Sedimentation in the Ritland Impact Structure, western Norway

By

Abdus Samad Azad

Dissertation presented for the degree of Philosophiae Doctor

Faculty of Mathematics and Natural Sciences
Department of Geosciences, University of Oslo
Oslo, Norway
May, 2013

Series of dissertations submitted to the
Faculty of Mathematics and Natural Sciences, University of Oslo
No. 1352

ISSN 1501-7710

Cover: Inger Sandved Anfinsen.
Printed in Norway: AIT Oslo AS.

Produced in co-operation with Akademika Publishing.
The thesis is produced by Akademika publishing merely in connection with the thesis defence. Kindly direct all inquiries regarding the thesis to the copyright holder or the unit which grants the doctorate.

Preface

The current thesis is the outcome of the three years (2009-2012) research funding granted by the Norwegian Research council (NFR). The research consists of two main components; the detailed field work and extensive laboratory analysis. Ten weeks of extensive field work in several field seasons from 2009-2012 were carried out in the Ritland impact structure, Hjelmeland, western Norway. This involved mapping the exposed sedimentary successions, detailed sedimentological logging of several sections, in field textural analysis of the coarser clastics and in depth documentation of the field observations. Laboratory investigations of the collected rock samples were undertaken at the University of Oslo, mostly in Geosciences department. 143 thin sections were examined under optical microscopes and X-ray diffraction analysis made of 57 bulk samples; in addition 20 selected samples were examined with the back-scattered scanning electron microscope. The results were presented to the scientific community through attending several conferences, both nationally and internationally. Three conference abstracts were published, representing the preliminary findings of the research, along with a poster presentation at Lunar and Planetary Science Conference at Houston, Texas, U.S.A. Network in Impact Research (NIR) worked as a useful forum for attending several training courses related to this research, mingling with impact researches around the world and also participating in excursions to several impact structures, i.e. Gardnos in Norway, Lappajärvi, Söderfjärden and Keurusselkä in Finland, Ries and Steinheim in Germany. The required courses (30 credits) for the PhD degree were taken mostly from University of Oslo, while 10 credit points on impact cratering and shock metamorphism were from University of Oulu, Finland.

The results of the dissertation consist of three scientific papers; the first paper has been published in the Norwegian Journal of Geology, the second is in print in the same journal and the third is in review in the Meteoritics and Planetary Science Journal. An introduction, geological setting, and a short summary of the papers are presented separately in the first three chapters. The appendix includes the conference abstracts and the poster.

The research has been supervised by Prof. Henning Dypvik (University of Oslo), while Fridtjof Riis (Norwegian Petroleum Directorate) and Dr. Elin Kalleson (Fyrstikkalleen High School) worked as the co-supervisors.

Acknowledgements

While writing this, I remember a phone call, offering me the position of Research Fellow at the University of Oslo. It was an enticing opportunity for me to work with a rather rarely discussed but very interesting topic of Geosciences. My foremost acknowledgment goes to my supervisor Prof. Henning Dypvik, who introduced me to the field of Impact Geology. He has been always available for discussion on many critical aspects of this research. He was very prompt in sending me feedback, always encouraging, and a perfectionist towards any of my writing. I also wish to thank my co-supervisors Fridjof Riis and Dr. Elin Kalleson for sharing their experiences and for their many valuable suggestions and guidance which helped to improve the thesis.

I equally acknowledge my wife Ummul Khayer T. Dina for always being supportive, providing the mental strength and so patiently taking care of our child Zahin Abrar Azad, helping me to concentrate on the research full time. I acknowledge the patience of our little boy, missing me during my extended working hours at the department. I am also thankful to my parents and family members who were always supportive and courageous, despite missing me for several years during my stay in Norway.

The Norwegian Research Council (NFR) generously granted the funding of the Ritland research project. I express my acknowledgement to the NFR authority. I am also grateful to other Ritland project members: Michal Tomczyk (University of Bremen, Germany) and Ronny Setså (University of Oslo) for helping me during field work and also for being available for group discussions. I extend my acknowledgement to other members who were involved for rather shorter periods but contributed a lot to the Ritland Project, e.g. Dr. Valery Suvalov (Russian Academy of Sciences), Dr. Simon Buckley (University of Bergen), Tonny Spencer (Statoil) and Claus Beyer.

I am thankful to the reviewers of my papers, Drs. Kevin Evans, Alex Deutsch and David Jolley for their thoughtful comments and constructive criticism, which improved the manuscript considerably. I express my gratitude to Dr. Trond Slagstad, Editor, Norwegian Journal of Geology, for prompt responses to all my questions related to publications. I am grateful to my Ph.D. thesis evaluation committee, Drs. Philippe Claeys, Lars Harald Blikra and Prof. Annik M. Myhre for the scientific evaluation of this dissertation. Adrian Read helped me improving the language of the manuscript, I am highly grateful to him. Finally, I want to thank the laboratory technicians, particularly Mufak Naoroz, Salah Akahvan and Berit Løken, and people at Ritland, especially the Sven Egil and Kari Sørensen family, for their kind support and hospitality.

Sedimentation in the Ritland Impact Structure, western Norway

Abstract

Abdus Samad Azad, Department of Geosciences, University of Oslo.

The Ritland structure is the remnants of a 2.7 km diameter, 350 m deep, Early to Middle Cambrian marine impact crater, located in Hjelmeland, western Norway. The impact origin of this structure was proposed in 2001 based on geological mapping. In 2007, further investigation confirmed the presence of rocks of melt origin and the subsequent shock-metamorphic features. Detailed field mapping and sedimentological and mineralogical analyses of the crater infill, explaining the possible depositional mechanisms, sedimentary environments and provenance, were the main objectives of this study. The Ritland crater infill studies were further extended into a comparative analysis with some selected marine crater infills, aiming to achieve a better understanding of the post-impact depositional mechanisms and sedimentary environments.

The Ritland crater was excavated in the gneissic sub-Cambrian peneplain by a bolide impact of ~115 m diameter. Recent studies on the lower Palaeozoic sediments outside the crater and intercalated ejecta beds indicate that the Ritland target site probably had experienced the Early Cambrian marine transgression when the bolide impacted, possibly into shoreface-close environments in the inner shelf. The Ritland crater infills were broadly classified into three sedimentation stages: A) late syn-impact, B) early post-impact, and C) late post-impact. Late syn-impact crater sedimentation represents an early stage of crater modification, where sediments were derived from collapse of the transient cavity and eventually avalanched down towards the crater centre. In the Ritland crater, extremely clast-rich breccias accompanied with the occasional appearance of reworked particles of melt origin, suggested to be deposited from rock avalanches, probably were deposited within seconds after impact. The rock avalanche deposits were overlain by debris flow deposits representing a water-wet condition related to the resurge of the seawater, thus deposited in the early post-impact stage. A pronounced shift from clast-supported to matrix-supported texture occurred in the upper part of these debris flow deposits. This transition probably reflects flow transformations, where debris flows were transformed into hyperconcentrated density flows during downslope transport, caused by dilution with the gradual ingress of sea water (seeping/breaching through the crater rim). The crater cavity soon (probably hours/days) filled with water and turbidity flows started to dominate. The sandstone succession exposed in the Ritland crater was deposited from turbidity currents, possibly representing minor submarine fans. The coarser clastics were deposited along the unstable, steep crater walls (derived from continued local erosion and slope-failure), while fine-grained

sediments were deposited to the crater centre. The clast and matrix mineralogy of the late syn-impact and early post-impact crater-infilling sediments are comparable and dominated by local basement lithologies (target site) suggesting that these sediments were mostly derived from impact-generated debris.

The late-post impact succession in the Ritland crater is mostly fine-grained, e.g. sandstones, silty shale and shales deposited during later stages in comparatively stable crater conditions. The base of the late post-impact succession is marked by ~6 m of fine- to medium-grained sandstones and alternating fine-grained sandstones and silty shales. A marked increase in the textural maturity (increase in quartz/feldspar ratio), and an evidence of Cambrian marine life within these sandstones (unlike to early post-impact sandstones) suggest a transition from early post impact to late post-impact stage. These successions gradually shift upwards into dark grey to black shales with an about 180 m thick unit in the crater centre. The late post-impact sedimentation in the Ritland crater is suspension dominated with only minor episodes of turbidity current deposition observed in the transitional sandstones. Localised occurrences of coarser clastics within the marine shales along the steep crater wall suggest that gravity slides and screes were sporadically active along the crater wall for a long time after the impact, until the crater was eventually topped by marine clays.

Comparative analysis of the Ritland crater infill to the Gardnos, Kärdla, Lockne and Chesapeake Bay crater-filling deposits revealed almost a common order of occurrence of different sedimentary processes dominating at the different stages of crater sedimentation. The thickness and compositional variations are explained by differences in crater size, target lithology and water depth.

Rock avalanches dominated during the late syn-impact stage in the Ritland and Gardnos craters, mainly due to their crystalline target sites covered with only a thin veneer of marine sediments. Bolide impact into target sites with thick sedimentary cover will most likely generate large-scale collapses of the transient cavity and water-saturated rim layers, resulting in repetitive events of rock avalanches, slumping and gravity-slides as observed in the Kärdla and Chesapeake Bay craters. Impact in deeper water target sites, e.g. Lockne, does not show any clear-cut large-scale gravity-collapse but rather represents an early resurge.

Impact into crystalline target sites with a thin cover of shallow marine sediments in the Ritland and Gardnos craters resulted in well developed and elevated rim formation. The crater rim walls probably acted as a barrier and hindered the large-scale resurge-generated debris flow events within the craters in their early post-impact stage. Impact into thicker sedimentary cover at the

target sites resulted in relatively weaker rim formation in the Kärdla and brim development in the Lockne and Chesapeake Bay craters, allowing multiple events of large-scale debris flows.

Turbidites were commonly observed at the waning stage of the resurge during early post-impact to the late post-impact stage. The Kärdla and Lockne craters represent thick resurge/back-surge turbidites. Ritland and Gardnos turbidites may have partially derived from back-surge but dominantly, most likely, form later slope-failure, erosion and reworking of the impact-derived debris. The turbidites in the Chesapeake Bay crater may either have been derived from the back-surge or from later slope-failure. Suspension deposition dominates in all the compared craters at the late stages when the crater cavities reached a more stable condition.

Scientific Results

List of papers

Paper 1: Azad, A. S., Dypvik, H., Tomczyk, M., Kalleson, E. & Riis, F. 2012: Late syn-impact and early post-impact sedimentation in the Ritland impact structure, western Norway. *Norwegian Journal of Geology, Vol. 92(4), p. 405-431.*

Paper 2: Azad, A. S., Dypvik, H., Riis, F. & Kalleson, E. 2013: Late post-impact sedimentation in the Ritland impact structure, western Norway. *In print, Norwegian Journal of Geology, Vol. 93(1), p. 37-58.*

Paper 3: Azad, A. S., & Dypvik, H. 2013: Sedimentation in marine impact craters - Insight from the Ritland impact structure. *In review, Meteoritics and Planetary Science Journal.*

List of conference abstracts and poster

Abstract 1: Azad, A. S., Tomczyk, M., Dypvik, H., Kalleson, E., & Riis, F., 2011: Syn-impact and early post-impact sedimentation in the Ritland impact structure, Abstracts and Proceedings of the NGF. Stavanger, Norway.

Abstract 2: Azad, A. S., Dypvik, H., Kalleson, E., & Riis, F., 2012: Late-post impact sedimentation in the Ritland impact structure, Conference abstract in 30th Nordic Geological Winter Meeting. Reykjavik, Iceland.

Abstract 3: Azad, A. S., Dypvik, H., Kalleson, E. & Riis, F. 2012: Sedimentation in the Ritland impact structure, western Norway. 43rd Lunar and Planetary Science Conference, Houston, Texas. (Abstract # 1281).

Poster 1: Azad, A. S., Dypvik, H., Kalleson, E. & Riis, F. 2012: Sedimentation in the Ritland impact structure, western Norway. 43rd Lunar and Planetary Science Conference, Houston, Texas.

Table of Contents

Introduction

CHAPTER 1

1. INTRODUCTION

1.1. Definition and importance of impact cratering

'Impact cratering' can be defined as a combination of processes by which impact craters are formed. The processes include highly dynamic, continuous, complicated sequences of events that take place in minutes. The term 'impact' or 'hypervelocity impact' refers to the collision of two planetary bodies at or nearly at cosmic velocity through which the original kinetic energy of the projectile is transferred into a target rock at a point surface. The shock wave generated from the collision travels both into the target and into the projectile. The term 'impact crater' or 'hypervelocity impact crater' is used for a structure which generally occurs as a depression in the topography and was formed by the cosmic projectile.

The importance of impact cratering has recently been summarised by Reimold (2003), French (2004), Pati and Reimold (2007), Reimold and Koeberl (2008) and French and Koeberl (2010). Impact cratering, once ignored or ridiculed, has now grown into a fully developed multidisciplinary research subject within the earth and planetary sciences. Most disciplines of earth and planetary sciences have touched upon these revolutionary concepts (French, 2004; Reimold, 2003). Results from advanced research on impact cratering are now able to shed light on many unresolved questions related to the origin of the Solar system, e.g. formation of the early crust and atmosphere on Earth, and transfer of water as well as life on to the Earth by interplanetary objects, i.e. dust particles, asteroid airburst, comets and meteorites. In addition, increased knowledge of impact cratering has been instrumental in discovering commercial accumulations of mineral and hydrocarbon deposits in impact structures.

Studying impact cratering may have key significance in answering the most vital question; is mother Earth on the brink of a potential threat from a large bolide impact? Fortunately, mankind on Earth has not experienced any large-scale impact event in historical time. Nevertheless, collisions of fragments of Shoemaker-Levy 9 into the atmosphere of Jupiter on July 1994 and the Tunguska event of June 1908 over Siberian forests appeared as warnings of the tremendous disasters that can be caused by hypervelocity impacts. The Earth has been under a constant bombardment of objects from space since its origin. The objects cover a wide compositional range: asteroids, comets, near-Earth objects, and they vary in size from dust to planetoids. Every day hundreds of tons of dust enter the upper atmosphere. Bombardment by objects of a few

metres' diameter occurs every year; every century or so there are bigger impacts; and over longer periods, (from hundreds of thousands to millions of years) objects with a diameter of up to several kilometres hit the Earth with consequences for life as a whole. Most of the dust or sand-sized particles burn up in the atmosphere due to air friction on their travel through the atmosphere, never reaching the Earth's surface.

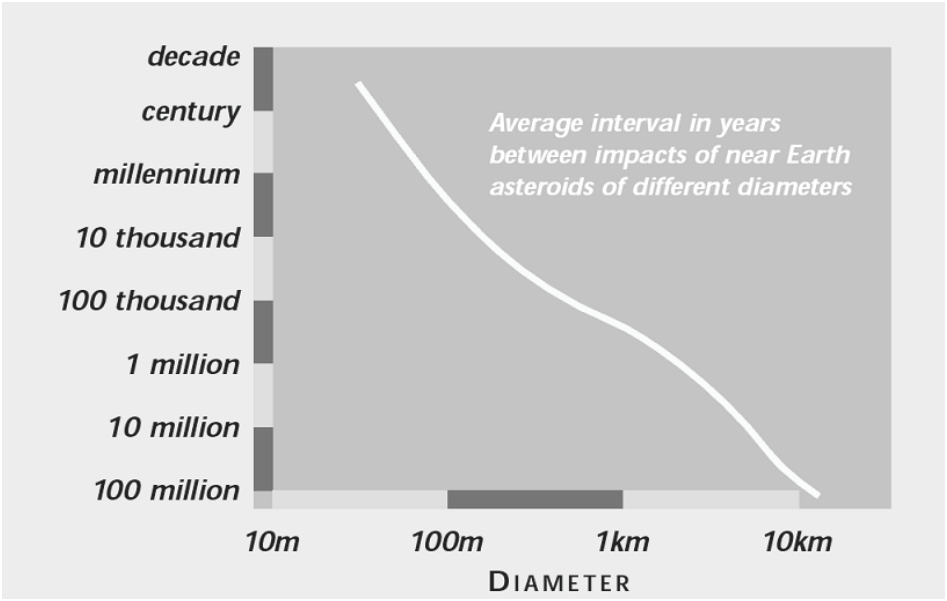

Fig. 1.1. Average interval of years between impacts on the Earth of near-Earth asteroids of different diameters. Small impactors are more frequent compared to larger objects (Atkinson et al., 2000).

Larger objects (50-100 m) may strike the ground as one piece or as a cluster of fragments, depending on their size and composition. The really large ones (>100 m in diameter), especially if they are coherent enough (e.g., iron meteorites), pass through the atmosphere without disintegrating or slowing down and strike the ground surface close to their original cosmic velocities (between 11 km/s and 72 km/s, average ~20 km/sec). A strong inverse correlation has been found between the size of the objects colliding with the Earth and the rate of collision in number of years (Fig. 1.1) (Atkinson et al., 2000). Small objects hit the earth much more frequently than the larger ones, reflecting the size distribution of objects in the asteroid belt that is supposed to be the main source of objects colliding with the Earth.

1.2. History of impact cratering science

The lunar craters have been studied since the advent of telescope in the sixteenth century. Many hypotheses have been proposed since, on the origin of lunar craters (Drake and Komar, 1984). The modern concept of 'impact cratering' is the outcome of the space program in the late 1960s.

Robert Hooke (1635-1703) was the first to draw sketches of the lunar craters, and interpreted the 'pits' on the lunar surface as analogous to the craters on Earth 'on the tops of some hills' caused by eruptive forces. He advanced two theories to explain the existence of the lunar 'pits'. First, he bombarded a mixture of tobacco-pipe clay and water with a heavy body as a bullet to produce pits similar to those on the Moon. But he failed to explain the source originating the pits since meteorites were unknown in his days. He worked on the other experiment with a pot of boiled alabaster. Hook noticed that if he removed the pot from the fire while it was boiling, the alabaster ceased to boil, and the whole surface, especially where some last bubbles had risen, started to form small pits shaped like those of the Moon. Hooke's description was close to that of a steam explosion, a concept of crater formation that has persisted in various forms ever since, e.g. boiling of soup by Rozet (1846) and St. Clair (1891), bubbling of gases by Mills (1969), even the tidal theory (Hannay, 1892), all implying a hot liquid condition of the Moon.

G. K. Gilbert (1843-1918) challenged the liquid state of the primeval Moon and the idea of vast circular cliffs on the Moon as the result of cyclopean bubbles bursting. The reality of meteorites was established at that time by the work of E.F.F. Chladni and E. Biot (Drake and Komar, 1984). Gilbert performed bombardment experiments with clay balls on a clay surface to model impact craters. Gilbert's (1893) *The Moon's Face* challenged the volcanic theory for the origin of lunar craters; a theory adhered to by many nineteenth-century scientists (Drake and Komar, 1984).

Alfred Wegner (1880-1930) also performed series of cratering experiments and reviewed the four dominant existing hypotheses: bubble, tidal, volcanic and impact. His experimental results only supported the impact hypothesis for a satisfactory explanation to the origin of lunar craters (Wegener, 1921). However, the debate continued until the best analogous terrestrial crater 'Meteor Crater' was found. Although an immense collection of meteorites of undisputable extraterrestrial origin was found at northern Arizona's crater in 1891, nearly fifteen years had been passed before a satisfactory explanation of linking the meteorites to the impact origin was established (Barringer, 1905; Tilghman, 1905).

Alfred Wegner (1921) and Barringer (1924) strongly supported the impact theory for the formation of 'Meteor crater'; however, there was still much opposition to this idea and much

support for the volcanically-driven steam explosion concept. This was partly due to the battle between the catastrophists and uniformitarianists (Marvin, 1999). The geological community was surprisingly less receptive to the idea of a catastrophic origin for 'Meteor Crater', as catastrophism was being ignored and abandoned while Lyellian uniformitarianism dominated geological reasoning throughout the western world during the nineteenth century.

In time, the need for physical evidence for proving the impact origin of the 'Meteor Crater' became evident. Shoemaker (1960) drew upon new observations of crater excavation associated with nuclear explosions and developed an analytical model for the penetration mechanics of hypervelocity impact events, and also presented physical evidence of shock metamorphic features in the mineral grains. Dietz (1947, 1959) found *shatter cones* in the impact-derived rocks and proposed that they were unique products of meteorite impacts. Dietz' arguments gradually became accepted during the 1960s and 1970s, especially when shatter cones were found to be associated with petrographic features such as planar deformation features (PDFs). In addition, the discovery of high-pressure silica 'coesite' and 'stishovite' (Chao et al., 1960; 1962) in impact structures also provided evidence of formation of extremely high pressure rocks. Similarly, lunar craters were proven to be of meteoric origin when lunar samples from the Apollo missions became available for mineralogical and chemical analysis, and many of them also showed signs of shock metamorphic deformation.

Impact cratering came into mainstream geosciences when Alvarez et al. (1980) provided the first geochemical evidence for a connection between a large impact event and the major biological extinction at the K-Pg (formerly K-T; Cretaceous-Tertiary) boundary 65 Ma ago in a thin clay layer. They discovered a strong enrichment of platinum group elements, including iridium, within the clay layer, which do not have any obvious terrestrial sources. Since the concentration of iridium in most meteorites is higher than in the Earth's crust by several orders of magnitude, this iridium anomaly could result from catastrophic impact event. Alvarez et al. (1980) hypothesis brought a fresh impetus to the twentieth century's geological research.

1.3. Formation of impact craters

The sequential events in hypervelocity impacts include several stages which are dominated by a specific set of major physical and mechanical processes (Melosh and Ivanov, 1999). Conventionally three main stages are distinguished: i) contact and compression, ii) excavation and transient crater growth, and iii) modification (slumping and collapse) of the transient cavity (Gault et al., 1968; Melosh, 1989; French, 1998; Turtle et al., 2005).

1.3.1 Contact and compression

The contact and compression stage is the briefest of all the stages. It starts as soon as the projectile hits the target surface (Fig. 1.2.a) and lasts as long as it takes the projectile to enter the target and transfer its energy in the form of shock waves (Melosh and Ivanov, 1999). The contact and compression stage lasts no more than a few seconds, even for impacts of very large objects (more than 100 km diameter transient crater) (French, 1998). When the projectile hits, it compresses and accelerates the target mass. Shock waves originate at the point or points of contact; propagate through the projectile and into the target. When the shock wave reflects back into the projectile, on reaching the back end of the projectile it is then reflected forward into the projectile as a rarefaction wave or release wave (Fig. 1.2.b). As the release wave passes through the projectile back to its front again, the projectile is unloaded from the shock pressures. This results in transfer of most of the projectile's initial kinetic energy into kinetic and internal energy in both the projectile and the target (Turtle et al., 2005). The residual kinetic energy is spent ejecting material and opening the transient cavity. The internal energy heats the projectile and the target, causing melting and/or vaporisation at the impact point in the case of sufficiently strong shocks (Turtle et al., 2005).

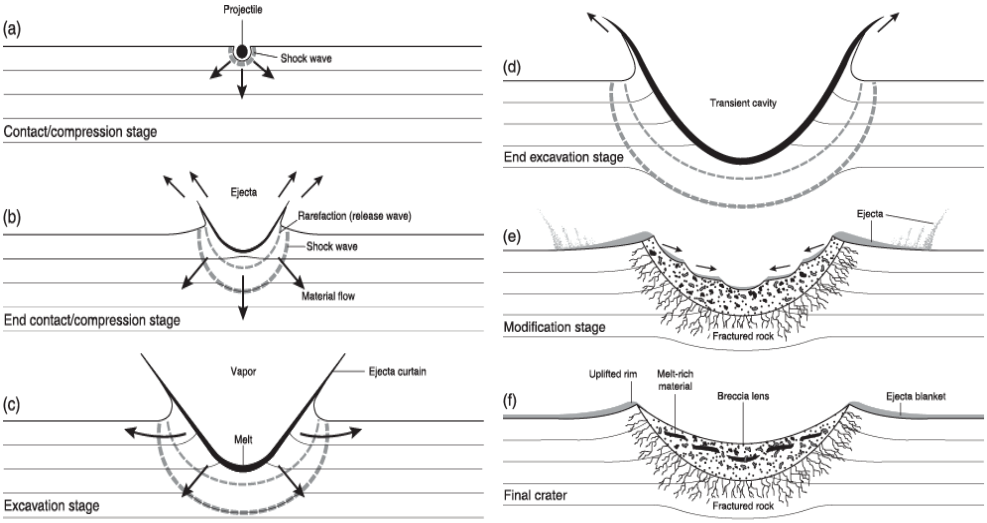

Fig. 1.2 Development of a simple impact structure (from French, 1998). Description of the progressive development of the structure is given in the text.

1.3.2 Excavation and transient crater growth

The brief contact and compression stage grades immediately into a relatively longer excavation stage. The excavation stage may last from seconds to minutes, depending on the velocity of the near-surface excavation flow and the diameter of the transient crater (French, 1998). During *the excavation stage*, an open cavity is formed (Fig. 1.2.c) due to the complex interaction of the hemispherical down and outward movement of the shock wave and upward-directed pressure gradient formed by the rarefaction waves. These complex processes drive the target rock outward from the impact point, producing a systematic excavation flow around the centre of the developing structure. In the upper levels, the target materials mainly move upward and outward; at lower levels, target materials moves dominantly downward and outward, thus quickly producing a bowl-shaped depression (the transient cavity) in the target rocks (Fig. 1.2.d).

1.3.3 Modification of the transient cavity

Gravity is the ultimate driving force during the modification or collapse of the transient cavity which produces the final crater shape. When the transient crater grows to its maximum size, the subsequent modification stage begins immediately (Fig. 1.2.e). For simple craters the transient crater modifies into final crater simply by debris sliding down the steepest parts of the crater wall to accumulate as a breccia lens on the crater floor, making the 'apparent crater' wider and less deep (Fig. 1.2.f). The inward and upward material motion during modification stages results in a complex mixture of breccia and impact-melts inside the crater depression (Fig. 1.2.f). In the case of large impact events, structural uplift of the sub-crater material results in complex and extensive slumping of the crater rim, and the transition from the transient cavity growth to collapse may not be defined explicitly, indeed the processes of excavation and collapse can overlap (Turtle et al., 2005). Sub-horizontal units of allogenic breccias and impact-melts (thickening along the crater walls and thinning at the central uplift) may occur as crater-fill materials (French, 1998).

1.4. Crater morphology

Irrespective of which planet**,** the fresh simple crater has classic bowl-shaped morphology, uplifted rim area, crater walls with exposed stratified target rocks, rather flat crater floor and well defined ejecta blanket (Figs. 1.3. a, b & c). Complexity in the crater morphology occurs with increasing crater diameter for both terrestrial and Martian impact craters (Figs. 1.3 d & e).

Fig. 1.3 Examples of simple and complex terrestrial and Martian craters. (a) Aerial photo of the 1.2 km diameter Barringer (Meteor Crater), Arizona, U.S.A. image credit: NASA (b) Martian simple crater 1 km in diameter, 260 m deep (c) Ground photo of the Barringer crater showing inside crater morphology, image credit: Earth Impact Database, (d) The complex/multi-ring Vredefort impact structure, 300 km in diameter, Free State, South Africa. Image source: Earth Impact Database. (e) The Zunil, 10.4 km Martian complex crater.
Image source (b): http://viewer.mars.asu.edu/planetview/inst/moc/R1502146#start
Image Source (e): http://www.uahirise.org/PSP_002252_1880

Three distinct types of impact structure can be formed: simple craters, complex craters and multi-ring basins (French, 1998). The small, simple impact structures have a nearly parabolic interior profile which is less than a few kilometres across (Melosh and Ivanov, 1999) (Figs. 1.3 a & b). Barringer or Meteor Crater in Arizona, U.S.A. is a well-preserved terrestrial simple impact crater with bowl-shaped morphology (Figs. 1.3 a & c). Tear faults cross-cut the area to produce a square shaped plan view (Kring, 2007). This crater is 1.2 km in diameter, 180 m deep, and has a crater rim that rises 30 to 60 m above the surrounding plain. On Earth, the transition from simple to complex crater morphology commonly occurs near a diameter of 2.5 km in sedimentary target materials and about 4.5 km in crystalline target rocks (Grieve, 1987). Fresh simple craters have an apparent depth (i.e., the distance from the top of crater rim to present-day crater floor) of about one-third of the apparent crater diameter (both of these apparent values are dependant on the degree of erosion) (Reimold and Koeberl, 2008). In a simple crater, probably half of its original (transient) depth is immediately filled by the mixture of re-deposited fall-back ejecta and debris slumped in from the crater walls and rim (French, 1998). Complex craters are characterised by a centrally uplifted region (central peak), a generally flat floor, and extensive inward collapse around the rim. Apparent crater depth for complex structures is more like one-fifth to one-sixth of their apparent diameter (Reimold and Koeberl, 2008). Multi-ring geometries can be formed in the complex structures due to the collapse of the central peak (Pati and Reimold, 2007). On Earth only three large impact structures are considered to be 'multi-ring basin' type; i) the 2.02 Gyr old and 250-300 km diameter Vredefort in South Africa (Fig. 1.3d), ii) the 1.85 Gyr old and 200-250 km diameter Sudbury in Canada, and iii) the 65 Ma age and 180 km diameter Chicxulub in Mexico (Spudis, 1993).

1.5. Impact rocks (impactites)

A wide variety of distinctive rock types are formed during impact processes. A general term 'impactite' is used for describing the rocks that are affected by or produced by the shock waves and other processes generated by a hypervelocity meteorite impact event (French, 1998). Based on the lithological components, texture, degree of shock metamorphism and mode of occurrence (in or outside the crater), impactites are classified and defined in detail by Stöffler and Grieve (2007) and French (1998). A brief summary of the major impactites is described, here mostly based on the classification and definitions proposed by French (1998).

French (1998) classified the impactites into four rock units based on their distribution with respect to the crater structure: i) crater floor and sub-crater: parautochthonous rocks, cross-cutting allogenic units, and pseudotachylite, ii) crater interior: allogenic crater-fill deposits

(lithic breccias, suevite breccias and impact-melt breccias); iii) crater rim region: proximal ejecta deposits, and iv) distant from crater: distal ejecta.

Crater floor and sub-crater: Parautochthonous rocks may occur as coherent target rocks or lithic breccias (French, 1998). Sub-crater rocks that are generally displaced as large individual blocks (typically measuring tens to hundreds of metres, or even larger), where the original stratigraphy and structural features are well preserved, can be termed coherent target rocks or blocks. Shock pressures in the parautochthonous rocks vary widely; highest pressures (25-30 GPa) occur near the centre of the structure and decrease rapidly outward towards the margin (≤ 2 GPa at the rim). Lower shock pressures may produce shatter cones in the deeper regions near the centre of the crater. Impactite breccias, termed parautochthonous lithic breccias, are formed by shattering and pulverising of target rocks essentially in place (autoclastic), typically forming irregular bodies tens to hundreds of metres in size and showing gradational contact against areas of similar and more coherent target rocks. The lithic breccias are composed of fragments, derived from local target rocks, and the breccias may be monomict or polymict, depending on the lithological variety of the target rocks. Distinctive shock-metamorphic effects, e.g. PDFs, are generally absent in the rock fragments, and the breccias show no evidence of significant transport. Cross-cutting breccias in the sub-crater bedrock contain significant amounts of clasts from elsewhere and therefore considered as allogenic breccias. These breccia bodies tend to have regular shapes and show sharp contacts and clear cross-cutting relations against the sub-crater bedrock. Cross-cutting breccias often occur as distinctive breccia dikes, typically range from less than a metre to tens of metres in width and may be as much as a kilometre long (Dressler and Sharpton, 1997). A wide variety of cross-cutting breccias has been reported from several impact structures: a) melt-free, polymict lithic breccias with clastic matrix, b) melt-fragment breccias, c) impact-melt breccias, d) impact-melt rocks. 'Pseudotachylite' is an unusual type of impact breccia that results from frictional melting during the rapid movements of late-stage crater development and modification (Spray, 1997). The origin of pseudotachylite has been controversial ever since the term was first used (Shand, 1916). However, impact-induced pseudotachylite breccias were distinguished from tectonic ones on the basis of their shape and dimensions. Unlike small-scale (few metres wide) linear bodies of tectonic pseudotachylite, impact-produced pseudotachylites found in the Sudbury and Vredefort structures are more irregular in form and may reach tens to hundreds of metres in size (Spray and Thompson, 1995).

Crater interior: Crater-fill breccias consist of several different components: a) collapse debris from the crater walls and rims of the original transient crater, b) materials ejected with nearly vertical trajectories, c) large and small bodies of impact melt, and d) ejecta originally deposited

near the transient crater rim and caught up in the subsequent collapse. All these components result in a partially filled cavity with a complex mixture of rock-fragments (both shocked and un-shocked) together with bodies of impact melt. In bowl-shaped, simple craters the final crater-fill may fill the crater to about half of its original depth. In larger, complex structures, particularly those formed in crystalline target rocks, the crater-fill typically contains discrete units of breccias and impact-melts that may form large annular deposits, thickening along the crater-walls and thinning around the central uplift. The crater-fill breccias are subsequently overlain by younger crater-fill sediments deposited by conventional sedimentary processes.

Melt-free breccias (lithic allogenic breccias) form a common distinct lithology in both large and small impact structures. These breccias consist of rock and mineral fragments within a clastic matrix of fine-grained material of comparable lithology. Unlike the parautochthonous lithic breccias, the crater-fill lithic breccias are more polymictic, as their fragments have been derived from a wider region of the target area. Distinctive shock effects are rarely observed in crater-fill fragments as they are derived from less-shocked regions around the walls and rim of the transient crater. Within the crater-fill deposits, lithic breccias are often associated with melt components, either as discrete fragments or as a matrix for lithic fragments. Breccias with a few percent or more of melt components are regarded as melt-bearing breccias, but the transition between the lithic breccias and melt-bearing breccias appears continuous, with no formal boundary explicitly defining those (French, 1998). Melt-fragment breccias, also known as suevites, are composed of discrete fragments of rocks and minerals, together with bodies of melt, in a clastic matrix of similar but finer-grained materials. In melt-matrix breccias or impact-melt breccias, the melts occur as a matrix, typically constituting 25-75 volume % of the rocks and may range from glass to completely crystalline igneous rock.

Ejecta deposits: Two main types of ejecta deposit are distinguished; the proximal ejecta (deposited near the crater) and the distal ejecta (deposited far from the crater). In terms of crater radius (R_c), during impact approximately half of the ejecta is deposited within $2R_c$ from the centre to form a continuous ejecta blanket. This may be tens to hundreds of metres thick, depending on the crater size. At greater distances, the ejecta deposit becomes thinner and increasingly discontinuous. Most of the ejecta are deposited within about $5R_c$. The ejecta deposits around the craters are rarely homogeneous and could appear similar to crater-fill deposits, i.e. lithic breccias, suevites and impact-melt rocks. In terrestrial impact events, disruption of the atmosphere by the impact fireballs, ballistic ejection from the crater, and subsequent atmospheric transport may result in distribution of smaller ejecta particles (≤ 1 mm) to regional or global distances (Alvarez et al., 1980). The widely studied distal ejecta from the

Chicxulub structure in Mexico is distributed world-wide, delineating the K-Pg boundary. Interestingly, the evidence of these distal ejecta layers (with shocked quartz grains and small spherules of melted target rocks with iridium enrichments sourced from the projectile) was established long before the Chicxulub impact structure itself was identified. Tektites and microtektites (cm to mm size) consist of pure glass/melt are the unique variety of distal ejecta that may be found far away from the impact site and distributed over wide areas (strewnfields).

1.6. Identification of impact craters

The number of confirmed impact structures discovered so far on Earth is 183 (http://www.passc.net/EarthImpactDatabase/), and it is estimated that many more remain to be identified (French and Koeberl, 2010). Identification of terrestrial impact structures is not always as easy as on the Moon and other planetary bodies. There the lack of an appreciable atmosphere, and less active geological processes, means that meteorite impact craters are well preserved and can commonly be recognised from morphological characteristics (French and Koeberl, 2010). In contrast the Earth's surface is constantly changing through different geological processes. Plate tectonics, active volcanism, weathering, erosion and sedimentation may alter, and eventually erase, the impact structures. Although circular morphology, circular geophysical anomalies, fracturing and brecciation etc. are typical for impact craters, identification based on these characteristics alone is ambiguous. Structures comparable to impact craters may have been formed by more conventional endogenic geological processes. Remote sensing techniques, digital elevation models and geophysical data sets may be useful in indicating the existence of potential impact structures or add supplementary information to the proven ones (Koeberl, 2007). Meteorite fragments, an unambiguous indication of impact structures, are rarely preserved in the target area. The impacting projectile is either melted or vaporized during impact (Melosh, 1989), or may be destroyed by post-impact weathering and erosion and have a little chance to survive for geologically longer periods of time (French and Koeberl, 2010). The most unambiguous identification of impact structures is based on a small set of distinctive shock-metamorphic effects (Koeberl, 1997; French, 1998; French and Koeberl, 2010). Shock-produced deformation effects which are considered to be the diagnostic indicators for shock metamorphism and meteorite impact are: chemical and isotopic projectile signature, shatter cones, high pressure (diaplectic) mineral glasses, high-pressure mineral phases, high temperature glasses and melts, planar deformation features (PDFs) and planar features (PFs) in quartz (French and Koeberl, 2010). Some of the features which can be produced by meteorite impact, however, may also be formed by other geological processes, viz. kink bending in micas,

mosaicism in crystals, pseudotachylite and pseudotachylite breccias, spherules and microspherules (French and Koeberl, 2010).

1.6.1. Shock metamorphism

Shock metamorphism (French, 1968) is generally defined as 'all the changes in rocks and minerals resulting from the passage of transient, high-pressure shock waves'. Hypervelocity impact results in peak shock pressures ranging from ≤2 GPa (near the final crater rim) to ≥100 GPa (near the impact point) (French, 1998). These pressures are far outside the range of normal endogenic metamorphism (Fig. 1.4) which can attain pressures of up to 2 GPa (Montanari and Koeberl, 2000). The temperature produced by the endogenic metamorphism generally ranges within 1000^{o}C (Fig. 1.4). In contrast, the temperature produced during shock metamorphism near the impact point is up to several thousand ^{o}C, high enough to produce melting and even vaporisation within the target. The shock-wave pressure is also different from normal geologic processes as it is brief and sudden, and passes through the rocks in microseconds, producing unique effects in the rocks. The most diagnostic features are produced at pressures ≥10 GPa which include planar deformation features (PDFs) in quartz grains, diaplectic mineral glasses, high pressure mineral phases and ultrahigh-temperature melting effects (French and Koeberl, 2010). However, low-pressure shock waves (≤5 GPa) can produce both megascopic (e.g., shatter cones and brecciation of the target rocks) and microscopic deformation features (e.g., kink bands in micas, several types of planar micro-fractures and related deformation in quartz, feldspar and other minerals).

Planar deformation features (PDFs): PDFs are generally accepted as unique indicators of high shock pressures and therefore of meteorite impact. The PDFs in quartz grains consist of multiple sets of thin (1-3 μm), parallel, closely spaced (2-10 μm) planes (Fig. 1.5.a) which traverse a significant fraction of width of the individual quartz grains containing them (French and Koeberl, 2010). The PDFs are oriented to the specific crystallographic planes with low Millar-Bravis indices. Depending on the peak pressure, PDFs are observed with ~2 to 10 orientations per grain (Koeberl, 2002). To confirm the presence of PDFs, it is necessary to measure the crystallographic orientations of a statistically significant number of PDFs in each sample (>20-50 grains from each thin section) by using either a universal stage or a spindle stage set-up (French and Koeberl, 2010). The details of PDFs formation have not been clearly understood, although their formation involves interactions between the passing shock-waves and specific directions in the quartz crystal lattice. Fresh PDFs can be produced in laboratory experiments. Commonly natural PDFs occur in altered form, where the original glass has been recrystallized to quartz

and the original planes are marked by planar arrays of small fluid inclusions known as 'decorated PDFs'. PDFs, although most well developed in quartz, can also be found in minerals such as feldspar, zircon, garnet and apatite (French and Koeberl, 2010).

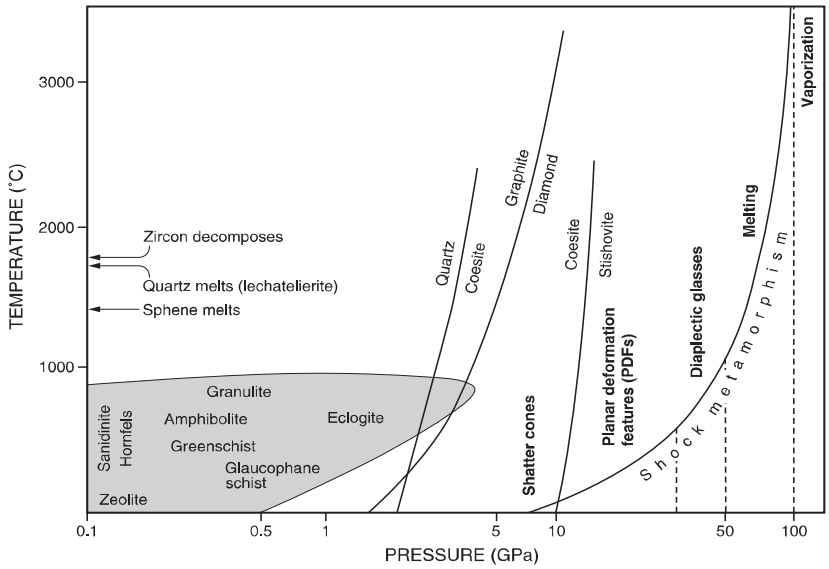

Fig. 1.4. Pressure and temperature plot showing comparative statement between normal crustal metamorphism and shock metamorphism (French, 1998).

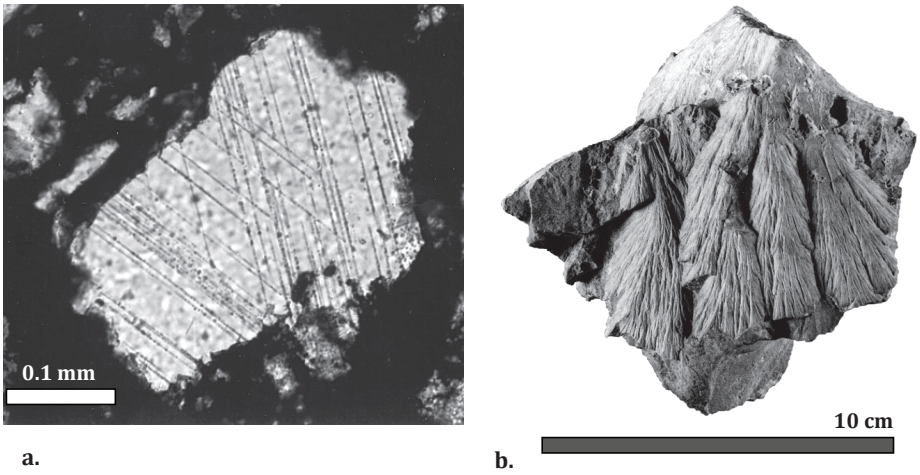

Fig. 1. 5. (a) Planar deformation features (PDFs) in a quartz grain from the carbon-bearing crater-fill breccia from the Gardnos structure, Norway. (b) Shatter cones in fine-grained limestone from the Haughton structure, Canada, (French, 1998).

Planar fractures: Multiple sets of open parallel fractures (PFs) can be produced by low level shock-waves (<10 GPa) in quartz grains. These fractures are relatively thin (typically 3-10 μm), but thicker than PDFs, appear as similar to the cleavage plane with multiple (usually 2-3) sets per grain. These fracture sets may be from 0.5 to 5 mm long, depending on the size of the host grain and may be oriented at specific angles to the c-axis of the host quartz grain (French, 2004). The planes consist of open fractures, often filled with secondary minerals and more widely spaced than PDFs (from 20 μm, to 100-500 μm). Sets of parallel PFs in quartz grains may form a more complex geometry in some established impact structures, where smaller, subparallel, closed planes of fluid inclusions diverge from the PF planes to form rather unusual and distinctive 'feather structures' (French, 2004; Ferrière and Osinski, 2009; Poelchau and Kenkmann, 2009). Multiple PF sets in quartz grain can be used as an impact criterion, especially if they are accompanied by other possible criteria for a meteorite impact.

High pressure mineral polymorphs: High pressure shock waves can also convert target rock minerals into new phases that are normally stable only at high static pressures, corresponding to the lower crust or mantle of the Earth (French and Koeberl, 2010). Two high pressure polymorphs of quartz: stishovite at shock pressures of >12-15 GPa and coesite at >30 Gpa (Stöffler and Langenhorst, 1994), are recognized as indicators of shock metamorphism in impact structures. Shock-produced diamond (mm-sized) formed in graphite or coal-bearing target rocks (Hough et al., 1995; Gilmour, 1998) is also a recognised high-pressure phase at a large number of established impact structures, and provides evidence of impact. However, the use of coesite and diamond as impact criteria remained equivocal as both the minerals, in addition, can also be found in non-impact environments in deep-seated terrestrial rocks, where they are formed in equilibrium at high static pressure (O'Brien et al., 2001). Some other high pressure polymorphs, reidite from zircon (Glass et al., 2002), TiO_2 polymorphs from rutile, and anastase (Jackson et al., 2006) have been reported in recent studies; however, using them alone as evidence of impact should be treated cautiously (French and Koeberl, 2010).

Diaplectic mineral glass: At higher shock pressures (>30-50 GPa), quartz and feldspars are converted into distinctive amorphous or 'glassy' phases without actual melting; these phases are called diaplectic glasses (Engelhardt and Stöffler, 1968). Diaplectic glass is one of the unique and distinctive criteria for the recognition of shock-metamorphosed rocks in impact structures.

High temperature impact-melts: Higher shock pressure (>50 GPa) produces increasingly high residual temperatures in the target rocks through which they pass. A post-shock temperature of >1500°C is sufficient to melt and decompose minerals that remain unaffected by the lower

temperatures produced in non-impact geological environments. The most common indicator of such impact-produced high temperature mineral melt is *lechatelierite* or silica glass. The presence of *lechatelierite* indicates temperature ≥1750°C, far above that of natural near-surface geological processes and can serve as independent evidence of meteorite impact (French and Koeberl, 2010). An unusual texture called 'ballen quartz' or 'ballen cristobalite' found in some silica grains in high-temperature impactites may also be related to the impact-produced formation of *lechatelierite* or diaplectic quartz glass. In 'ballen quartz', the original silica grains show distinctive fine-grained granular or internal texture composed of small spherical or rounded bodies which may be isotropic or partly to completely microcrystalline (French et al, 1970). Ballen quartz is considered to be formed due to the back-transformation from shock-induced states. Ferrièra et al. (2010) have recently suggested that the ballen quartz or the 'toasted' ballen quartz is formed due to vesicle formation after pressure release, at high post-shock temperatures, representing the beginning of quartz breakdown due to heating.

Shatter cones: These features were the first to be proposed as a diagnostic impact criterion (Dietz, 1947) and remain as the only diagnostic shock effect which is visible at macroscopic and megascopic (hand-specimen and outcrop) scales. Shatter cones are distinctive multiple sets of striated conical fractures that develop at relatively low shock pressures (≥2 GPa) in the rocks of terrestrial impact structures (Fig. 1.5.b). Shatter cones are commonly observed in the uplifted parautochthonous rocks of the central uplift, in individual rock fragments in the allochthonous breccias above the crater floor, or outside the crater (rim and ejecta). Depending on shock pressure and rock type, shatter cones may contain PDFs and even diaplectic glass (Dressler, 1990). The quality of shatter cones varies greatly with the rock type in which they form; fine-grained rocks (such as limestone and dolomite) produce excellent, finely detailed cones, while coarser rocks (sandstones, quartzite and other crystalline rocks) produce cruder cones which are often difficult to recognise. In such cases, careful observation is needed to distinguish them from non-impact features such as slickensides, wind-abrasion surfaces, cone-in-cone structures in sedimentary rocks, or even artificial blast cones in quarries and road cuts. The mechanism of formation of shatter cones is still not well understood. However, Ferrière and Osinski (2010) put forward some insights to the mechanism of shatter cone formation: a) shatter cones within crater-fill breccias are probably formed at an early stage of the cratering process, i.e. prior to crater excavation, b) they record shock-pressures up to ~20 Gpa and challenges the models related to low shock-pressure (3-6 Gpa) (Baratoux and Melosh, 2003) and c) the occurrence of shatter cones with complete cones and apices pointing in opposite directions also negates the hypothesis of shatter cone formation from branched, rapid fractures as proposed by Sagy et al. (2004).

Pseudotachylite and pseudotachylitic breccias: Pseudotachylitic breccias were first reported by Shand (1916) from the Vredefort structure, South Africa. Since then there has been continuous controversy regarding their character, nomenclature, origin and use as unique impact criterion. Two fundamental types of pseudotachylite have been recognised in the field. One type occurs as small, typically cm-length veinlets, composed of glassy materials and often containing high-pressure phases or PDFs in quartz-bearing clasts (Martini, 1991; Spray, 1998). The second type is longer, forming large veins and irregular bodies consisting of target rock fragments in a dark matrix, composed of partially or completely melted material. Individual pseudotachylite bodies observed at some structures, e.g. Vredefort (South Africa) and Sudbury (Canada), may extend over hundreds of metres to kilometres (Dressler and Reimold, 2004). The origin of pseudotachylite bodies and their relation to the process of crater development is still in discussion. Recent studies have suggested that similar types of pseudotachylite bodies can be produced by tectonic processes, as a result of frictional melting between rapidly moving blocks of crustal rocks (Spray, 1998). Reimold (1998) opposed challenged this view, mentioning the absence of significant movement between pseudotachylite walls. However, similar relations are also observed in fault zones unrelated to impacts, where pseudotachylites generated along shear planes have been injected as veins into nearby dilatational fractures without showing significant lateral movement (Snoke et al., 1998).

1.6.2 Geochemical anomalies

A large concentration of meteorite fragments in a geologically fresh crater certainly is a powerful criterion for recognition of impact craters. Unfortunately, this is rarely found and probably has limited use in identifying geologically old or deeply buried, eroded impact structures (French and Koeberl, 2010). During the large impact events, the projectile is subjected to shock pressures >100 GPa and often subjected to complete melting and vaporisation. Survival of the un-melted meteorite fragments in the resulting impact structure is extremely rare. Furthermore, meteorite fragments that survive the impact processes and are deposited in and around the newly-formed impact structure will be unlikely to survive for geologically longer periods of time before being destroyed by post-impact weathering. The Late Pliocene Eltanin impact event in the South Pacific Ocean (Bellingshausen Sea) is exceptional in being represented by large concentrations (~1 gm/cm^2) of meteoritic ejecta (both impact-melt rocks and un-melted meteorite fragments), deposited over an area of at least 2500 km^2 (Kyte, 2002). The relatively high abundance of Ir in a sediment core collected in the mid-1960s by the USNS *Eltanin* suggested the concept of impact origin (Kyte, 1981). Meteorite fragments from iron meteorite projectiles have been found otherwise only in some young impact structures, e.g. Meteor Crater

in Arizona, Henbury and Wolfe Creek in Australia. No preserved meteorites have been found associated with terrestrial impact crater more than 0.5 Ma. old (Grieve, 1991).

Distinct chemical and isotopic signatures in rocks inherited from the dispersed projectile (meteoritic) can be conclusively identified and thus provide reliable evidence of a meteoritic impact event. During impact, the original projectile material is heavily diluted by mixing with a vast volume of vaporised, melted and fragmented target rock. The actual amount of projectile material incorporated into impact lithologies is generally <1 wt% (French and Koeberl, 2010). Such small amounts of extraterrestrial matter may lead to only slight geochemical anomalies. Siderophile elements such as Ni, Co, Cr, Au and the platinum group elements (PGEs): Ru, Rh, Pd, Os, Ir, and Pt, are rare in the Earth's crust but are highly enriched in several classes of meteorite. In particular, Ir analysis has been effectively used to recognise impact origins, particularly for the K-Pg boundary layer (Alvarez et al., 1980). An elevated concentration of Ir (several hundred times the background value) was found at the K-Pg boundary (Alvarez et al., 1980) and interpreted to be linked with the Chicxulub impact (Hildebrand et al., 1991; Sharpton et al., 1992). Claeys et al. (2002) also recorded a positive Ir anomaly at the K-Pg boundary at 85 different sites around the world and suggested a homogeneous global distribution of Ir. In addition to the Ir anomaly as a powerful tool for recognising terrestrial craters, siderophile-element analyses are also instrumental to indicate the type of the projectile, as different meteorite classes have different elemental ratios (Palme et al., 1981; Palme, 1982, Koeberl, 2007). The distribution of the osmium (Koeberl and Shirey, 1993: Lee et al., 2006) and chromium (Shukolyukov and Lugmair, 1998; Koeberl et al., 2007) isotopic systems is also useful for establishing the presence of a meteorite component in impact melt rocks and breccias.

The Rhenium-Osmium (Re-Os) isotopic system: The first successful application of the Re-Os method is attributed to the Bosumtwi impact structure in Ghana (Koeberl and Shirey, 1993). Generally, meteorites have osmium concentrations that are several orders of magnitude higher than in terrestrial crustal rocks. In meteorites, the abundance of rhenium is much lower than the osmium abundance, resulting in Re/Os ratios less than or equal to 0.1. On the other hand, the Re/Os ratio of terrestrial rocks is usually no less than 10, due to the higher concentration of Re and lower concentration of Os. The $^{187}Os/^{188}$ Os ratio increases rapidly with time in the older crustal rocks; in contrast, meteorites have low $^{187}Os/^{188}$ Os ratios. As osmium is much more abundant in meteorites, addition of meteorite material to terrestrial material will increase the osmium content and cause a decrease in the $^{187}Os/^{188}$ Os ratio.

Chromium isotope analysis: Chromium isotopes are not only used as a criterion for recognition of the extraterrestrial component in the impactites, but also provide information for determining meteorite type (Shukolyukov and Lugmair, 1998, Shukolyukov et al., 2000). The chromium isotope analysis is based on the determination of the relative abundances of ^{53}Cr, which is the daughter product of the extinct radionuclide ^{53}Mn. Terrestrial rocks do not show any variation in the $^{53}Cr/^{52}Cr$ ratio, because homogenisation of the Earth was completed long after all primordial ^{53}Mn had decayed. In contrast, some meteorite classes show a variable excess of ^{53}Cr relative to terrestrial samples. The range ($^{53}Cr/^{52}Cr$) for meteorites is about +0.1 to +1.3ε depending on meteorite type, except for carbonaceous chondrites which show an apparent deficit of about -0.4ε. These variations in Cr isotopic composition reflect heterogeneous ^{53}Mn distribution in the early solar system and early Mn/Cr fractionation in the solar nebula and in meteorite parent bodies (Shukolyukov and Lugmair, 1998). The negative ε value for carbonaceous chondrites is an artifact of using the $^{54}Cr/^{52}Cr$ ratio of the fractionation correction, because these meteorites carry a pre-solar ^{54}Cr component (Shukolyukov et al., 2000). The actual, un-normalised $^{53}Cr/^{52}Cr$ ratio is similar to that of other undifferentiated meteorites, and the apparent ^{53}Cr deficit in the carbonaceous ones is actually due to an excess of ^{54}Cr . The presence of ^{54}Cr excess in bulk carbonaceous chondrites allows them to be distinguished from other classes of meteorite (Shukolyukov et al., 2000).

1.7. Sedimentation in marine impact craters

Of the known terrestrial impact structures, roughly 15% are known to be formed in contemporary marine target sites, but only a very few (6) of these are now located in a marine environment (Dypvik et al., 2004; McCall, 2009; Dypvik and Kalleson, 2010). This limited number of recognised marine craters (considering ~70% of the Earth has been covered by sea water) is attributed to several reasons: a) role of plate tectonics: generation of oceanic crust and an eventual destruction by subduction, with resulting formation of basaltic, deep oceanic crust of relatively of young age (~200 million years), b) lack of finely detailed knowledge of the ocean floor topography, and c) lack of complete understanding of the morphology and physical characteristics of marine craters formed in a thinner, basaltic oceanic crust (Dypvik et al., 2004; McCall, 2009, Dypvik and Kalleson, 2010). Recent study shows an estimated number of occurrences of ~300 impact structures on seafloor targets over the last 3.0 billion years (Mcgall, 2009). Except for the late Pliocene Eltanin structure in the South Pacific Ocean, all of these marine craters are formed in shelf or epicontinental shallow seas (Dypvik et al., 2004). The sea water depth, during impact, within these marine craters varied roughly within a range of a few

tens of metres to a few hundreds of metres, with the exception of Eltanin where a water depth of a few thousand metres has been estimated (Dypvik and Jansa, 2003; Kyte, 2002).

Craters formed in shallow seas may have a bowl-shaped morphology, fairly comparable to the subaerial craters or concentric sombrero morphology, depending on the impactor size, water depth and target composition (Ormö and Lindström, 2000). Simple craters formed at a very shallow sea water depth target site with thin sedimentary cover on crystalline basement usually have elevated crater rims; initial sedimentation in such craters is fairly comparable to subaerial craters. Concentric sombrero morphology occurs in relatively larger, complex craters formed on a target site consisting of a thicker sedimentary cover on crystalline basement. Radial channels (resurge gullies) are formed in such craters due to erosive resurge currents.

Post-impact sedimentation in marine impact craters has been discussed by Ormö and Lindström (2000), Dypvik and Jansa (2003), Dypvik et al. (2004); while Dypvik and Kalleson (2010) endeavoured to group the crater-infilling sediments into three main sedimentation stages: 1) late-syn impact, ii) early post-impact, and iii) late post-impact, according to so-called 'crater modification' stages (Melosh, 1989). Dypvik and Kalleson (2010) referred their 'late syn-impact' stage of crater sedimentation to an early stage of crater modification where the crater-infilling processes are dominated by gravity-driven processes, e.g. slides, slumps, screes, rock avalanches or debris avalanches. The early post-impact stage of crater sedimentation is erosion dominated, representing relatively later stages of crater modification, where brim development, secondary slumping, faulting and resurge activities dominate. Water surges back into the crater at this stage generating powerful mass-flow processes, e.g. debris flows, density flows and turbidity flows operate to in-fill the crater. Eventually the crater becomes in-filled/inundated by sea water, leading to more fluid-flow activities. The late post-impact stage represents rather stable crater conditions that are mostly dominated by turbidity flows and suspension-deposition, and shows a gradual return to the original pre-impact conditions (Dypvik and Kalleson, 2010).

Ejecta distribution in marine craters differs from that of land-target craters. According to Melosh (1989) water vapour formed during impact will both accelerate and increase the ejecta formation and distribution over an area of larger radius than to that in their subaerial counterparts. Shuvalov and Dypvik (2004) argued that for a water depth comparable to or larger than the size of the impacting bolide, the expansion of the ejecta would be restricted by both the wall of the transient cavity as well as water surge. In such cases, no distal ejecta are expected to form. However, for impact into shallow seas, where the water depth is less than the diameter of the impacting bolide, they mentioned that the solid ejecta may have higher escape velocities

than in land-target impacts. This is due to the presence of volatile-rich (wet) sediments which are more prone to vaporisation and expansion. The ejected material moves further out from the crater as ground-hugging/base-surge debris flows (ballistic sedimentation) or may appear as more fluidised flow with the availability and incorporation of water within the ejecta curtain (Melosh, 1989). Fluidised ejecta distribution has been reported at Lonar crater in India, diverging from the ballistic model and ending in terminal rampart crater morphology (Schultz and Gault, 1979), suggesting that the ejected debris that were fluidized at the time of emplacement (Maloof et al., 2010).

CHAPTER 2

2. GEOLOGICAL SETTING

2.1. Regional geology

The Ritland structure is a recently recognised impact structure (Riis et al., 2011) located in the mountainous terrain of the Hjelmeland municipality, Rogaland, western Norway (Fig. 2.1A). A bolide of about 115 m diameter (Shuvalov et al., 2012) probably impacted during the Early to Middle Cambrian period on the sub-Cambrian peneplain, forming the Ritland crater. The sub-Cambrian peneplain, covering extensive areas of Scandinavia, represents a long hiatus between Pre-Cambrian high grade metamorphic and igneous rocks and the overlying Cambro-Silurian successions. The prolonged subaerial exposure of this peneplain surface probably gathered a number of asteroid impacts as illustrated by the formation of the Cambrian Ritland and Gardnos impact structures. The sub-Cambrian peneplain essentially consists of Precambrian granitic/gneissic rocks. Today, it is well exposed to the southeast of the crater, as remnants of a wide and slightly undulating weathered surface, where the Ritland crater forms a topographic depression of about 350 m below the peneplain (Fig. 2.1B). The occurrence of a few metres of marine shales overlying the peneplain in the southeastern part of the Ritland crater suggests a shallow marine setting at the time, part of the extensive early Cambrian epicontinental sea (Riis et al., 2011; Kalleson et al., 2012). The highly deformed and fractured granitic/gneissic basement rocks and the well exposed outcrop of crater-filling sediments (approximately 2.7 km in diameter) outline a nearly circular three dimensional crater depression (Figs. 2.1A & B). This was initially filled by impact generated coarser clastics and subsequently finer-grained sediments were deposited (Figs. 2.1A & 1B). The crater-filling successions were probably buried by several kilometres of Caledonian thrust nappes during the Mid-Silurian to Early Devonian period (Figs. 2.1A & B) (Gee et al., 2008). Succeeding tectonic episodes from the late Palaeozoic to Cenozoic and several glacial episodes in the Quaternary period helped exhumed the present day structure (Riis et al., 2011).

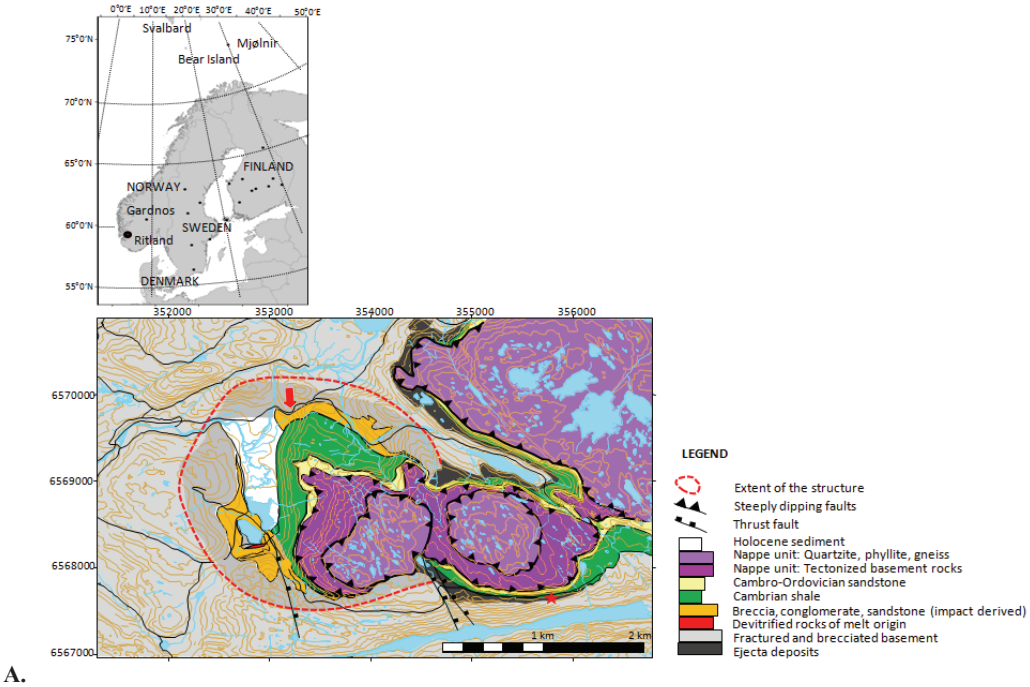

A.

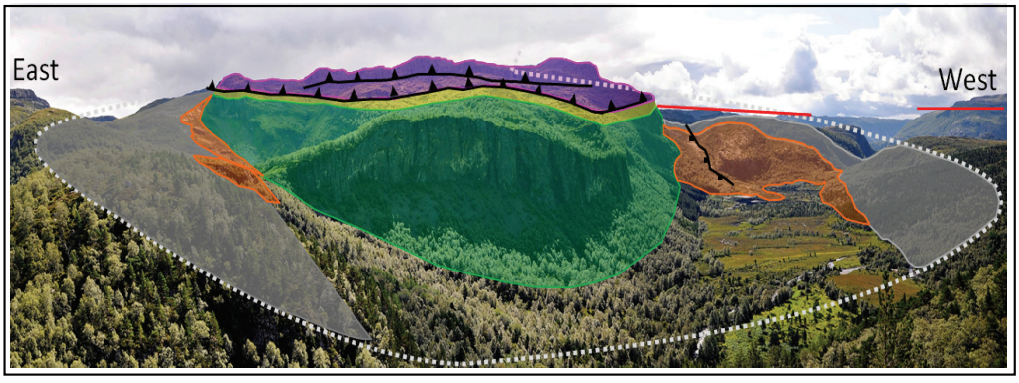

B.

Fig. 2.1. A. Geological map of the Ritland impact structure based on topographic map. The map shows a general outline of the crater-filling sediments and the major lithological units inside and outside the crater (slightly modified after Riis et al., 2011). The red hatched line illustrates the outline of the circular crater depression which is presented in detail in Fig. 2.2. The red star within the ejecta deposits shows the location where the shatter cones were found. B. View from the north (indicated by red arrow in Fig. A) into the Ritland impact structure. The impact derived coarser clastics, e.g. breccias, conglomerates and sandstones, are shown in orange, fine-grained marine clay in green, Cambro-Ordovician sandstone in yellow, thrust nappes in pink and the fractured and brecciated basement are shown in light grey. The solid red line in the in the background represents the reference level of the sub-Cambrian peneplain surface (Photo Courtesy: Knut Vindfallet).

2.2. The Ritland impact structure

The Ritland impact structure is recognised by its highly deformed and fractured basement rocks and the well exposed crater-filling succession distributed within a circular area of about 2.7 km diameter. In the central part, nearly 300 m thick, late post-impact, fine-grained Cambrian-Ordovician sediments are exposed in the depression below the sub-Cambrian peneplain (Figs. 2.1A & B, 2.2). The late syn-impact and early post-impact coarser clastics (Fig. 2.2) (deposited during the early stages of crater modification) are exposed along the crater wall showing fan-like geometries developing from the crater wall and extending towards the crater centre. The southwestern part of the crater wall (Svodne-Ritlandsfjellet area) reveals the most complete stratigraphic sequence of late syn-impact and early post-impact crater-infill (Fig. 2.2). More than 80 m of these sedimentary successions are exposed within this area (Azad et al., 2012). This is the only area where a ~2 m thick, devitrified rock succession of melt-origin has been found overlying the brecciated basement, illustrating the impact-origin of the Ritland structure (Fig. 2.2). The melt-fragments occur together with lithic clasts in a dominantly fine-grained clastic matrix (Riis et al., 2011). Planar deformation features (PDFs), mostly with two sets of crystallographic axes, have been identified in the quartz grains of the melt-bearing rocks (Fig. 2.3A) (Riis et al., 2011). The melt-bearing rock unit is overlain by impact generated breccias; subsequently conglomerates and sandstones were deposited during the early stages of the sedimentation (Fig. 2.2). Along the western margin (Stemhaugen area) much of the crater infill has been subjected to local rock slides and erosion (Fig. 2.2). In the northern margin (Bjødnabuhaugen area), at least 60 m of the upper part of the late syn-impact and early post-impact crater-infill are well exposed (Fig. 2.2). Sediments of the lower stratigraphic part are scarce in this area, and mostly covered with vegetation. The upper part of the early post-impact sediments is found in topographically higher areas in the northeastern crater margin (Bjødnabu and Dormålsknuten areas) (Fig. 2.2). In the Dormålsknuten area, these coarser clastics are found impinging in the dark grey to black marine shales and represent local screes that encroached onto unconsolidated marine clays (Azad et al., 2012 *submitted*). In addition to the well preserved crater-infills, the Ritland impact structure is unique for having a well-preserved and well-exposed ejecta layer in the northeastern and southeastern parts, ranging in distance from approximately 2 to 6 km from the crater centre (Kalleson et al., 2012). PDF features were observed in quartz grains from several localities within the ejecta layer. An assemblage of shatter cones consisting of pure calcite (Fig. 2.3B) was found in the Raudkleiv area located within 2 km of the crater margin (location marked with red star in Fig. 2.1A) (Kalleson et al., 2012).

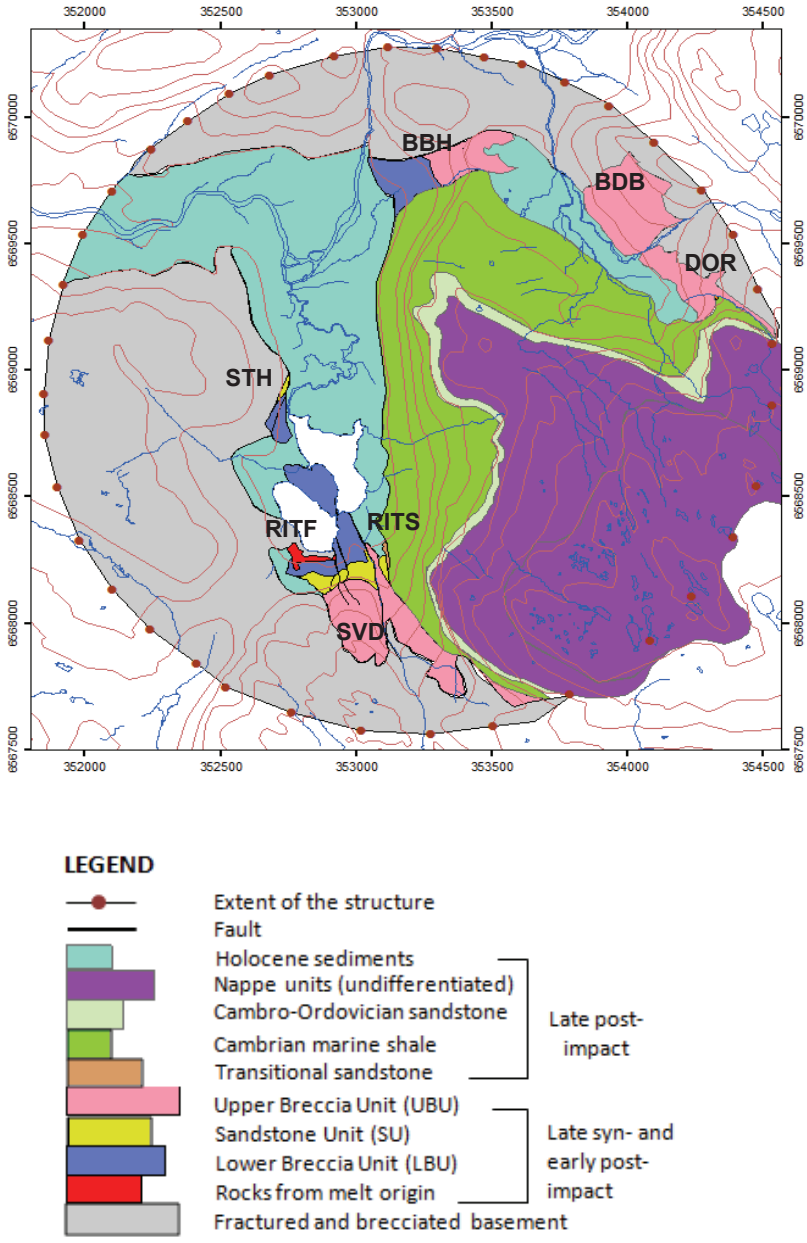

Fig. 2.2 Lithofacies map of the Ritland impact structure. The exposed sedimentary successions were logged in different areas of the crater wall. SVD-Svodene, RITF-Ritlandsfjellet, RITS-Ritlandstjønna, STH-Stemhaugen, BBH-Bjødnabuhaugen, BDB-Bjødnabu, and DOR-Dormålsknuten.

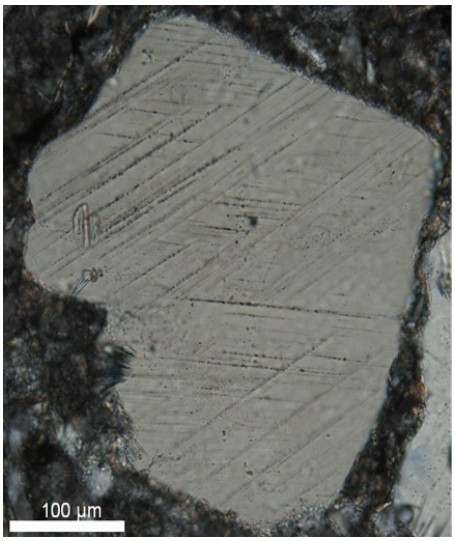

A.

B.

Fig. 2.3.A. Photomicrograph of one quartz grain from devitrified rocks of melt origin showing decorated planar deformation features (PDFs) (Photo courtesy: Elin Kalleson). B. Shatter cones found in the ejecta layer in Raudkleiv area (red star in Fig. 2.1A) (Photo Courtesy: Henning Dypvik).

2.3. Previous studies and identification of the structure

Previous geological studies in the Ritland area mostly focused on the well preserved Cambrian fossils in the 180 m thick shale unit exposed in the central part of the crater (Figs. 2.1A & B); the crater itself remained unrecognised for a long time. Bjørn Andersen first discovered the Cambrian fossils at the Ritland locality in 1949. Later Henningsmoen (1952) documented a trilobite fauna together with brachiopods, an orthoid, hyoliths, sponge spicules and various problematica within the shale unit, concluding that the fauna was of early Middle Cambrian age. Henningsmoen (1952) envisaged a shallow-water marine setting for the Ritland area. In the upper part of the shale unit a bed of limestone concretions containing an abundant inarticulate brachiopod fauna was correlated with the upper Middle Cambrian Andrarum Limestone of Southern Sweden (Bruton et al., 1989; Bruton and Harper, 2000). The presence of polymictic, immature breccias containing angular blocks of gneiss, (several metres across) below this Cambrian marine shale unit, was noted by Spjeldnæs (1985). He suggested that these rather immature, spectacular breccias could be associated with rifting and faulting in a tectonically active environment and probably were deposited from debris flows in alluvial fan settings.

Bruton and Harper (2000) studied a mid-Cambrian shelly fauna from the Ritland area and confirmed the shallow-water marine depositional conditions. Later, Knaust (2004) studied trace-fossils from the Cambro-Ordovician sandstones (upper part of the shale unit) (Figs. 2.1A & B) and suggested a late shallowing of the Cambrian sea with sand deposition in an offshore-shoreface area. An impact origin for the Ritland structure was first proposed by Riis (2001) while mapping the nappes and claiming an unusual thickness variation of the shale unit, about 120 m in the structure compared with a thin (20 m) veneer overlying the flat-lying nappe remnants in the adjacent areas. The topographic depression of about 350 m below the sub-Cambrian peneplain, with a concentric structure of about 3 km diameter, first suggested the idea of an impact crater. Detailed mapping of the exposed successions in the depression along with the intensely deformed and brecciated basement delineated the possible impact crater. Later, in 2007, the presence of melt-bearing rocks along with the planar deformation features (PDFs) in quartz grains confirmed its impact origin (Riis et al., 2008).

2.4. Present and further studies

'Ritland Project' was funded by the Norwegian Research Council (NFR), from July 2009 until July 2012. The work involved several field seasons and detailed laboratory analysis of the rock samples. The results have been presented to the scientific community and general public through several national and international seminars and conferences, local meetings, newspaper articles and TV programmes. The project aimed to answer several questions with regards to the processes and mechanisms of the Ritland crater formation and its modification and structural development through time, as well as the depositional mechanism and sedimentary environment of the crater infills. In particular, the project focused on the characterisation of the impact breccias and melt-bearing impactites and the distribution and mechanism of ejecta formation, as well as age dating of the impact events.

The first scientific paper outlining the general geology of the Ritland impact structure and a brief description of the impactites and crater-infilling sedimentary succession was published by Riis et al. (2011). The second paper on numerical modelling of the Ritland crater formation, discussing mechanisms and development of the crater formation (i.e. impact energy, bolide size, impact velocity, ejecta curtain distribution, target stratigraphy and rock-properties, physical processes during impact) was published by Shuvalov et al. (2012). Detailed study and characterisation of the impactites i.e. impact breccias and melt-bearing breccias, was carried out

and submitted to the Meteoritics and Planetary Science Journal (Kalleson et al., *submitted*). The present thesis consists of three scientific papers which include a detailed description of the crater-infill and discussion of related depositional mechanisms. The first paper describes the lower part of the stratigraphic successions i.e. late syn-impact and early post-impact sedimentary successions (Azad et al., 2012). The second paper discusses the upper stratigraphic column of the crater-infill (late post-impact) and has been submitted to the Norwegian Journal of Geology (Azad et al., 2012 *submitted*). The third paper aims at giving a general comparison of the Ritland crater infill to the crater-infilling succession of selected marine impact craters that had comparable geological settings (Azad and Dypvik, 2013 *submitted.*). A detailed description of the ejecta layers and the mechanism of the ejecta formation have also been studied and the manuscript is under preparation (Kalleson et al., *in prep.).* Apart from the scientific papers, two Masters' theses, one describing the crater-infills (Tomczyk, 2010) and the other describing the ejecta layers (Setså, 2011) were submitted to the Department of Geosciences, University of Oslo.

The current research can be extended to address some of the questions that remain unresolved:

- Age dating of the impact event; relatively fresh and well preserved impact breccias (although subjected to a certain degree of metamorphism due to Caledonian deep burial) may provide better estimation of the impact age.

- Detailed analysis of the deformation of the target surface i.e. sub-Cambrian peneplain caused by the impact; well exposed impact breccia in the crater floor and in steep rim areas can allow detail studies of the impact energy and stress distribution.

- Due to time constraints, the crater-infills of the Bjødnabu and Dormålsknuten area (Fig. 2.2) have not been studied in detail; a conclusive study on the stratigraphy of the crater-infills should be undertaken.

- A clear comparison between the Ritland and Gardnos impactites could also be done.

- Study of the well-preserved crater rim in the northeastern part outside the crater may also provide a better understanding of the mechanism of crystalline rim formation in simple impact craters.

CHAPTER 3

3. THE PAPERS

3.1 Theme of the thesis

The Ritland impact structure is probably one of the better preserved and exposed impact structures among the 183 recognised terrestrial impact structures (Earth Impact Data Base, http://www.passc.net/EarthImpactDatabase/). The outcrop of the crater-infilling sedimentary successions were observed along the crater wall and in the central part of the crater (Riis et al., 2011; Azad et al., 2012, Azad et al., 2013 *in print*) while ejecta deposits were clearly seen at several sites outside the crater depression (Setså, 2011; Kalleson et al., 2012). More than 80 m thick succession of late syn-impact and early post-impact coarse-grained sediments in the southwestern part of the crater wall, ~6 m early post-impact to late post-impact transitional sediments and ~180 m of fine-grained late post-impact sediments (Azad et al., 2012; Azad et al., 2013, *in print*) exposed in the central part of the crater area provides a good overview of complete crater-infill stratigraphy. The main theme of this research was to undertake a detailed sedimentological and mineralogical analysis of the crater-infilling successions, an interpretation of their depositional mechanisms, sedimentary environments and possible provenance analyses.

The late syn- and early post-impact crater-filling sediments include dramatic and unique episodes of high energy sedimentation in the crater depression, recording a cataclysmic event in the geological column. In the late post-impact stage the crater depression generally infills by common sedimentary processes (often low-energy sedimentation) and eventually become buried by prolonged sedimentation. Over geological periods a crater depression may be exhumed by later erosion or tectonics, partially or fully exposing the crater infill. Unfortunately only a very few of the recognised terrestrial impact structures are well exposed and well preserved. Thus impact structures like Ritland are particularly important as they may provide more information and improve our understanding of the catering mechanisms, depositional processes and environments. Such a crater can act as a basis for comparison to other craters with comparable geological settings. A comparative analysis of the Ritland crater-infilling succession with other impact craters of related geological setting was also a theme of this study.

The dissertation consists of three scientific papers: i) the first paper describes the late syn- and early-post impact crater sedimentation (lower stratigraphic level), ii) the second paper describes late post-impact crater sedimentation (upper stratigraphic level), and iii) the third

paper compares the Ritland crater-infilling succession with the crater infills of some selected marine impact structures of comparable geological setting.

3.2 Paper I

Azad, A. S., Dypvik, H., Tomczyk, M., Kalleson, E. & Riis, F. 2012: Late syn-impact and early post-impact sedimentation in the Ritland impact structure, western Norway. *Norwegian Journal of Geology, Vol. 92, pp. 405-431.*

Paper I presents a subdivision of the Ritland crater-infilling succession based on detailed field mapping and sedimentological investigations. An attempt is made to frame the suggested crater sedimentation stages (Dypvik and Kalleson, 2010) with crater modification stage (Melosh, 1989; Turtle et al., 2005). Synchronising these two stages is often difficult, but has significant importance for a better understanding of the crater modification processes, post-impact depositional mechanisms and sedimentary environments, as well as for systematic study of the crater infills. Three sedimentation stages were introduced aiming to understand the Ritland crater infills systematically: i) Late syn-impact, ii) early post-impact, and iii) late post-impact.

The late syn-impact and early post-impact sediments (Paper 1) were deposited during the initial stages of crater-modification, representing the lower part of the crater-infilling stratigraphy. These sediments were further classified into different sedimentary units and facies types. The Ritland crater was excavated in the crystalline basement rocks, probably during Early to Middle Cambrian time, by a 115 m diameter bolide impact (Riis et al., 2011). At the time of impact the basement is suggested to have been topped by a thin veneer of marine sediments beneath the epicontinental sea (Riis et al., 2011). The crater depression was surrounded by a well developed, elevated crystalline rim, where the rim wall was most likely exposed to the atmosphere. The crater depression acted almost like a close trap and the sediments were mostly derived from erosion of the crater wall and rim. Very coarse, angular to subangular, extremely clast-rich, matrix-poor impact-generated breccias along with reworked particles from melt origin initially filled the crater depression. These sediments were derived from the collapse of the transient cavity and deposited from rock avalanches, probably within a few seconds after the impact. The crater sedimentation at this stage (late syn-impact) was fairly similar to that of subaerial craters.

Mass flow processes, e.g. debris flows and density flows, were activated as soon as water surged back into the crater depression during the early post-impact stage. Clast-supported conglomerates, matrix-supported conglomerates and conglomeratic sandstones were deposited at this stage. Once the crater cavity was filled with water, fluid flow activities, e.g. turbidity-

flows, dominated, depositing sandstones in the crater cavity. The steep crater walls were unstable for a significant period of time, depositing coarser clastics along the crater wall derived from continued slope-failure and local erosion and deposited by scree, rock avalanches or debris avalanche processes. The crater cavity preserved all these infilling sediments and for a long time remained as a partially-filled depression beneath the sea. Through time as the crater cavity approached more stable conditions, fine-grained, suspension deposition dominated (late post-impact), eventually completely filling the crater cavity. The comparable clast and matrix mineralogical composition of the late syn-impact and early post-impact crater-infilling sediments to the local basement lithology (target site) suggests that these sediments were mostly derived from the impact-generated debris.

3.2 Paper 2

Azad, A. S., Dypvik, H., Riis, F. & Kalleson, E. 2013: Late post-impact sedimentation in the Ritland impact structure, western Norway. *In print, Norwegian Journal of Geology, Vol. 93, pp. 37-58.*

Paper 2 addresses the late post-impact sediments that represent the upper stratigraphical successions of the crater infill. These sediments are exposed in the central, southeastern and northeastern part of the crater and show onlapping relations to the upper part of the early post-impact sediments (exposed higher up in the northeastern crater wall). The late post-impact succession is relatively fine-grained, e.g. sandstones, silty shale and shale deposited during later stages in comparatively stable crater conditions. The base of this succession is marked by a few metres (~6 m) of fine- to medium-grained sandstones and alternating fine-grained sandstones and silty shales, representing a transition between the early post-impact and late-post impact crater sedimentation. The transitional fine- to medium-grained sandstones are texturally more mature and quartz-rich compared to the early post-impact sandstones (paper 1) and also contain traces of early Cambrian marine life. The upper part of the late post-impact succession consists of dark grey to black shales which attain a maximum thickness of about 180 m in the crater centre and thin towards the crater margin. The upper part of this shale unit is referred to as mid-Cambrian alum shale by Knaust (2004).

Suspension deposition dominated in the late post-impact stage of crater sedimentation with only minor episodes of turbidity flow deposition observed in the lower part of the succession. These turbidites were probably derived from later slope failure, base-slope erosion and further reworking of the crater infills. Through time, reduced rate of crater wall erosion and limited influx of extra-crater sediments eventually resulted in suspension deposition. The gradual upward transition of the late post-impact sediments into dark grey to black shales suggests that

anoxic to hypoxic bottom water conditions prevailed within the crater depression. This thick shale unit were probably deposited through an extensive (millions of years) period of suspension deposition. A few (3) clast-supported conglomerate beds (each ~1 m thick) were observed intercalated with black shales in the easternmost steep crater wall. The local occurrence of these clast-rich conglomerates within the black shales suggest that gravity slides and screes were occasionally active along the crater wall for a long time after impact, interrupting long quiet periods with clay deposition.

3.3 Paper 3

Azad, A. S. and Dypvik, H. 2013: Sedimentation in marine impact craters - Insight from the Ritland impact structure. *In review, Meteoritics and Planetary Science Journal.*

Paper 3 is intended to compare the crater-infilling succession of the Ritland impact structure with the crater infills of some selected marine impact structures, viz. Gardnos, Kärdla, Lockne and Chesapeake Bay, which had geological settings similar to Ritland. The aim of this study was to compare how the sedimentary processes vary in different craters in terms of the magnitude and order of occurrence at different stages of crater sedimentation. The study also aimed to look at how these sedimentary processes and the crater infills are quantitatively and qualitatively controlled by differences in crater size, target lithology and water depth during impact.

Different sedimentary processes (e.g. rock avalanches, slides and slumps; debris and density flows; turbidity and suspension deposition) dominating at the different stages of crater sedimentation (i.e. late syn-impact, early post-impact and late post-impact), occur in almost the same order in all the compared marine craters, irrespective of the crater size, target lithology and water depth. The common order of occurrence of these sedimentary processes resulted in comparable crater infills. The thickness (quantitative) and compositional variations (qualitative) of the deposits are, however, explained by differences in crater size, target lithology and water depth.

Sedimentary processes such as rock avalanches that occurred during the late syn-impact stage are commonly observed in the Ritland and Gardnos craters due to the close similarity of their target sites (crystalline target covered with thin veneer of marine sediments and a comparable water depth) and an absence of large-scale faulting and slumping of the crater wall in the Gardnos crater. Bolide impact into a thick, low-strength sedimentary cover at the target site with a water depth comparable or less than the impactor size resulted in large-scale collapses of the transient cavity and water-saturated rim layers in the case of Kärdla and Chesapeake Bay

craters. Repetitive events of rock avalanches, slumping and gravity slides were observed during the late syn-impact stage within these two craters. Impact into a deeper water target site at Lockne does not show clear-cut large-scale gravity-collapse of the transient seafloor cavity or rim wall; instead, powerful resurge processes from the collapse of the transient water cavity were seen to have occurred immediately.

Crystalline target sites with a thin cover of shallow marine sediments in the Ritland and Gardnos impacts resulted in well developed and elevated crater rim formation in much the same way as observed in subaerial craters. Well developed and elevated crater rim walls formed in these two craters probably acted as a barrier and reduced the instantaneous resurge energy. Comparable debris flow events observed in the Ritland and Gardnos craters during the early post-impact stage of crater sedimentation were of only limited extent. The thickness and compositional variations (clast-supported in Ritland, matrix-supported in Gardnos) of the debris flow deposits are explained by differences in crater size and impact energy. Impact into crystalline target sites with thicker sedimentary cover resulted in relatively weaker rim formation in the Kärdla crater and brim development in the Lockne and Chesapeake Bay craters, allowing instantaneous, powerful resurge of the debris-loaded water. Series of large-scale debris flow events were observed within these craters.

Turbidity flows are commonly observed at the waning stage of the resurge during early post-impact to the late post-impact stage of crater sedimentation. Thick resurge/back-surge turbidites were commonly observed in the Kärdla and Lockne craters. The Ritland and Gardnos turbidites may have partially derived from the delayed resurge through suspension-settling but could have been dominantly derived from later slope-failure, base-slope erosion and reworking of the impact-derived debris. The turbidites in the Chesapeake Bay crater may either have been derived from the back-surge, depositing through suspension-settling, or could have been derived from later slope-failure and reworking of the impact-generated sediments as seen in the Ritland and Gardnos cases. Suspension deposition dominates in all the compared craters at the late stages of crater sedimentation when the crater cavities attained a more stable condition.

REFERENCES

Alvarez L. W., Alvarez W., Asaro F. and Michel H. V. 1980. Extraterrestrial cause for the Cretaceous-Tertiary extinction: experiment results and theoretical interpretation. *Science* 208:1095-1108.

Atkinson H., Tickell C. and Williams D. 2000. Report of the Task Force on potentiality hazardous Near Earth Objects. *British National Space Centre, London*. www.neartheearthobject.co.uk *(Accessed on 12.10.2012).*

Azad A. S., Dypvik H., Tomczyk M., Kalleson E., and Riis F. 2012. Late syn-impact and early post-impact sedimentation in the Ritland impact structure, western Norway. *Norwegian Journal of Geology* 92(4):405-431.

Azad A. S., Dypvik H., Riis F., and Kalleson E. 2013. *In print*., Late post-impact sedimentation in the Ritland impact structure, western Norway. *Norwegian Journal of Geology 93(1):37-58*

Azad A. S. and Dypvik H. 2013. *In review,* Sedimentation in marine impact craters - Insight from the Ritland impact structure. *Meteoritics and Planetary Science Journal.*

Baratoux D. and Melosh H. J. 2003. The formation of shatter cones by shock waves interference during impacting. *Earth and Planetary Science Letters* 216:43-54.

Barringer D. M. 1905. Coon Mountain and its crater. *Proceedings of the Academy of Natural Sciences in Philadelphia* 57:861-886.

Barringer D. M. 1924. Further notes on Meteor Crater in northern central Arizona. *Proceedings of the Academy of Natural Sciences in Philadelphia* 76:275-278.

Bruton D. L., Harper D. A. T., and Repetski J. E. 1989. The stratigraphy and faunas of the Parautochthon and Lower Allochthon of southern Norway, In *The Caledonide geology of Scandinavia,* edited by Gayer R. A., Graham and Trotman, pp. 231-241.

Bruton D. L. and Harper D. A. T. 2000. A mid-Cambrian shelly fauna from Ritland, western Norway and its palaeogeographical implications. *Bulletin of the Geological Society of Denmark 47*:29-51.

Chao E. C. T., Soemaker E. M., and Madsen B. M., 1960. First natural occurrence of coesite. *Science* 132:220-222.

Chao E. C. T., Fahey J. J., Littler J., and Milton D. J. 1962. Stishovite SiO_2, a very high pressure new mineral from Meteor Crater, Arizona. *Journal of Geophysical Research* 67:419-421.

Claeys P., Kiessling W., and Alvarez W. 2002. Distribution of Chicxulub ejecta at the Cretaceous-Tertiary boundary. In *Catastrophic Events and Mass Extinction*, edited by Koeberl C. and MacLeod K.G., Boulder, Colorado: Geological Society of America Special Paper 356. pp. 55-68.

Dietz R. S. 1947. Meteorite impact suggested by the orientation of shatter-cones at the Kentland, Indiana disturbance. *Science* 105:42-43.

Dietz R. S. 1959. Shatter cones in cryptoexplosion structures (meteorite impact?). *Journal of Geology* 67:496-505.

Drake E. T. and Komar P. D. 1984. Origin of impact craters: Ideas and experiments of Hook, Gilbert, and Wegener. *Geology* 12:408-411.

Dressler B. O. 1990. Shock metamorphic features and their zoning and orientation in the Precambrian rocks of the Manicouagan Structure, Quebec, Canada. *Tectonophysics* 171:229-245.

Dressler B.O. and Sharpton V. L. 1997. Breccia formation at a complex impact crater: Slate Islands, Lake Superior, Ontario, Canada. *Tectonophysics* 275:285-311.

Dressler B. and Reimold W. U. 2004. Order or chaos? Origin and mode of emplacement of breccias in floors of large impact structures. *Earth Science Reviews* 97:1-54.

Dypvik H. and Jansa L. F. 2003. Sedimentary signatures and processes during marine bolide impacts: A review. *Sedimentary Geology* 161:309-337.

Dypvik H., Burchell M. J., and Claeys P. 2004. Impacts into marine and icy environments-A short review. In *Cratering in marine environment and on ice*, edited by Dypvik H., Burchell M. J, and Claeys P. New York: Springer-Verlag, pp. 1-20.

Dypvik H. and Kalleson E. 2010. Mechanisms of late synimpact to early postimpact crater sedimentation in marine-target impact structures. *Geological Society of America Special Papers* 465:301-318.

Earth impact database, http://www.unb.ca/passc/ImpactDatabase/ *(Accessed on 02.01.2013)*.

Engelhardt W. V. and Stöffler D. 1968. Stages of shock metamorphism in crystalline rocks of the Ries Basin, Germany. In *Shock Metamorphism of Natural Materials,* edited by French B. M. and Short, N. M. Baltimore, MD: Mono Book Corp., pp. 159-168.

Ferrière L. and Osinksi G. 2009. Characterization of shock-metamorphic effects in quartz from sandstones at the Houghton impact structure, Canada *(Abstract # 5377) Meteoritics and Planetary Science* 44:A68.

Ferrière L. and Osinksi G. 2010. Shatter cones and associated shock-induced micro-deformations in minerals -New investigations and implications for their formation. (*Abstract # 1392) 41st Lunar and Planetary Science Conference,* CD-ROM.

Ferrière L., Koeberl K., Libowitzky E., Reimold W. U., Greshake A., and Brandstätter F. 2010. Ballen quartz and cristobalite in impactites: New investigations. In *Large Meteorite Impacts and Planetary Evolution IV*, edited by Gibsen R. L. and Reimold W. U., Boulder, Colorado: The Geological Society of America Special Paper 465 pp. 609-618.

French B. M. 1968. Shock metamorphism as a geological process. In *Shock Metamorphism of Natural Materials* edited by French B. M. and Short N. M. Baltimore, MD: Mono Book Corp., pp. 1-17.

French B. M., Hartung J. B., Short N. M., and Dietz R. S. 1970. Tenoumer Crater, Mauritania: age and petrologic evidence for origin by meteorite impact. *Journal of Geophysical Research* 75:4396-4406.

French B. M. 1998. Traces of catastrophe: A handbook of shock-metamorphic effects in Terrestrial meteorite impact structures. *LPI Contribution No. 954, Houston, Lunar and Planetary Institute,* 120p.

French B. M. 2004. The importance of being cratered: The new role of meteorite impact as a normal geologic process. *Meteoritics & Planetary Science* 39(2):169-197.

French B. M. and Koeberl C. 2010. The convincing identification of terrestrial meteorite impact structures: What works, what doesn't and why. *Earth Science Reviews* 98:123-170.

Gault D. E., Quaide W. L., and Oberbeck V. R. 1968. Impact cratering mechanics and structures. In *Shock Metamorphism of Natural materials*, edited by French B.M. and Short N.M., Baltimore, MD: Mono book Corp., pp.87-99.

Gee D. G., Fossen H., Henriksen N., and Higgins A. K. 2008. From the early Palaeozoic platforms of Baltica and Laurentia to the Caledonide orogen of Scandinavia and Greenland. *Episodes* 31(1):44-51.

Gilbert G. K. 1893. The Moon's face: A study of the origin of its features (Presidential address delivered December 10, 1892). *Philosophical Society of Bulletin* 12:241-292.

Gilmour I. 1998. Geochemistry of carbon in terrestrial impact processes. In *Meteorites: Flux with time and impact effects* edited by Grady M. M., Hutchison R., McCall G. J. H., and Rothery D. A. *Special publications, Geological Society of London* 140, pp. 205-216.

Glass B. P., Lu S., and Leavens P. B. 2002. Reidite: an impact-produced high-pressure polymorph of zircon found in marine sediments. *American Mineralogist* 87:562-565.

Grieve R. A. F. 1987. Terrestrial Impact Structures. *Annual Review of Earth and Planetary Sciences* 15:245-270.

Grieve R. A. F. 1991. Terrestrial impact: the record in the rocks. *Meteoritics* 26:175-194.

Hannay J. B. 1892. Formation of lunar volcanoes. *Nature* 47:7-8.

Henningsmoen G. 1952. Early Middle Cambrian fauna from Rogaland, SW Norway. *Norsk Geologisk Tidsskrift 30*:13–31.

Hildebrand A. R., Penfield G. T., Kring D. A., Pilkington M., Camargo Z. A., Jacobsen S., and Boynton W. V. 1991. Chicxulub crater: a possible Cretaceous/Tertiary boundary impact crater on the Yucatán Peninsula, Mexico. *Geology* 339:345-360.

Hough R. M., Gilmour I., Pillinger C. T., Arden J. W., Gilkes K. W. R., Yuan J. and Milledge H. J. 1995. Diamond and silicon carbide in impact melt rock from the Ries impact crater. *Nature* 378:41-44.

Jackson J. C., Horton Jr. J. W., Chou I. M., and Belkin H. E. 2006. A shock-induced polymorph of anatase and rutile from the Chesapeake Bay impact structure, Virginia, U.S.A. *American Mineralogists* 91:604-608.

Kalleson E., Riis F., Setså R., and Dypvik, H. *in preparation.* Ejecta Distribution and Stratigraphy - Field evidence from the Ritland impact structure.

Kalleson E., Dypvik H., and Riis F. *Submitted*. The melt-bearing impactites in the Ritland structure. *Meteoritics & Planetary Science.*

Kalleson E., Riis F., Setså R., and Dypvik, H. 2012: Ejecta Distribution and Stratigraphy - Field Evidence from the Ritland Impact Structure. *(Abstract # 1351) 43rd Lunar and Planetary Science Conference,* CD-ROM.

Knaust D. 2004. Cambro-Ordovician trace fossils from the SW-Norwegian Caledonides. *Geological Journal* 39:1–24.

Koeberl C. and Shirey S. B. 1993. Detection of a meteorite component in Ivory Coast tektites with rhenium-osmium isotopes. *Science* 261:595-598.

Koeberl C. 1997. Impact cratering: The mineralogical and geochemical evidence. In *Ames Structure in Northwest Oklahoma and Similar Features: Origin and Petroleum Production,* edited by Johnson K. S., and Campbell J. A. (1995 Symposium). *Oklahoma: Geological Survey Circular* 100, pp. 30-54.

Koeberl C. 2002. Mineralogical and geochemical aspects of impact craters. *Mineralogical Magazine* 66(5):745-768.

Koeberl C. 2007. The geochemistry and cosmochemistry of impacts. In *Treatise of Geochemistry* edited by Davis A., New York: Elsevier, 1, pp. 1.28.1-1.28.52.

Kring D. 2007. Guidebook to the Geology of Barringer Meteorite Crater, Arizona. *Lunar and Planetary Science Contribution,* LPI contribution No. 1355, 139p.

Kyte F. T., Zhou Z., and Wasson J. T. 1981. High noble metal concentration in a late Pliocene sediment. *Nature* 292:417-420.

Kyte F. T. 2002. Unlimited meteoritic debris collected from Eltanin ejecta in *Polarstern* cores from expedition ANT XII/4. *Deep-Sea Research II* 49:1067-1071.

Lee S. R., Horton Jr. J. W., and Walker R. J. 2006. Confirmation of a meteorite component in impact-melt rocks of the Chesapeake-Bay impact structure, Virginia, USA – evidence from osmium isotopic and PGE systematic. *Meteoritics and Planetary Science* 41:819-833.

Maloof A. C., Sarah T. S., Benjamin P. W., Samuel A. S., Nicholas L. S., Karin L. L., Bethell I. G., and Poussart P. M. 2010. Geology of Lonar Crater, India. *Geological Society of America Bulletin* 122(1-2):109-126.

Martini J. E. J. 1991. The nature, distribution, and genesis of the coesite and stishovite associated with the pseudotachylite of the Vredefort Dome, South Africa. *Earth and Planetary Science Letters* 103:285-300.

Marvin U. B. 1999. Impacts from space: the implications for uniformitarian geology. *Geological Society of London Special Publications* 150:89-117.

McCall G. J. H. 2009. Half a century of progress on terrestrial impact structures: A review. *Earth Science Reviews* 92:99-116.

Melosh H. J. 1989. Impact cratering: a geological process. *New York, Oxford University Press, 245p.*

Melosh H. J. and Ivanov B. A. 1999. Impact crater collapse. *Annual Review of Earth Planetary Sciences* 27:385-415.

Mills A. A. 1969. Fluidization phenomena and possible implications for the origin of lunar craters. *Nature* 224:863-866.

Montanari A. and Koeberl C. 2000. Impact Stratigraphy: The Italian Record*. Lecture notes in Earth Sciences,* New York, Springer Verlag 93, pp.364.

O'Brien P. J., Zotov N., Law R., Khan M. A. and Jan M. Q. 2001. Coesite in Himalayan eclogite and implications for models of India-Asia collision. *Geology* 29:435-438.

Ormö J. and Lindström M. 2000: When a cosmic impact strikes the sea bed. *Geological Magazine* 137:67-80.

Palme H., Grieve R. A. F., and Reimold W. U. 1981. Identification of the projectile at the Brent crater, and further considerations of projectile types at terrestrial craters. *Geochimica et Cosmoschimica Acta* 45:2417-2424.

Palme H. 1982. Identification of projectiles of large terrestrial impact craters and some implications fro the interpretation of Ir-rich Cretaceous/Tertiary boundary layers. In *Geological Implications of Impacts of Large Asteroids and Comets on the Earth*, edited by Silver L. T. and Schultz P. H., Boulder, Colorado: Geological Society of America Special Paper 190, pp. 223-233.

Pati J. K and Reimold W. U. 2007. Impact cratering-fundamental process in geoscience and planetary science. *Journal of Earth System Science* 116:81-98.

Poelchau M. H. and Kenkmann T. 2009. Feather textures-a possible shock-feature in quartz, diagnostic of low shock pressures, *Meteoritics and Planetary Science* 44:A170.

Reimold W.U. 1998. Exogenic and endogenic breccias: A discussion of major problems. *Earth Science Reviews* 43: 25-47.

Reimold W. U. 2003. Impact cratering comes of age. *Science* 300:1888-1890.

Reimold W. U. and Koebrel C. 2008. Catastrophes, extinctions and evolution: 50 years of impact cratering studies. *Golden Jubilee Memoir of the Geological Society of India* 66: 69-110.

Riis F. 2001. En kraterstruktur i det subkambriske peneplanet ved Ritland, Ryfylke—sannsynligvis dannet ved meteorittnedslag. *(Abstract) Geonytt: Medlemsblad for Norsk Geologisk Forening*: 94.

Riis F., Dypvik H., and Krøgli S. O. 2008. The Ritland Crater - An early Cambrian impact structure in West Norway (Abstract # PIS-01805L). *International Geological Congress, Oslo* Norway *(published online at http://www.cprm.gov.br/33IGC/1338980.html).*

Riis F., Kalleson E., Dypvik H., Krøgli S.O., and Nilsen O. 2011. The Ritland impact structure, southwestern Norway. *Meteoritics and Planetary Science 46*:748-761.

Rozet (M. Le capitaine) 1846. Mémoire sur la selénologie: *Comptes Rendus* 22: 470-473.

Sagy A., Fineberg J., and Reches Z. 2004. Shatter cones: Branched, rapid fractures formed by shock impact. *Journal of Geophysical Research* 109, B10:20p.

Schultz P. H. and Gault D. E. 1979. Atmospheric effects on Martian ejecta emplacement. *Journal of Geophysical Research* 84:7669-87.

Setså R. 2011. The Ritland impact structure: Characteristics and distribution of the ejecta layer and associated Lower Paleozoic sedimentary succession, *M.Sc. Thesis, University of Oslo, Norway,* 111p.

Shand S. J. 1916. The pseudotachylyte of Parijis (Orange Free State) and its relation to 'trapshotten gneiss' and 'finty crushrock'. *Quarterly Journal of the Geological Society of London* 72:198-221.

Sharpton V. L., Dalrymple G. B., Marin L. E., Ryder G., Schuraytz, B. C., and Urrutia Fucugauchi J. 1992. New links between the Chicxulub impact structure and the Cretaceous/Tertiary boundary. *Nature* 359:819-821.

Shoemaker E. M. 1960. Penetration mechanics of high velocity meteorites, illustrated by Meteor crater, Arizona, *21st International Geological Congress, Copenhagen*, pp. 418-434.

Shukolyukov A. and Lugmair G. W. 1998. Isotopic evidence for the Cretaceous-Tertiary impactor and its type. *Science* 282:927-929.

Shukolyukov A., Kyte F. T., Lugamir G. W., Lowe, D. R. and Byerly G. R. 2000. The oldest impact deposits on Earth –First confirmation of an extraterrestrial component. In *Impact and the early Earth*, edited by Gilmour, I. and Koeberl C., *Lecture notes in Earth Sciences 91,* Berlin-Heidelberg: Springer, Verlag, pp. 99-116.

Shuvalov V. and Dypvik H. 2004. Ejecta formation and crater development of the Mjølnir impact. Meteoritic and Planetary Science 39(3):467-479.

Shuvalov V., Dypvik H., Kalleson E., and Setså, R. 2012. Modelling the 2.7 km, shallow marine Ritland impact structure. *Earth Moon Planets* 108:175-188.

Snoke A. W., Tullis J., Todd V. R. (Eds.) 1998. Fault-related rocks: A photographic Atlas. New Jersey, Princeton, Princeton University Press, 617p.

Spary J. G. and Thompson L. M. 1995. Friction melt distribution in a multi-ring impact basin. *Nature* 373:130-132.

Spjeldnæs N. 1985: Biostratigraphy of the Scandinavian Caledonides. In *The Caledonide Orogen-Scandinavia and Related Areas,* Part 1, edited by Gee D.G. and Sturt B. A. Chichester, Wiley, pp. 317–329.

Spray J. G. 1997. Superfaults. *Geology* 25:579-582.

Spray J. G. 1998. Localized shock- and friction-induced melting in response to hypervelocity impact. In *Meteorites: Flux with time and Impact Effects* edited by Gardy M. M., Hutchison R., McCall G. J. H., and Rothery D., *Geological Society of London Special publications* 140, pp.195-204.

Spudis P. D. 1993. The geology of multi-ring impact basins: The moon and other planets. *New York*, *Cambridge University Press,* 263p.

St. Clair Humphreys A. 1891. A hypothesis of lunar formation. *British Astronomical Association Journal* 3:132-136.

Stöffler D. and Langenhorst F. 1994. Shock metamorphism of quartz in nature and experiment: Basic observation and theory. *Meteoritics* 29:155-181.

Stöffler D. and Grieve R. 2007. Impactites, In *Metamorphic Rocks-A classification and Glossary Terms,* edited by Fettes D. and Desmond J., *Cambridge: Cambridge University Press*, 243p.

Tilghman B. C. 1905. Coon Butte, Arizona. *Proceedings of the Academy of Natural Sciences in Philadelphia* 57: 887-914.

Tomczyk M. 2010. Post-impact sedimentation in the Ritland impact structure, South-western Norway, *M.Sc. Thesis, University of Oslo, Norway,* 92p.

Turtle E. P., Pierazzo E., Collins G. S., Osinski G. R., Melosh H. J., Morgan J. V., and Reimold W. U. 2005. Impact structures: What does crater diameter mean? In *Large Meteorite Impacts III,* edited by Kenkmann T., Hörz F. and Deutsch A. Boulder, Colorado: *Geological Society of America Special Paper 384*, pp.1–24.

Wegener A. L. 1921. Die Entstehung der Mondkrater: Braunschweig, Druck und Verlag von Freiedrich Vieweg und Sohns, In *the origin of lunar craters:* (Translated by A.M. Célal Sengör, 1975), *The Moon* 14: 211-236.

Papers

Paper 1

Late syn-impact and early post-impact sedimentation in the Ritland impact structure, western Norway.

By

Azad, A. S., Dypvik, H., Tomczyk, M., Kalleson, E. & Riis, F.

Norwegian Journal of Geology, 2012, *Vol. 92, p. 405-431.*

Late syn-impact and early post-impact sedimentation in the Ritland impact structure, western Norway

Abdus Samad Azad, Henning Dypvik, Michal Tomczyk, Elin Kalleson & Fridtjof Riis

Azad, A.S., Dypvik, H., Tomczyk, M., Kalleson, E. & Riis, F.: Late syn-impact and early post-impact sedimentation in the Ritland impact structure, western Norway. *Norwegian Journal of Geology,* vol. 92., pp 405-431, Trondheim 2012. ISSN 029-196X.

The 2.7 km in diameter, Ritland impact structure was excavated probably during Early to Mid Cambrian time in the gneissic sub-Cambrian peneplain. Based on field mapping and sedimentological study the crater infills are broadly classified as: A) late syn-impact, B) early post-impact and C) late post-impact sediments. Units A) and B) are subdivided into: i) Lower Breccia Unit (LBU), ii) Sandstone Unit (SU) and iii) Upper Breccia Unit (UBU). The lowermost sediments of the LBU contain dispersed particles of melt origin, suggesting a late syn-impact origin, probably related to rock avalanches. Debris-flow events took place during the early post-impact phase. Shift from clast-supported to matrix-supported texture in the upper part of the LBU represents flow transformation from cohesive to hyperconcentrated density flows, probably due to a result of resurge of seawater. The SU overlying the LBU represents suspension-dominated sedimentation after the crater was filled with water. The UBU represents sedimentation in the marginal part of the crater basin. Scree, rock-avalanche or debris-avalanche processes dominated in this sequence.

Abdus S. Azad, Henning Dypvik & Elin Kalleson, Department of Geosciences, University of Oslo, P.O. Box 1047 Blindern, 0316 Oslo, Norway Michal Tomczyk, Department of Geosciences, University of Bremen, P.O. Box 330440, 28334, Bremen, Germany. Fridtjof Riis, Norwegian Petroleum Directorate, P.O. Box 600, 4003 Stavanger, Norway.

E-mail corresponding author (Abdus S. Azad): m.a.s.azad@geo.uio.no

Introduction

Among 19 impact structures so far documented in Fennoscandia (Dypvik et al., 2008), two were previously recognised in Norway: Gardnos (Dons & Naterstad, 1992; French et al., 1997; Kalleson et al., 2009, 2010) and Mjølnir (Gudlaugsson, 1993; Dypvik et al., 1996). Ritland is the third and most recently recognised impact structure, located in the Hjelmeland municipality, Rogaland, western Norway (Fig. 1A). Presently, the structure shows a nearly circular depression excavated in Precambrian gneisses. The highly deformed and fractured basement and the exposed crater-filling sediments outline a simple impact structure (Riis et al., 2011).

Earlier geological studies in the Ritland area mostly focused on the well preserved Cambrian fossils. Bjørn Anderson first discovered the Cambrian fossils from the Ritland locality in 1949, and they were later described by Henningsmoen (1952). Sigmond (1978) produced the first regional geological map of the area. The presence of polymictic, immature breccias with gneissic blocks in the Ritland area was suggested to be related to rifting or faulting (Spjeldnæs, 1985). Bruton & Harper (2000) studied a Middle Cambrian shelly fauna from the Ritland area and explained its implications for the shallow-water marine setting of this locality. Later, Knaust (2004) studied trace fossils from the Cambro–Ordovician sediments of the Ritland area and commented on their depositional environment. An impact origin for the Ritland structure was first proposed by Riis (2001) based on geological mapping of the circular structure and deformed basement. Later, in 2007, the presence of impact-melt rocks and quartz grains with shock-metamorphic features confirmed its impact origin (Riis et al., 2008).

The present study focuses on the distribution, texture, mineralogical composition, structure and geometry of the crater-filling sediments, aiming to infer the depositional processes and to deduce a relevant crater-filling history. In this study, the crater-filling sediments are grouped into three broad units: A) late syn-impact sediments, B) early post-impact sediments and C) late post-impact sediments. The 'late syn-impact' sediments (Dypvik & Kalleson, 2010) refer to the start of the crater modification stage (Melosh, 1989) and were deposited upon collapse of the transient cavity and slumping back into the crater. The time required for the deposition of the late syn-impact sediments was probably less than a minute for a simple impact structure like Ritland (Shuvalov et al., 2012). Early post-impact sediments (Dypvik & Kalleson, 2010) were derived from erosion of the cavity walls and rims and deposited

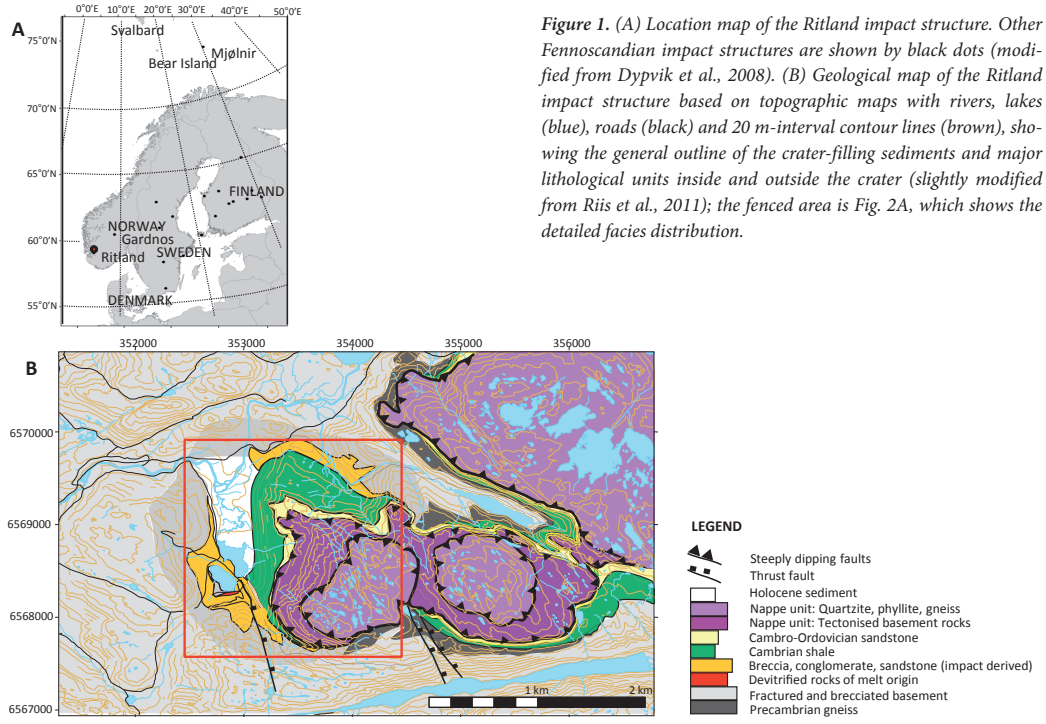

Figure 1. *(A) Location map of the Ritland impact structure. Other Fennoscandian impact structures are shown by black dots (modified from Dypvik et al., 2008). (B) Geological map of the Ritland impact structure based on topographic maps with rivers, lakes (blue), roads (black) and 20 m-interval contour lines (brown), showing the general outline of the crater-filling sediments and major lithological units inside and outside the crater (slightly modified from Riis et al., 2011); the fenced area is Fig. 2A, which shows the detailed facies distribution.*

by gravity-controlled processes at early stages of crater modification, which began minutes after the impact. These successions are more erosion dominated and were deposited under water-saturated conditions (Dypvik & Kalleson, 2010). The late post-impact successions filled the crater in the late stages of crater sedimentation and represent part of a widespread regional succession. Only the late syn-impact (A) and early post-impact (B) sediments are discussed in this paper.

Regional geology

The granitic/gneissic sub-Cambrian peneplain, overlain by a thin, marine, Cambrian sedimentary cover, was the target surface for the Ritland impact (Riis et al., 2011). The peneplain represents a long hiatus between the Precambrian basement and deposition of the overlying Cambro–Silurian successions. The timing of crater formation is assumed to be Early to Mid Cambrian (Riis et al., 2011).

Lower Cambrian strata are found on the peneplain surface at several places in southern and western Norway (e.g., Hardangervidda, Mjøsa) (Martinsson, 1974; Nielsen & Schovsbo, 2011). A thin (1–3 m) sequence of conglomerate, shaly sandstone and limestone resting on the basement and overlain by phyllitised alum shales in the northern part of Rogaland has been described by Goldschmidt (1925). This basal conglomerate has been interpreted as reworked, weathered basement deposited during the early stages of a marine transgression (Andresen, 1982). Outside the Ritland crater, a thin layer (<30 cm) of basal conglomerate has been found consisting of quartz, feldspar and gneissic clasts in a sandy-silty matrix, covered by a *c.* 10 m-thick silty-shale layer (Setså, 2011). These sediments were probably deposited before the impact, as evidenced by their stratigraphical position and the presence of a possible overlying ejecta layer (Setså, 2011). The Middle Cambrian successions across Baltoscandia are characterised by 'Alum Shale' (Bergström & Gee, 1985; Nielsen & Schovsbo, 2007). The great areal extent indicates deposition on a stable, shallow-marine, epicontinental sea platform (Bruton et al., 2010). Deeper water conditions of the epicontinental sea prevailed in the western parts of Oslo (Bruton et al., 2010) whilst a shallow-water facies belt has been identified in Sweden and western Norway (Bruton & Harper, 2000). Hallam (1981) suggested a water depth of <200 m for this epicontinental sea.

When the bolide impacted, Ritland was probably part

of an epicontinental shallow-marine setting. Middle Cambrian fossils (Bruton & Harper, 2000) found in the upper part of the thick marine shales within the crater suggest that the crater was completely submerged during that time (Riis et al., 2011). A regionally developed sandstone unit caps the Cambrian shale across the crater margin, representing a later shallowing of the Cambrian sea (Riis et al., 2011). The Caledonian Orogeny led to the extensive formation of thrust sheets (Bergström & Gee, 1985) associated with transport towards the east and southeast with emplacement above the crater-filling sediments (Fig. 1B).

Impact geological setting

At Ritland, a *c.* 300 m-thick succession of Cambro–Ordovician sedimentary rocks is found at a level below the sub-Cambrian peneplain, indicating the presence of a topographic crater depression 2.7 km in diameter (Riis et al., 2011). The approximate crater depth is considered to be 350 m (Riis et al., 2011). According to the scaling laws of Melosh (1989) and numerical simulation (Shuvalov et al., 2012), the diameter of the projectile responsible for the Ritland crater is estimated to be 115 m. The transient cavity and depth can be calculated as 2.2 km and 776 m, respectively, while the crater-rim height and the apparent crater depth can be calculated as 110 m and 550 m, respectively (Earth Impact Effects Program, http://impact.ese.ic.ac.uk).

Materials and methods

Detailed field investigations were carried out in order to map the sedimentary successions exposed at Ritlandsfjellet, Ritlandstjønna, Svodene, Bjødnabuhaugen and the Stemhaugen area (Fig. 2A). Sedimentological logs (Figs. 3, 5, 10 and 11) were prepared for all of these sections in order to understand the facies distribution. A geological profile from the hypothetical crater centre to the Svodene–Ritlandsfjellet area was constructed to define the stratigraphical relations of the sediments to the crater wall and rim (Fig. 2B). Three sedimentary logs (RITF–1, RITF–3 and RITF–4) were constructed within close vicinity to the Svodene–Ritlandsfjellet area to obtain a three-dimensional impression of the crater-filling sediments at the crater's southwestern margin (Fig. 3).

Detailed clast counts (sub)parallel to the bedding planes of the breccia and conglomerates were carried out for textural and compositional analysis. Twenty square grids (0.5 m x 0.5 m) for the lower stratigraphical part and thirty square grids (1.0 m x 1.0 m) for the upper stratigraphical part were selected where clast composition, size and shape were documented (Fig. 6). The average size of the ten biggest clasts within each bed divided by bed thickness has been used as a proxy for studying the competence vs. flow thickness throughout the logged sections (Figs. 5, 10 and 11).

At the Bjødnabuhaugen section, a comprehensive log of the crater-filling sediments was constructed covering the northern margin of the crater wall (Figs. 2A and 10). A log of the Stemhaugen area (Figs. 2A and 11) shows crater-filling sediments at the western margin of the crater wall. The relative proportions of matrix and clasts were estimated in the field and documented in the sedimentary logs.

The matrix-clast proportions and the matrix compositions also were studied in thin-sections. A total of 106 thin-sections have been examined under optical and scanning electron microscopes. Modal compositions (400 grain counts) were determined for 27 of these thin-sections (Table 1). Semiquantitative determination of mineralogical composition for 40 bulk samples was based on peak heights (Morris et al., 2008) of data from XRD (X-ray diffraction) analysis, using a Philips X'Pert MPD, at the University of Oslo. The results are presented in Table 2. Quartz, K-feldspar, plagioclase, calcite, dolomite, mica and chlorite were quantified with respective peak values of (d = 4.26 Å), (d = 3.24 Å, 3.25 Å), (d = 3.18 Å, 3.19 Å), (d = 3.03 Å), (d = 2.89 Å), (d = 10 Å) and (d = 7 Å). The Wentworth (1922) scale was used for grain-size classification. Folk's (1974) classification scheme was used for identification of breccia, conglomerate, conglomeratic sandstone, sandstone, etc.

Field observations

The late syn- and early post-impact sediments in the Ritland impact structure have been described from three different depositional areas showing individual fan-like distributions developed from different parts of the crater wall. The three different depositional areas are: 1) Svodene–Ritlandsfjellet, 2) Bjødnabuhaugen and 3) Stemhaugen (Fig. 2A). Of these three, the crater-filling sediments are particularly well exposed at the southwestern margin of the crater at Svodene–Ritlandsfjellet (Fig. 2A). The base of the late syn-impact sediments and the top of the early post-impact sediments has been found only in this area (Fig. 2A). An informal lithostratigraphical unit 'Svodene' has been proposed for describing these crater-filling sediments (Riis et al., 2011). At Bjødnabuhaugen, along the northern margin of the crater, the upper stratigraphical column is well exposed (Fig. 2A), whereas the sediments of the lower stratigraphical column are more scarce. Along the western margin at Stemhaugen, much of the late syn- and early post-impact sediments have been subjected to local rock slides and erosion (Fig. 2A). In the east and towards the centre, late post-impact fine-grained sediments are exposed, whereas impactites in the central part of the crater are covered by Holocene sediments (Fig. 2A).

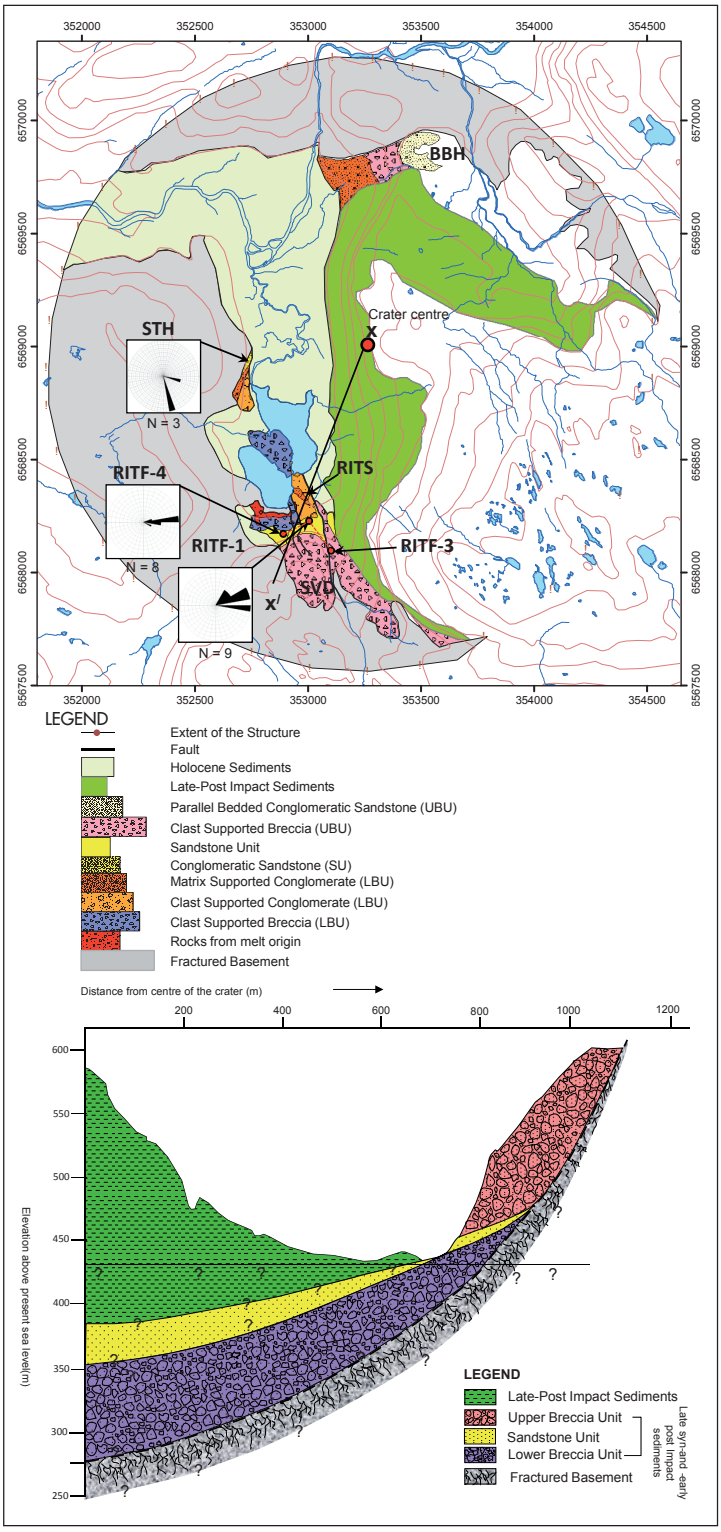

Figure 2. (A) Facies-distribution map of the Ritland impact structure, with rose diagrams showing the flow directional measurements (strikes) of different sedimentary structures logged in the RITF–Ritlandsfjellet and STH–Stemhaugen sections. The other locations on the map are RITS–Ritlandstjønna, SVD–Svodene and BBH–Bjødnabuhaugen. Sedimentary units, LBU–Lower Breccia Unit, UBU–Upper Breccia Unit, SU–Sandstone Unit. Cross section along X– X' is shown in Fig. 2B and a stratigraphical profile (red, dotted line) of the SVD–RITF section is shown in Fig. 3. (B) Geological cross-section (X– X' in Fig. 2A) illustrating the stratigraphical relationship of the major sedimentary units from the crater centre towards the Svodene–Ritlandsfjellet area. The base of the crater and the subsurface distribution of the different sedimentary units have been drawn conceptually.

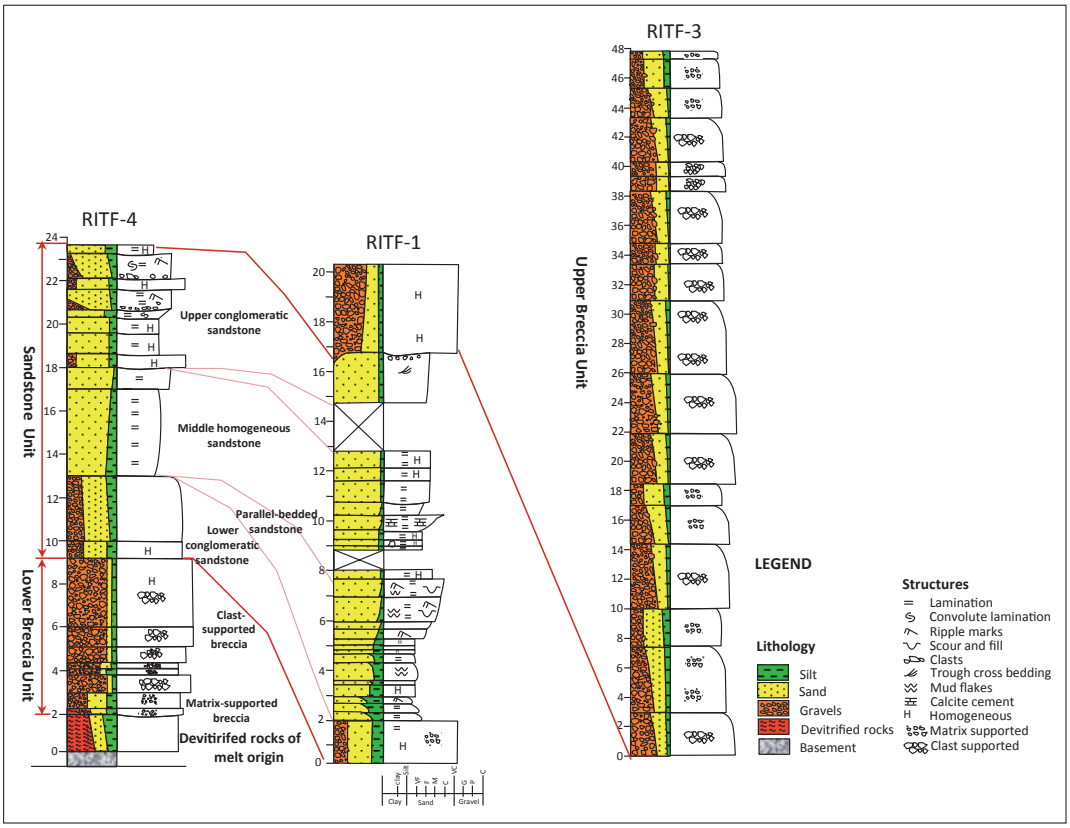

Figure 3. Generalised stratigraphy of the late syn-impact and early post-impact sediments based on the exposed successions of the southwestern crater wall, Svodene–Ritlandsfjellet area (modified from Tomczyk, 2010). Geographical positions of the RITF logged sections can be seen in Fig. 2A.

Svodene–Ritlandsfjellet area

The sedimentary succession of the Svodene–Ritlandsfjellet area is composed of three general stratigraphical units: i) Lower Breccia Unit, ii) Sandstone Unit and iii) Upper Breccia Unit (Fig. 3). The minor (~2 m thick), dark, devitrified rock succession of melt origin present at the lowermost stratigraphical position (overlying brecciated basement) (Figs. 2A and 3) is not discussed in this paper as it will be presented in Kalleson et al. (submitted).

Lower Breccia Unit (LBU)

The total thickness of the Lower Breccia Unit (LBU) at Svodene–Ritlandsfjellet is approximately 11 m, with the lower 7 m exposed in the Ritlandsfjellet area (Figs. 2A, 3 and 4), whilst the upper 4 m is exposed in the Ritlandstjønna area (Figs. 2A and 5). At Ritlandsfjellet, the LBU overlies a thin rock succession of melt origin (Figs. 2A, 3 and 4). The contact between the rock succession of melt origin and overlying LBU is rather diffuse. In most cases the breccias containing particles of melt origin interfinger both laterally and vertically with clastic breccias (Fig. 4). The LBU consists mainly of breccias referable to four major facies: i) matrix-supported breccia, ii) clast-supported breccia, iii) clast-supported conglomerate and iv) matrix-supported conglomerate (Figs. 3, 4 and 5).

Matrix-supported breccia: In the Ritlandsfjellet area (log RITF–4 in Fig. 3), the lowermost part of the LBU is marked by two breccia beds showing a matrix-supported texture (Fig. 4). These beds consist of angular, granitic/gneissic clasts 2–3 cm in size in a dark-grey to blackish sandy matrix. The lowermost bed contains brownish, centimetre-size, elongate, reworked particles of melt origin (Fig. 4) and displays a slightly erosional contact to the underlying devitrified rock succession of melt origin (Kalleson et al., submitted) and a gradational contact to the overlying beds. The particles of melt origin (0–20%) vary both laterally and vertically. The uppermost bed is dominated by lithic clasts with only sporadic particles of melt origin.

Table 1: Modal composition (thin-section study) of the different facies from three sedimentary units from different depositional areas (400 grains were counted in each slide to determine the percentages). Quartz/feldspar ratio of the individual samples and their average (representing individual facies) from Svodene–Ritlandsfjellet, Stemhaugen and Bjødnabuhaugen are shown in two different columns. Graphical presentations of these average values are shown in Figs. 12 and 13. (FUP–fining-upward sequence, CUP–coarsening-upward sequence, LCS–low-angle cross-stratified sandstone, UHS–upper homogeneous sandstone bed, UCS–upper conglomeratic sandstones, UHS–upper homogeneous sandstone).

Sedimentary unit	Depositional area	Facies	Sample no.	Quartz	Feldspar	Qtz/Felds	Average Qtz/Felds	Carbon-ates	Chlorite	Mica	Matrix	Rock fragments	Heavy minerals	Siderite	Amphi-bole	Sericite
Upper Breccia Unit	Bjødnabu-haugen	Matrix-supported breccia/ conglomerate	BBH_01_16	26	16	1.63	1.15	38	0	4	0	1	0	0	0	15
			BB_01_14	23	34	0.68		2.5	3	5.5	0	30	trace	1.5	0	0
		Clast-support. breccia	BBH_01_10	13	51	0.25	0.25	0	0	12	9	8	1	4	0	2
	Svodene–Ritlandsfjellet	Matrix-supported breccia/ conglomerate	RITF_3_6_09	13	16	0.81	0.76	0	3	19	32	12	0	0	5	0
			RITF_3_3_09	14	20	0.70		19	0	11	16	14	1	0	0	4
		Clast-support. breccia	RITF_3_2_09	16	40	0.40	0.40	0	18	10	9	6	1	0	0	0
Sandstone Unit	Stemhaugen	Conglomeratic sandstone	STH_04_06_09	12	24	0.50	0.59	0	4	12	24	19	1	1	0	3
			STH_04_05_09	15	21	0.71		0	6	7	40	5	0	0	1	5
			STH_04_04_09	14	26	0.54		trace	5	3	42	8	trace	0	1	0
			STH_04_03_09	14	23	0.61		0	6	4	43	6	1	2	0	1
	Svodene–Ritlandsfjellet	Upper cong. sst (UHS)	RITF_4_8_09	22	37	0.59	0.55	12	2	8	8	10	0	0	0	1
		Upper cong. sst (UCS)	RITF_4_7_09	14	28	0.50		0	0	8	6	43	0	0	0	1
		Middle homo. sandstone	RITF_1_5_09	25	52	0.48	0.66	0	12	5	0	5	1	0	0	0
		Middle homo. sst. (LCS)	RITF_1_4_09	26	31	0.84		29	0	10	0	0	0	0	0	4
		Parallel-bedded sst. (CUP)	RITF_1_6_09	29	31	0.94	0.94	0	6	8	17	7	2	0	0	0
		Parallel-bedded sst (FUP)	RITF_1_2_09	31	26	1.19	1.35	0	3.5	7.5	30	1	1	0	0	0
			RITF_1_1_09	27	18	1.50		0	6	18	28	1	1	1	0	0
		Lower cong. sandstone	RITF_4_5_09	19	25	0.76	0.76	0	8	6	34	5	0	0	1	2
Lower Breccia Unit	Stemhaugen	Matrix-supported conglomerate	STH_04_02_09	15	26	0.58	0.58	1	4.5	3	45	0	trace	0	2	3
		Clast-supported conglomerate	STH_03_04_09	11	31	0.35	0.47	6	7	4	22	18	0	0	0	1
			STH_01_05_09	15	26	0.58		0	14	2	22	20	1	0	0	0
	Svodene–Ritlandsfjellet	Matrix-supported conglomerate	SVDL_04_03_10	15	34	0.44	0.40	1	3	8.5	17	10	trace	1.5	trace	9
			SVDL_04_02_10	15	38	0.39		15	1	8	7	7	0	0	0	10
			SVDL_04_01_10	15	40	0.38		0	2	8	11	13	1	1	1	8
		Clast-supported conglomerate	SVDL_02_05_10	14	25	0.63	0.64	0	1	8	14	19	0	1	4	14
			SVDL_02_03_10	13	20	0.65		13	1	11	20	9	0	0	5	8
		Clast-support. breccia	RITF_4_1_09	8	16	0.50	0.50	8	1	1	16	44	1	0	5	0

Table 2: Mineralogical composition of the different facies from three sedimentary units from different depositional areas and from the basement obtained from XRD analysis (semi-quantative). Quartz/feldspar ratios of the individual samples and their average (individual facies) are shown in two different columns. Graphical presentation of these average values is shown in Fig. 13. Trace of some minerals studied from SEM/XRD has been added to the column farthest to the right.

Sedimentary unit	Depositional area	Facies	Sample no.	Quartz	Plagio-clase	K-feldspar	Total Feldspar	Quartz/ Felds	Ave-rage	Calcite	Dolo-mite	Chlorite	Mica	Clay	Amphi-bole	Others	Trace (SEM and XRD)
Upper Breccia Unit	Bjødnabu-haugen section	Parallel-bed. conglo. sst.	BBH_01_21	25	31	40	71	0.35	0.35	0	0	0	4	0	0	0	
		Matrix-supported breccia/ conglomerate	BBH_01_17	23	37	37	74	0.31	0.34	0	0	0	3	0	0	0	
			BBH_01_14	26	54	16	70	0.37		0	0	4	0	0	0	0	
		Clast-supported breccia	BBH_01_12	20	36	37	73	0.27	0.30	0	0	2	5	0	0	0	
			BBH_01_10	26	58	6	64	0.41		0	0	0	10	0	0	0	
			BBH_01_05	20	62	4	66	0.3		0	3	5	6	0	0	0	
			BBH_03_05	5	35	5	40	0.13		0	2	13	40	0	0	0	
			BBH_03_03	21	31	28	59	0.36		9	0	9	1	0	1	0	
			BBH_02_08	29	50	12	62	0.47		0	2	0	7	0	0	0	
			BBH_02_06	8	72	3	75	0.11		2	1	8	6	0	0	0	
			BBH_02_05	26	53	15	68	0.38		1	0	3	1	0	0	1	
	Svodene–Ritlandsfjellet	Matrix-supported breccia/ conglomerate	RITF_3_6_09	28	50	10	60	0.47	0.27	0	3	2	0	0	6	1	Siderite
			RITF_3_3_09	4	36	36	72	0.06		14	0	1	7	0	2	0	
		Clast-supported breccia	RITF_3_1_09	8	58	25	83	0.1	0.10	0	1	2	3	0	3	0	
			RITF_3_2_09	6	43	41	84	0.07		0	0	5	3	0	0	2	Sepiolite
			RITF_3_4_09	9	13	75	88	0.1		0	2	0	1	0	0	0	
			RITF_3_5_09	6	41	2	43	0.14		0	1	1	48	0	1	0	
Sandstone Unit	Stemhaugen section	Conglomeratic sandstone	STH_04_06	19	38	39	77	0.25	0.20	0	0	3	1	0	0	0	Zircon
			STH_04_05	15	56	21	77	0.19		0	0	7	1	0	0	0	
			STH_04_04	12	57	25	82	0.15		0	0	6	0	0	0	0	Mica
			STH_04_03	15	54	23	77	0.19		1	0	7	0	0	0	0	Amphibole
	Svodene–Ritlandsfjellet	Upper cong. sst. (UHS)	RITF_4_8_09	5	38	38	76	0.07	0.06	11	0	4	3	0	1	0	
		Upper cong. sst. (UCS)	RITF_4_7_09	5	51	30	81	0.06		0	0	6	6	0	1	1	Siderite
		Upper cong. sst. (UHS)	RITF_4_3_09	4	51	33	84	0.05		0	0	10	1	0	0	1	Sepiolite
		Middle homo. sst.	RITF_1A_1_09	8	49	37	86	0.09	0.11	0	0	5	1	0	0	0	
		Middle homo. sst. (LCS)	RITF_1_3_09	3	13	12	25	0.12		66	0	0	5	0	1	0	
		Parallel-bedded sst. (CUP)	RITF_1_6_09	11	40	38	78	0.14	0.11	1	0	5	1	0	3	1	Hematite
			RITF_1_7_09	6	49	41	90	0.07		0	0	3	1	0	0	0	
		Parallel-bedded sst. (FUP)	RITF_1_2_09	14	37	41	78	0.18	0.21	0	2	5	1	0	0	0	
			RITF_1_1_09	15	27	38	65	0.23		2	0	14	3	0	0	1	Siderite
		Lower cong. sandstone	RITF_4_5_09	8	40	24	64	0.13	0.13	0	0	17	6	0	3	2	Ajoite
Lower Breccia Unit	Stemhaugen	Matrix-suppt. conglomerate	STH_04_02	16	47	28	75	0.21	0.21	0	0	4	5	0	0	0	Amphibole
		Clast-suppt. conglomerate	STH_03_04	15	63	18	81	0.19	0.19	0	0	4	0	0	0	0	Mica. apatite
	Svodene–Ritlandsfjellet	Matrix-suppt. conglomerate	SVDL_04_02	5	45	35	80	0.06	0.06	10	0	3	2	0	0	0	Hematite, sphene
		Clast-suppt. conglomerate	SVDL_02_02	15	45	34	79	0.19	0.19	0	0	3	3	0	0	0	Zircon, epidote, apatite
		Clast-suppt. breccia	RITF_4_1_09	7	34	34	68	0.1	0.1	8	2	1	10	0	2	2	Ankerite, ajoite
		Matrix-suppt. breccia	RITF_4_4_09	13	23	30	53	0.25	0.25	7	5	1	18	1	2	0	
Basement	Melands-grønna High	Basement breccia	MGH_2_1_10	14	26	55	81	0.17	0.26	0	0	0	1	0	0	4	Ankerite, apatite, pyrite
			MGH_10_3_10	14	18	62	80	0.18		1	0	0	2	0	0	3	Ankerite, apatite
	Ritlandsfjellet		RITT_12_01_09	24	54	0	54	0.44		0	0	0	15	0	0	7	Ankerite, apatite

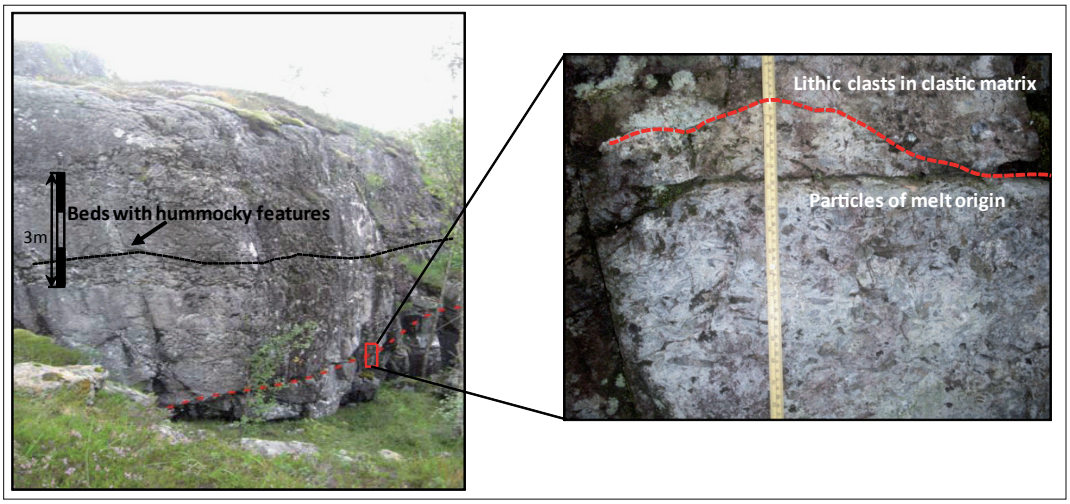

Figure 4. Sedimentary succession of the Lower Breccia Unit exposed in the Ritlandsfjellet area. The red, hatched line marks a possible boundary between the underlying rock succession of melt origin (~2 m thick) and overlying breccia beds (~7 m thick). The enlarged section displays matrix-supported breccias with centimetre-size, elongate, reworked particles of melt origin, laterally and vertically interfingering with lithic clasts in a dark grey to blackish sandy matrix. The overlying, clast-supported breccia beds are often visible in the terrain as elevated ridges and hummocky features (black, hatched lines).

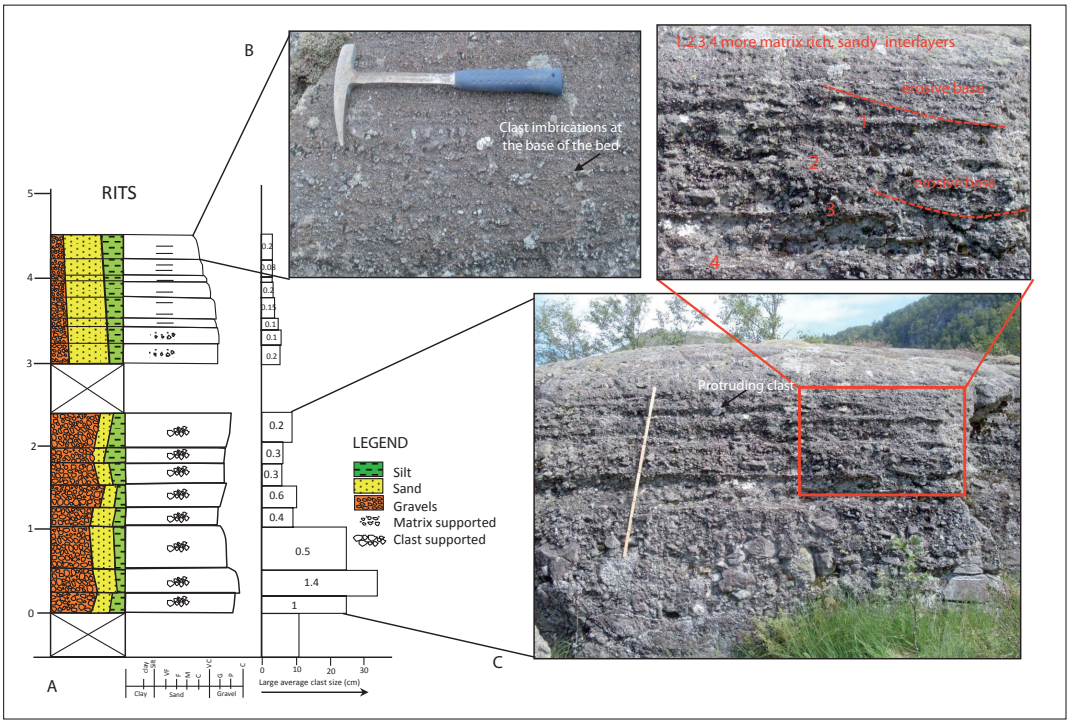

Figure 5. (A) Sedimentological log of the upper part of Lower Breccia Unit, Ritlandstjønna area. The average size of the ten largest clasts (MPS) is plotted (right side) against bed thickness (BTH) (the number represents the MPS/BTH ratio). (B) Conglomeratic sandstones, coarse clasts at the bottom and finer near the top, with evidence of clast imbrications at the base of the bed. (C) Clast-supported conglomerate; crudely stratified, poorly sorted, with an increased amount of sandy matrix; the enlarged part of the photo shows a faint erosional base and more matrix-rich sandy interlayers at the top.

Clast-supported breccia: Clast-supported breccia beds overlying matrix-supported breccia beds vary in thickness from 20 cm to 2–3 m (Figs. 3 and 4). They are very poorly developed, forming wedges and dip at 10° to 12° towards the crater centre. In the terrain, these beds are marked by elevated ridges and hummocky features (Fig. 4). The clasts range in size from a few centimetres (2–4 cm) to a few tens of centimetres (20–40 cm) and are angular to subangular, consisting of basement gneisses and dispersed pegmatitic clasts. The beds do not show any gradation and the matrix content is fairly low (5–10%).

Clast-supported conglomerate: These sediments are located in the Ritlandstjønna area (log RITS) (Figs. 2A and 5) and stratigraphically overlie the clast-supported breccia beds of the Ritlandsfjellet area (Figs. 3 and 4). The clast-supported conglomeratic beds dip at 2–4° towards the crater centre. The bed thickness varies from 15 to 50 cm (Fig. 5A). The beds are moderately developed, crudely stratified and sometimes show a faint erosional base to the underlying beds (Fig. 5C). The clasts are granitic and gneissic in composition; in a few cases, pegmatitic veins and an original gneissic foliation are preserved within these clasts. No trends of clast-size variation within the individual beds were found. The clasts vary in shape from angular to subangular, and subrounded to rounded. Locally, larger clasts protrude on the top of the bedding planes (Fig. 5C). The clasts are larger (10–20 cm) in the lower part of this subunit and smaller (4–8 cm) in the upper part, showing an overall fining-upward sequence (Fig. 5A). Thin pebbly/sandy interlayers are found at the top (Fig. 5C). Large outsize (30–40 cm) clasts have been found within this subunit. The maximum clast size (MPS) vs. bed thickness (BTH) ratio varies from 0.2 to 1.4 (Fig. 5A). Clast counting on the bedding plane revealed that the clast size varies from less than a centimetre to a few tens (10–20) of centimetres, but does not exceed 50 cm (Fig. 6).

Matrix-supported conglomerate: These beds form the uppermost part of the LBU and grade into conglomeratic sandstones above (Fig. 5A). The beds are 5 to 25 cm thick and relatively well developed. The clasts are mostly of quartzite, 0.5–2 cm, locally 5–7 cm, and are subrounded to rounded. A gradual decrease in clast size and a corresponding increase in matrix content become more evident towards top. The sediments are poorly sorted and show clast imbrications along the base of the bed (Fig. 5B).

Sandstone Unit (SU)

In the Svodene–Ritlandsfjellet area, the sandstone-dominated unit has been logged at two different sections (RITF–1 and –4) (Figs. 2A and 3). The thickness of this SU is about 15 m, with a gradual lower boundary to the LBU. Presently, the top surface of the SU is exposed at 460 to 480 m above sea level (Fig. 2B), approximately 260 m below the reference level of the peneplain. Palaeocurrent flow measurements in the SU, e.g., from cross-beds and ripple marks, strike within the range of 40°–110°, reflecting a unimodal (east-northeastward) palaeocurrent flow direction (Fig. 2A). Generally, the SU is an arkosic arenite, fine to medium grained with subangular to subrounded grains, and appears to be moderately sorted. It is characterised by significant lateral and stratigraphical textural variations. Different facies types were identified, e.g., massive sandstone, parallel-bedded sandstone, low-angle cross-stratified sandstone, conglomeratic sandstone, and soft-sediment deformed sandstone

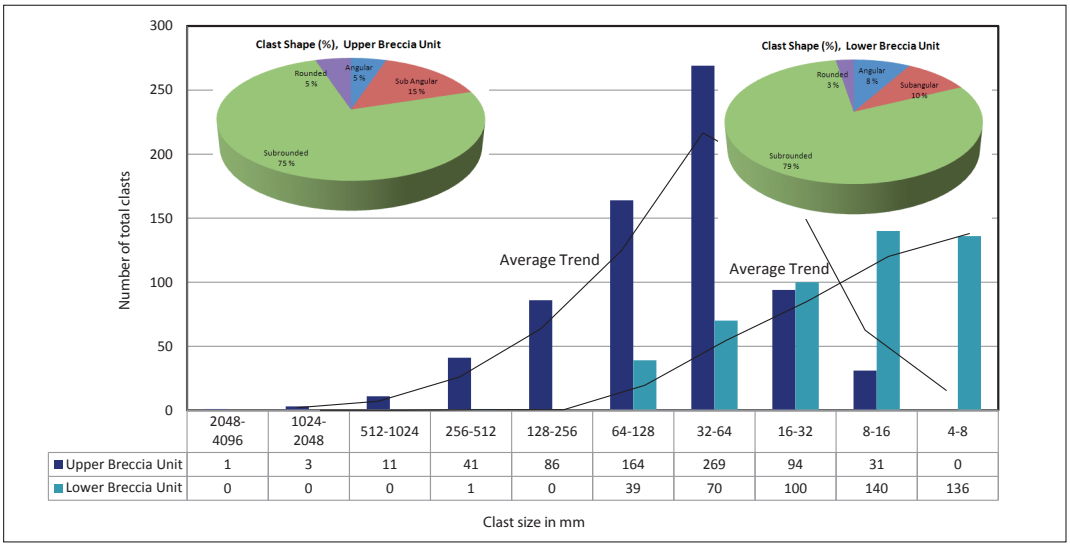

Figure 6. Comparison of average clast size and shape between the Lower Breccia Unit (LBU) and the Upper Breccia Unit (UBU). Clasts were counted along bedding planes in square grids in the Ritlandstjønna area for the LBU and on Svodene hill for the UBU.

(Tomcyzk, 2010). The SU is divided into four facies units: i) lower conglomeratic sandstone, ii) parallel-bedded sandstone, iii) middle homogeneous sandstone and iv) upper conglomeratic sandstone (Figs. 3 and 7).

Lower conglomeratic sandstone: The thickness of the lower conglomeratic sandstone varies from 2 to 4 m (Fig. 3), and the beds show a gradational transition towards the underlying breccias (Fig. 3). The clasts vary in size up to a few centimetres, and show an increasing roundness as compared to the LBU. The matrix is mostly a fine-grained sand which increases significantly in amount upwards in the unit.

Parallel-bedded sandstone: These sandstone beds are more or less parallel and 10–20 cm thick (Figs. 3 and 7), dipping with an angle of 10° to 15° towards the crater centre. The sandstones are fine to medium grained. Individual beds are capped by thin silt laminae (0.2–0.8 cm), thus showing a fining-upward pattern. The overall development of this unit displays a fining-upward succession in the lower part, shifting to an upward-coarsening trend in the upper part (Fig. 7). The lower, fining-upward intervals are conglomeratic at the base and medium to fine grained towards the top (Fig. 7A). The coarsening-upward succession in the upper part consists of fine sand at the base and medium-grained sand towards the top. Both successions display some erosional scours and wavy laminations, and very faint ripple marks (Fig. 7B) with occasional crenulated mud clasts 1–3 mm in size.

Middle homogeneous sandstone: The middle part of the SU is mostly homogeneous (Figs. 3 and 7). These sandstones are fine to medium grained with subangular granitic clasts (~50 cm) locally embedded within them. Approximately two-metre thick, low-angle (9°), cross-stratified sandstone beds are present and locally show erosional bases to the underlying sandstones (Fig. 7C). These particular sandstones are fine grained and consist of subangular grains of moderately sorted sand.

Upper conglomeratic sandstone: The uppermost part of the SU is mostly homogeneous but locally coexists with beds of conglomerate (Figs. 3 and 8). The conglomeratic beds show sharp, erosional and commonly irregular bases towards the underlying homogeneous sandstone

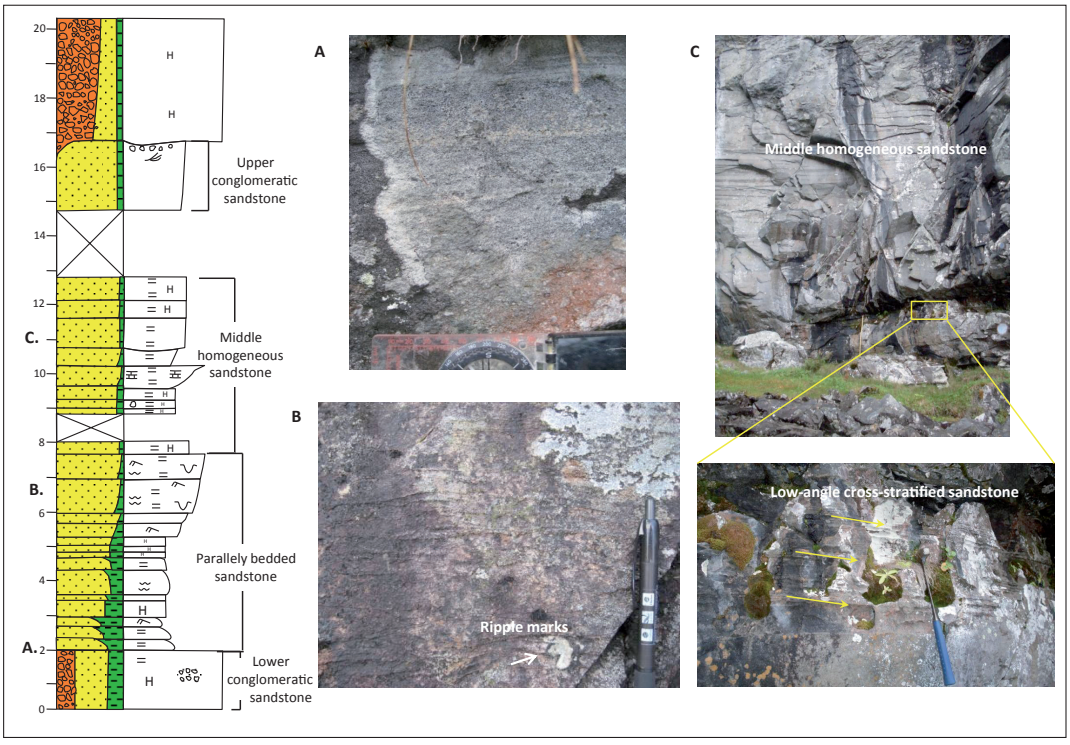

Figure 7. Sedimentological log of the Sandstone Unit, Ritlandsfjellet. Relative positions of the photos are shown to the left side of the log by photo number. (A) Fining-upward sequence, conglomeratic along the base and medium to fine grained with faint parallel lamination towards the top. (B) Wavy laminations and faint ripple marks in medium-grained sandstone. (C) Middle homogeneous sandstone, calcite-rich, low-angle, cross-stratified sandstone beds (yellow box) are enlarged in a separate photo. For legend, see Fig. 3.

beds (Fig. 8A) and range in thickness from 50 to 130 cm, dipping with an angle of 20° towards the crater centre (Fig. 8A). Clast sizes within the conglomerates range from 2 to 3 cm. Rare, large, outsize clasts (up to 90 cm) are found, commonly sitting on top of the sandstone beds (Fig. 8A). Different degrees of fracturing are commonly observed within these outsize clasts, which also contain dispersed pegmatitic veins (Fig. 8A). The clasts are subangular to subrounded and granitic to gneissic in composition, similar to the basement rocks. The sandstone beds are 40 to 100 cm thick and medium to coarse grained. Convolute laminations and very faint ripple marks have been found within the underlying sandstone beds (Fig. 8A). Convolute lamination was probably formed by compaction caused by the overloading pressure of the clast-rich beds during syn-depositional stages.

Upper Breccia Unit (UBU)

In the Svodene–Ritlandsfjellet area, the Upper Breccia Unit (UBU) reaches a maximum thickness of 50 m and thins rapidly to the west and east (Fig. 9A). This unit has an erosional contact towards the brecciated basement at the crater rim and progrades over the underlying SU (Fig. 9A). Sediments of the UBU occur as well-developed wedges and pinch out in the lower slope towards the crater centre. The individual beds dip at 20° and extend about 150 m from the steep crater wall towards the crater centre (Fig. 9A). The UBU in the Svodene–Ritlandsfjellet area is mainly clast-supported, but a few beds of matrix-supported breccias have been found. Clast-counting results along the bedding-plane surfaces at the Svodene hill show that clast size ranges widely from centimetres to a few metres (Fig. 6). The clasts are subrounded to subangular (Fig. 6), commonly intensively fractured and have a similar granitic/gneissic composition as in the successions below and in the basement itself.

Clast-supported breccia: The thickness of the individual beds of the clast-supported breccia ranges from 1 to 6 m with a fairly low matrix content (<20%) (Fig. 3). An increase in the matrix content towards the top of each bed defines a poorly developed normal grading (Fig. 3). The clasts are mostly subangular to angular in shape and range in size from a few centimetres to the metre scale (Fig. 9B). The matrix appears to be homogeneous and consists of medium- to coarse-grained sand.

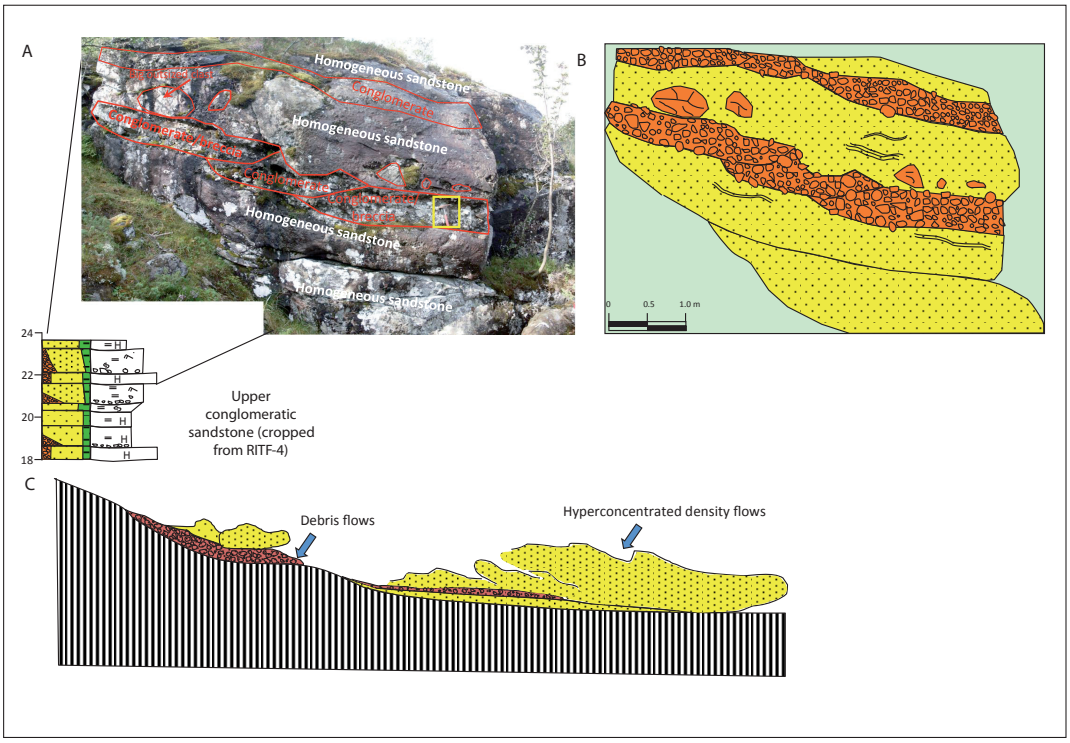

Figure 8. (A) Homogeneous sandstone beds intercalated with conglomeratic beds, forming a local, erosional/irregular contact to the underlying sandstone beds. Outsize clasts (~90 cm) with different degrees of fracturing are dispersed within the sandstone beds. (B) Conceptual sketch of the coexistence of the conglomeratic beds and sandstones. (C) Partial transformation of the precursor debris flows into concentrated density flows during downslope movement of the flow (modified after Haughton et al., 2003). For legend, see Fig. 3.

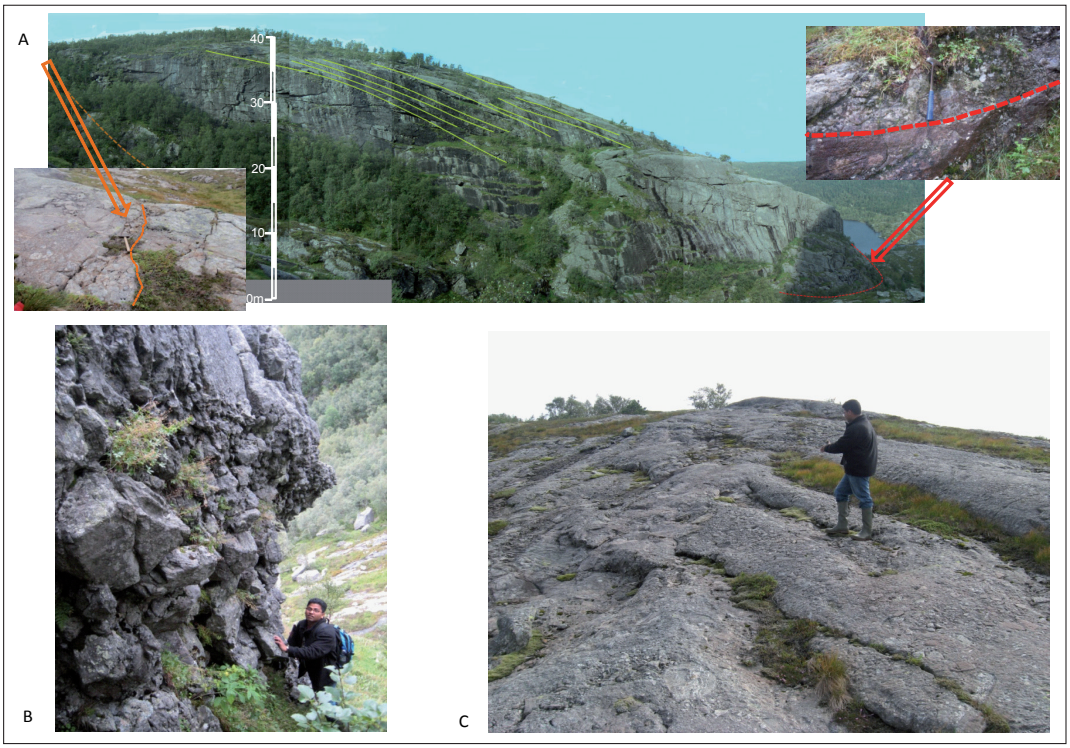

Figure 9. Sedimentary succession of Upper Breccia Unit (UBU), Svodene hill. (A) Fan-shaped geometry (convex up, east–west thinning) of the UBU sediments, extending from the crater rim to the crater centre, displaying an erosional contact (red, hatched line) to the underlying Sandstone Unit (enlarged photo to the right) and to the brecciated basement (orange, hatched line, enlarged photo to the left) at the crater rim. (B) Clast-supported breccia, the individual clasts are subangular to angular, extending to metre size. (C) Matrix-supported conglomerates with radially elongated lobes with large outsize clasts in the snout, UBU.

Matrix-supported breccia/conglomerate: Matrix-supported breccia beds are found intercalated with the clast-supported breccia beds (Fig. 3). The matrix-supported beds range in thickness from 50 cm to 4 m where the maximum clast size reaches up to 70 cm. The matrix consists of medium- to coarse-grained sand, light grey to pink in colour; it is moderately sorted and the content may reach up to 70–80%. Faint laminations and typical flow features have been observed within some of the matrix layers. At the top of the Svodene hill, there are 2 m-thick, matrix-supported conglomeratic beds displaying radially elongated lobes (Fig. 9C). The lobes are 10 m wide and large outsize clasts are typically found in the snout. The beds display a clast-supported texture at the base but are more matrix-rich at the top.

Bjødnabuhaugen area

At Bjødnabuhaugen, sediments of the upper stratigraphical column are well exposed (Fig. 2A) and can be correlated stratigraphically with the UBU of Svodene–Ritlandsfjellet area. The sediments of the lower stratigraphical column are scarcer in this area. The basal contact of the lower breccias is clearly erosional. Rare patches of the matrix-supported conglomerate have been found in lower stratigraphical positions; elsewhere it is mostly covered with vegetation. However, the field relationships suggest that the non-exposed section could be approximately 15 m thick.

Upper Breccia Unit

The UBU in the Bjødnabuhaugen area is composed of breccias with a stratigraphical thickness of at least 60 m. Its contact with the brecciated basement in the crater wall is not exposed. The individual beds dip from 20° to 30° degrees, extending approximately 100 m from the northern crater rim towards the crater centre and also showing well-developed wedges and pinch outs towards the crater centre. These sediments are mainly clast supported, but a few metres of matrix-supported breccia and conglomeratic beds have been found. The Bjødnabuhaugen sediments are divided into three facies units:

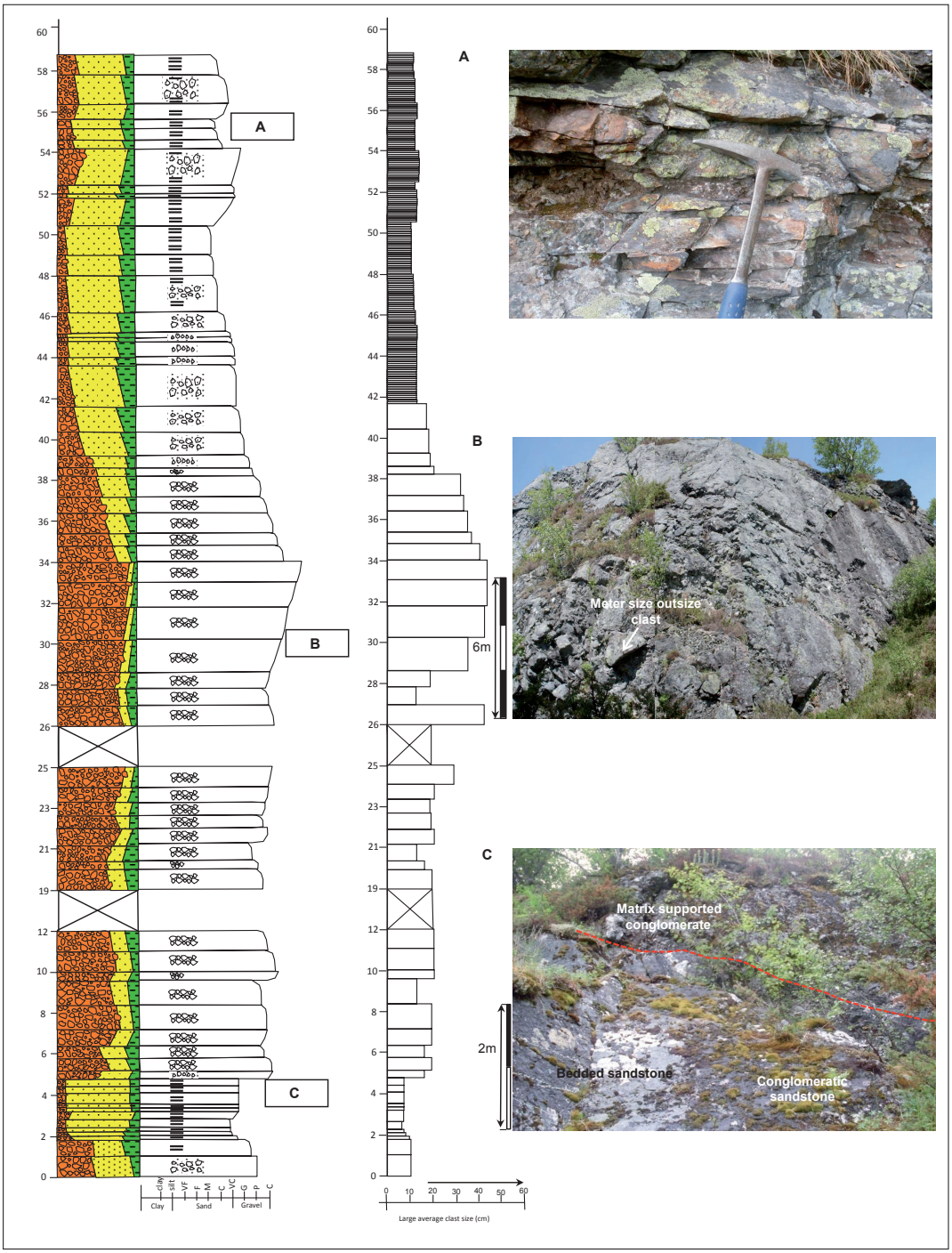

Figure 10. *Sedimentological log of the Upper Breccia Unit in the Bjødnabuhaugen area. To the right, the average size of ten large clasts (MPS) is plotted against bed thickness (BTH). The photos are marked on the log with boxed figure numbers. (A) Conglomeratic sandstone, well-developed beds with sheet-like distribution. (B) Clast-supported breccia, locally with very big outsize clasts. (C) Erosional contact between the conglomeratic sandstone (below) and matrix-supported conglomerate (top); at the right-hand side of the picture, the lateral transition of the sandstone into conglomerate can be seen. All the photos taken from the Bjødnabuhaugen section (Fig. 2A).*

Clast-supported breccia: In the Bjødnabuhaugen area, the thickness of individual clast-supported beds ranges from 1 to 2 m (Fig. 10). The average maximum clast size ranges from 30 to 50 cm. Metre-sized (outsize) clasts have also been found (Fig. 10B). The clasts display high degrees of fracturing with typical 'crackle' or 'jigsaw-breccia fabric' (Blair & McPherson, 1994). The bedding planes are generally poorly developed. Individual beds locally show crude reverse grading to almost no grading, displaying hummocks and arcuate ridges to the overlying beds (Fig. 10B). The maximum clast size vs. bed thickness plot shows that the largest clasts are in the thickest beds, and are found in the middle part of the section (Fig. 10). Thin beds with smaller clast sizes are found in the upper and lower parts (Fig. 10). Lateral changes in clast shape and size are commonly observed. The matrix is mostly coarse-grained sand, but locally a gravel-size matrix has been found. The matrix is light grey, and the grains in the matrix are angular to subangular in shape, poorly sorted and have a composition comparable to that of the common clasts.

Matrix-supported breccia/conglomerate: The matrix-supported breccias are found in the lower and upper parts of the section (Fig. 10). The matrix-supported beds range in thickness from 25 cm to 2 m. The average clast size of the matrix-supported beds is 5–10 cm, though bigger clasts up to 50 cm have been found. The matrix content varies from 40 to 80%, and the matrix itself is a medium- to coarse-grained sand of light grey to brown colour. Faint laminations have been found within these matrix layers. In the Bjødnabuhaugen area, matrix-supported beds grade into parallel-bedded conglomeratic sandstones (Fig. 10).

Parallel-bedded conglomeratic sandstone: A few metres of parallel-bedded conglomeratic sandstone beds have been found in the lower part of the Bjødnabuhaugen section (Fig. 10). The sandstone beds in the lower part are 5 to 10 cm thick, well developed, fine to medium grained and show a slight coarsening-upward trend (Fig. 10). Clasts up to 5 cm in size have been found within these sandstone beds, with the clast size appearing to increase upwards. The sandstone beds locally show a lateral variation from matrix-supported to clast-supported texture (Fig. 10C). Near the top, a 10 m-thick sequence of conglomeratic sandstone beds is present, which grades upward from matrix-supported conglomerate to conglomeratic sandstone (Fig. 10). These sandstone beds are 2–4 cm thick, well developed, crudely stratified and planar in nature, and commonly show a sheet-like distribution (Fig. 10A). They consist of grey to light brown, medium- to coarse-grained sand with some clasts. The clast size generally ranges from 5 to 10 cm, but locally up to 15 cm. Towards the top, outcrops of the conglomeratic sandstone beds are highly weathered and oxidised (Fig. 10A).

Stemhaugen area

The sedimentary succession at Stemhaugen is not well exposed; mostly covered by recent vegetation and commonly subjected to local rock slides. The contact between the sediments and the brecciated basement has not been found here. Field relationships suggest that the non-exposed missing section could be approximately 10 m in thickness. Presently, the sedimentary succession at Stemhaugen is only found at lower elevations (425–455 m), approximately 300 m below the reference level of the peneplain, thus representing the lower stratigraphical levels of the crater-fill sediments, possibly correlatable with the LBU and the lowermost part of the SU in the Svodene–Ritlandsfjellet area. The sedimentary succession in the Stemhaugen area is mainly clast supported at the base (~25 m thick), grading into matrix-supported conglomerate to conglomeratic sandstone (~12 m thick) towards the top (Fig. 11). Faint cross-beds found in the conglomeratic sandstones reflect a southeastward flow direction (Fig. 2A). A sedimentary succession (5–6 m) of very coarse (10 cm to >1 m), angular to subangular, clast-supported breccias with a fine-grained matrix has been found between the crater lakes (Fig. 2A), possibly representing a slumped (lowermost) section derived from the western part of the crater wall.

Clast-supported conglomerate: The base of the sedimentary succession in the Stemhaugen area is marked by clast-supported conglomerates. Bedding is poorly developed and shows normal grading to no grading in the lower part, whereas a crude reverse grading is seen in the upper part (Fig. 11A). The individual bed thickness ranges from 1 to 4 m. The clasts are subangular to subrounded, poorly sorted and granitic and gneissic in composition. In a few cases, pegmatitic veins and original gneissic foliation are preserved within these clasts. Clast size ranges generally from 4 to 20 cm, but a few clasts up to 50 cm have been found. The matrix content is fairly low (5–10%), consisting mostly of fine- to medium-grained sand with occasional patches of coarse-grained sand.

Matrix-supported conglomerate: The matrix-supported conglomerate beds (Fig. 11B) show gradational boundaries to the underlying clast-supported breccias. The beds are relatively well developed and range in thickness from 10 to 15 cm. Clast size ranges from 3 to 7 cm, and the clasts are subangular to subrounded with characteristic granitic and gneissic compositions. Some larger outsize clasts of 15 to 30 cm size have been found; an upward decrease in clast size and increase in matrix content (up to 75%) can be quite prominent in the individual beds. The matrix consists of light grey, fine- to medium-grained sand, locally showing faint laminations.

Conglomeratic sandstone: The conglomeratic sandstone unit (Fig. 11C) is approximately 8 m thick. Individual beds are well developed (10–15 cm thick), consisting of grey, moderately sorted, fine- to medium-grained sand with local indications of cross-bedding.

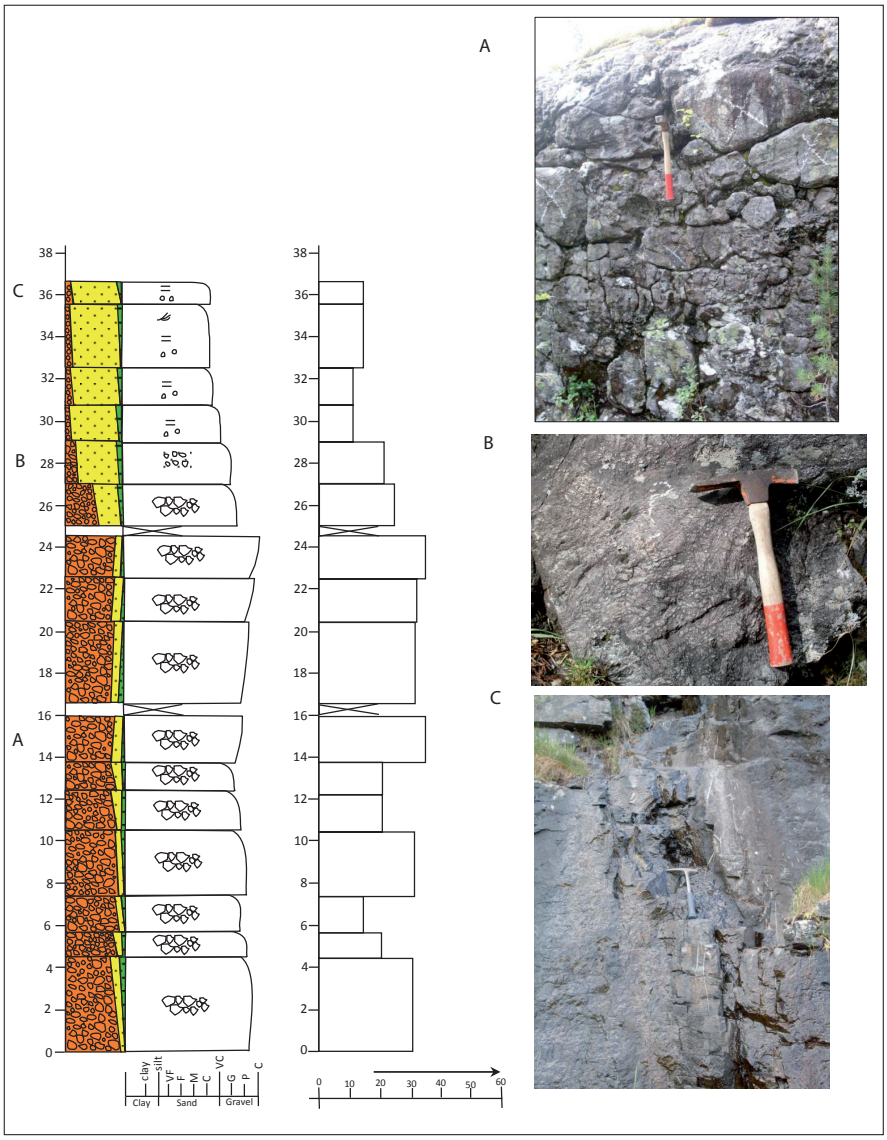

Figure 11. *Sedimentological log of the Stemhaugen section. To the right, the average size of ten large clasts (MPS) is plotted against bed thickness (BTH). The photos are marked on the left side of the log. (A) Clast-supported conglomerate showing crude reverse grading. (B) Matrix-supported conglomerate. (C) Conglomeratic sandstone with well-developed beds. For legend, see Fig. 3.*

Large, outsize clasts (10 to 12 cm) are locally present within these sandstone beds.

Mineralogical observations

Thin-section and x-ray diffraction (XRD) analyses of each facies from the three different depositional areas (Tables 1 and 2) show a very similar mineralogical composition and are comparable to the general composition of the granitic and gneissic basement (feldspar rich, quartz poor) (Table 2). The crater-filling sediments are rich in feldspar and poor in quartz, with an average quartz/feldspar ratio of 0.20 (XRD) (Tables 1 and 2). This can be compared with an average quartz/feldspar ratio of the gneissic basement rocks of 0.26 (XRD) (Table 2), indicating a short transport history and a very local source for these crater-filling sediments.

The clast-supported and matrix-supported conglomeratic beds at Stemhaugen were compared mineralogically to the similar facies in the Svodene–Ritlandsfjellet area

(Tables 1 and 2) in order to detect any difference in the sediment source between these areas. The clast-supported conglomerate beds from both these areas display comparable quartz/feldspar ratios (Figs. 12 and 13; Tables 1 and 2). The quartz/feldspar ratio of the matrix-supported conglomerate beds from the Stemhaugen section is higher than in the Svodene–Ritlandsfjellet area (Figs. 12 and 13; Tables 1 and 2). The K-feldspar content dominates in the LBU sediments from the Svodene–Ritlandsfjellet area compared to the sediments from the Stemhaugen area (Table 2).

The LBU sediments from both Svodene–Ritlandsfjellet and Stemhaugen generally have better rounded quartz grains compared to feldspar grains. Some exceptionally rounded quartz grains have been found within these sediments from both areas (Fig. 14A). Feldspar grains (up to 5 mm in size) are highly angular showing a high degree of grain fracturing and evidence of in situ disintegration (Fig. 14B). The SEM studies revealed that very fine-grained, recrystallised quartz and feldspar grains constitute the major part of the matrix components, whilst titanite, authigenic mica and pyrite are found in minor amounts. Melt particles and quartz grains with 'planar deformation features' (PDFs) have been found only in the lower part of the LBU sediments from the Svodene–Ritlandsfjellet area. The sporadic occurrence of calcite, mica and amphibole minerals is more common in the LBU sediments from Svodene–Ritlandsfjellet than in those from the Stemhaugen area (Tables 1 and 2). Apatite, monazite, iron oxides (e.g., haematite) (Fig. 14C) and carbonates (e.g., ankerite and siderite) are only found in small amounts in a few samples as a minor matrix component (Tables 1 and 2).

The mineralogy of the conglomeratic sandstones in the Stemhaugen area was compared to that in the lower conglomeratic sandstones of the Svodene–Ritlandsfjellet area. Both the thin-section and the XRD analyses show that the conglomeratic sandstones from Svodene–Ritlandsfjellet show slight differences in their quartz/feldspar ratio compared to the conglomeratic sandstones in the Stemhaugen section (Figs. 12 and 13; Tables 1 and 2). Greater amounts of chlorite, mica and amphibole have been found in the lower conglomeratic sandstones from Svodene–Ritlandsfjellet area as compared to similar stratigraphical levels at Stemhaugen (Tables 1 and 2).

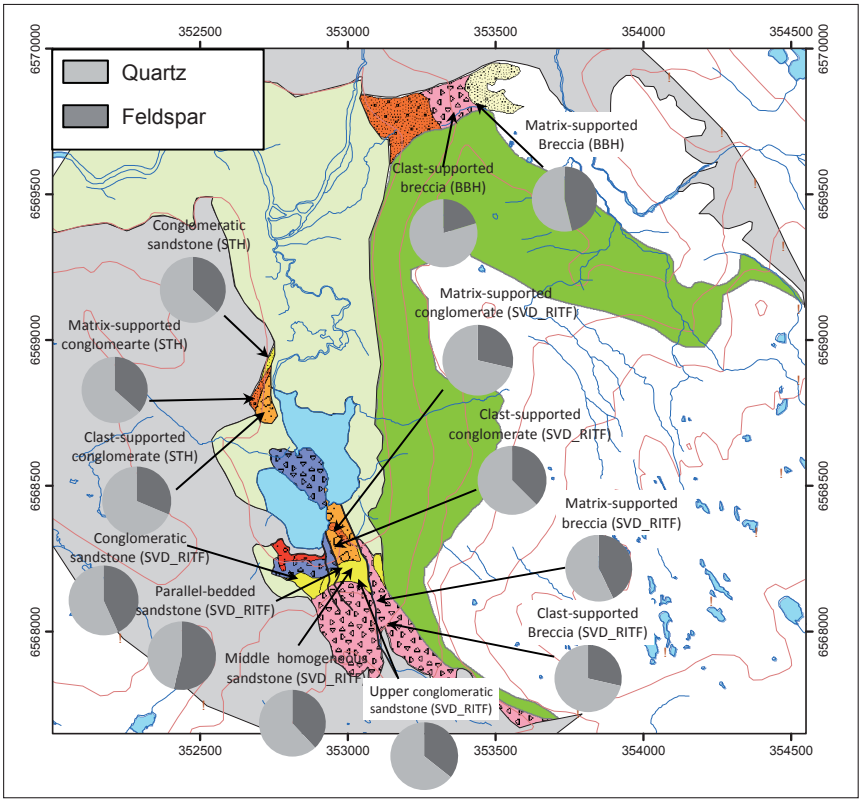

Figure 12. Quartz/feldspar ratios of the different facies types in different depositional areas. The quartz and feldspar contents are based on grain counts (400) in thin-sections. STH–Stemhaugen, RITF–Ritlandsfjellet, SVD–Svodene and BBH–Bjødnabuhaugen.

Sedimentary units	Facies	Litho-logy	Quartz/Feldspar	Major sedimentological characteristics	Interpretation
Upper Breccia Unit	Parallel-bedded conglomeratic sandstone		0.35	Well- to crudely-stratified, 2-4 cm thick, sheet-like distribution with some outsize clast	Hyperconcentrated density flow
	Matrix-supported breccia/conglomerates		0.27 0.34 0.76 1.15	Poorly to moderately developed beds, 70-80% matrix content, radially eloganted lobes	Debris flows
	Clast-supported breccia		0.10 0.25 0.40 0.30	Subangular to angular in shape, <20% of matrix, poorly developed beds, no grading to crude reverse grading or normal grading	Scree, rock avalanches, debris avalanches
Sandstone Unit	Upper conglomeratic sandstone		0.06 0.55	Coexistence of conglomeratic beds and homogeneous sandstones, convolute laminations, and very faint ripple marks	Linked debrites
	Middle homogeneous sandstone		0.11 0.66	Mostly homogeneous, boulder-size clast in fine- to medium-grained sand, 2m of low-angle cross-stratified sand with erosional base	Turbidity, channel mouth bar
	Parallel-bedded sandstone		0.11 (CUP) 0.94 0.21 (FUP)	Parallel beds, fining upward in the lower part and coarsening upward to the upper part, wavy laminations, mud clast, erosional scours	Surge or surge-like turbidites
	Lower conglomeratic sandstone		0.13 0.20 0.59 0.76	Gradational contact to the underlying breccia, homogeneous, upward increase in matrix	Debrisflows/Hypercon-centrated density flows
Lower Breccia Unit	Matrix-supported conglomerate		0.06 0.21 0.40 0.58	Relatively well developed beds, overall fining-upward trend, clast imbrications at the base	Hyperconcentrated density flows
	Clast-supported conglomerate		0.19 0.47 0.64	Moderately developed beds, high MPS/BTH ratio, no grading in beds, iron oxide coatings	Subaerial cohesive debris flows
	Clast-supported breccia		0.10 0.50	Angular to subangular clast, poorly developed beds formed wedges, elevated ridges, hummock	Rock avalanches
	Matrix-supported breccia		0.25 XRD_SVD-RITF XRD_STH XRD_BBH Thin_SVD-RITF Thin_STH Thin_BBH	2-3 cm, angular granitic/gneissic clast, cm-size particles of melt origin, very fine-grained qtz/feldspathic matrix, PDFs in quartz grain	Fall-back ejecta (?) mixed with slump-back breccia

Figure 13. Major sedimentological characteristics of different facies and their possible depositional mechanisms. Quartz/feldspar ratio obtained from thin-sections (400 grains counted) and XRD analyses of the different facies are also shown. (FUP–fining-upward sequence, CUP–coarsening-upward sequence, MPS–maximum particle size, BTH–bed thickness).

The quartz/feldspar ratio in different facies of the sandstone unit at Svodene–Ritlandsfjellet varies according to their grain size (Figs. 12 and 13). The parallel-bedded sandstones have higher quartz/feldspar ratios compared to other sandstone facies (Figs. 12 and 13; Tables 1 and 2). Fining-upward beds of the parallel-bedded sandstones have slightly higher quartz/feldspar ratios compared to the coarsening-upward succession (Fig. 13). Homogeneous sandstones (cross-stratified beds) at intermediate stratigraphic levels are rich in calcite cement (Tables 1 and 2). The cement shows a poikilotopic texture where it fully occupies the pore spaces and reflects an early stage of cementation (Fig. 14D). A decrease in the quartz/feldspar ratio has been observed in the upper conglomeratic sandstones compared to the other underlying sandstone facies (Figs. 12 and 13; Tables 1 and 2) in the Svodene–Ritlandsfjellet area.

The mineralogical composition of the UBU sediments of Svodene–Ritlandsfjellet was compared with the UBU sediments of Bjødnabuhaugen (Tables 1 and 2). The UBU sediments in both depositional areas have comparable quartz and feldspar contents with local enrichment of mica, calcite and amphibole (Tables 1 and 2). Gneissic clasts (up to 4–8 mm) and angular to subangular feldspar grains (up to cm size) with possible planar fractures are commonly found in the UBU sediments in both areas. Thin-section study shows that the clast-supported breccia beds of Svodene–Ritlandsfjellet have slightly higher quartz/feldspar ratios compared to the clast-supported breccia beds of the Bjødnabuhaugen area (Fig. 12; Table 1). The K-feldspar content of clast-supported breccia beds in the Svodene–Ritlandsfjellet area is higher than in the Bjødnabuhaugen area (Table 2). Matrix-supported breccia/conglomeratic beds in the Bjødnabuhaugen section have higher quartz/feldspar ratios compared to the matrix-supported beds of the Svodene–Ritlandsfjellet area (Fig. 12). Contents of accessory minerals, e.g., mica and amphibole, are slightly higher in the upper breccia sediments of Svodene–Ritlandsfjellet compared to those at Bjødnabuhaugen. Generally, matrix-supported breccias have higher quartz/feldspar ratios compared to the clast-supported breccias in both areas (Tables 1 and 2).

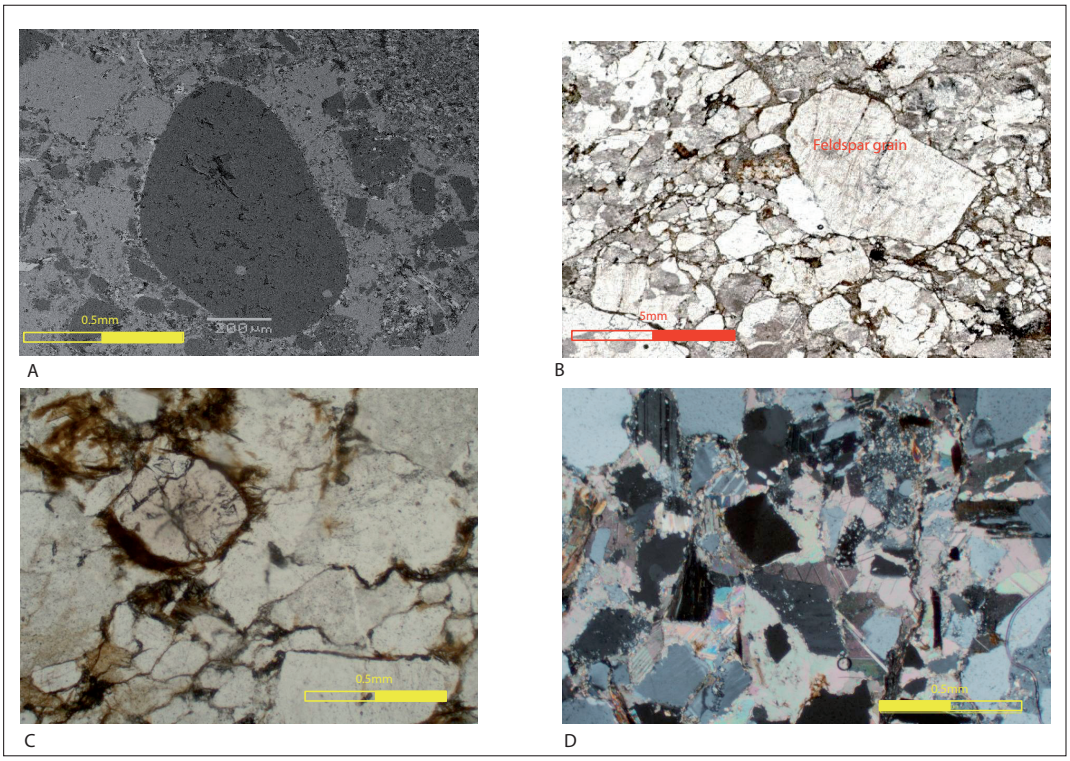

Figure 14. *Microphotographs of typical crater-filling sediments. (A) Exceptionally well-rounded quartz grain from Lower Breccia Unit (LBU) sediments, Ritlandsfjellet area. (B) Large (5 mm), fresh, highly angular and fractured feldspar grain from LBU sediments, Ritlandsfjellet. (C) Iron oxide minerals, locally found as coatings around grains within clast-supported conglomerates, LBU, Ritlandstjønna area. (D) Calcite-cemented sandstones, from middle homogeneous sandstones, SU, Ritlandsfjellet area.*

Discussion

The late syn-impact and early post-impact sediments from different depositional areas in the Ritland impact structure show dramatic differences in grain size and shape both laterally and stratigraphically. The mineralogy of the clasts and matrix, however, does not differ much and is very similar to that of the local gneissic basement. In all the studied sections, the clast size varies from centimetre to metre scale within very short lateral and vertical distances, representing short time intervals and a local history of gravity-controlled sedimentation. Insignificant amounts of finer-grained sediments, i.e., clay/silt fractions, within these sections represent a short and locally controlled transport of fresh, unweathered material which was probably derived from the different parts of the steep, unstable crater walls and rims, and deposited as individual fans prograding towards the crater centre.

Lower Breccia Unit

The presence of dispersed particles of melt origin and shock-metamorphic features in quartz grains from the lower part of the LBU in the Svodene–Ritlandsfjellet area confirms its late syn-impact origin. According to Melosh & Ivanov (1999), the crater modification stage of a simple impact structure starts with the slumping and collapse of the steep, transient cavity walls. Lenses of crushed rock generated by slumping of the transient cavity eventually slide and avalanche down towards the centre of the crater as different mass and gravity flows, depending on factors such as the composition of the target area, slope failure and temporal fluidisation of the sediments (Melosh, 1989).

The mechanism of large rock avalanches at impact craters was described by Davies (1982) and Melosh (1987), whilst Hewitt (1999) summarised some key morphological and sedimentary features of rock avalanche deposits. 'Rock avalanches' have been defined

by Kessler & Bédard (2000) as "large dislodged rock mass flows moving rapidly down slopes as a mobile, fluidal, close packing of blocks and fragments that jostle, bump, push, collide and fragment each other during their transport". Rock avalanche deposits are generally very poorly sorted with a mixture of mega-blocks, boulders and cobble-size fragments, gravel, sand and mud. The individual clasts are generally very angular and in some cases may form a jigsaw fit in the breccia. The rock avalanche mechanism has been compared to grain flows, having an erosional base and variably developed reverse grading (Blair & McPherson, 1994).

The clast-supported breccias (Figs. 2, 3 and 4) exposed in the Svodene–Ritlandsfjellet area show evidence of having been deposited from rock avalanches. These sediments are very poorly sorted and consist of a similar lithology to the basement (target surface) breccia, displaying the original gneissic foliation within the clasts. The matrix content within the clast-supported breccia is fairly low (5 to 10%) and the mineral composition is comparable to that of the clasts. All these features show close a similarity with rock-avalanche deposits. Clast-supported breccia at the lower stratigraphical level has been found neither in the Stemhaugen succession nor in the Bjødnabuhaugen section. However, the sedimentary succession (5 m) occurring between the lakes in the Ritlandstjønna area (Fig. 2A) possibly represents remnants of a major slump involving rock avalanches.

The 2 m-thick, clast-supported conglomerate beds of the Ritlandsjønna area (Fig. 5) stratigraphically overlying the breccia beds of the Ritlandsfjellet area most likely represent a debris-flow unit and could be classified as cohesive debris-flow deposits. Cohesive debris flows display *en masse* depositional characteristics, with the cohesive strength of the matrix acting as the dominant clast-support mechanism; the matrix is typically fine grained with a significant content of clay-sized particles (Costa & Williams, 1984; Gani, 2004). The matrix content within the clast-supported conglomerate beds in the Ritlandsjønna area is fairly low and consists mostly of fine- to medium-grained sand and silt, with an insignificant clay fraction. The cohesive strength can be enhanced by a number of other factors in subaerial debris flows, e.g., buoyancy and pore pressure (Mulder & Alexander, 2001). The diagnostic features of a cohesive debris-flow deposit include basal inverse grading (shear flow), an ungraded flow body (plug flow) and a sandy upper part (water lain) (Larsen & Steel, 1978; Nemec & Steel, 1984; Hubert & Filipov, 1989). The clast-supported conglomerate beds of Ritlandsjønna have some similarities with typical cohesive debris-flow deposits. Very large, outsize clasts occur locally at the weakly erosional bases of the beds, but no obvious reverse grading was found (Fig. 5C). The clasts in-between the beds are highly irregular in shape and are commonly ungraded. Well developed, horizontally stratified, sandy layers are found in the upper parts capping the ungraded beds (Fig. 5C). Outsize (30–40 cm) clasts have locally been found embedded within the clast-supported sediments, displaying variable degrees of fracturing. Larger clasts were also found along the bedding planes (Fig. 5C). This can be due to the 'rolling' motion (Iverson, 1997) generated in the debris flows where the larger grains are engulfed at the flow head and dispersed away from the flow through increased frictional strength (Mulder & Alexander, 2001).

These clast-supported conglomeratic beds were probably deposited during the seawater resurge when the crater was behaving more like a subaerial target crater. These debris-flow deposits are more reminiscent of subaerial deposition and were probably deposited under open atmospheric conditions. Nemec & Steel (1984) summarised some of the typical distinguishing features for subaerial and subaqueous debris-flow deposits. They claimed that subaqueous debris-flow deposits generally have higher matrix contents and have better clast alignment, imbrications and grading, and a marked upward increase in matrix content. They are typically capped by massive or rippled fine-grained sandstones, and commonly possess sand sills and dykes and deformation structures. Subaerial debris-flow deposits have sheet-like configurations with insignificant basal erosion, and beds are ungraded to well graded, quite commonly containing large, outsize clasts and showing a significant positive correlation between their bed thickness and maximum clast size. The maximum particle size (MPS)/bed thickness (BTH) ratio for the subaerial debris-flow deposits normally is higher (3 or less) than for subaqueous debris-flow deposits. The clast-supported conglomeratic beds in the Ritlandstjønna area show similarities with the diagnostic features of subaerial debris-flow deposits. The MPS/BTH ratio of these sediments (Fig. 5A) varies between 0.2 and 1.5, with an average value of 0.5. A significant positive correlation between bed thickness and maximum clast size is also evident.

The relatively thick sequence of clast-supported conglomerates found at the Stemhaugen section (Fig. 11) can be stratigraphically correlated with clast-supported conglomerates from the Ritlandsjønna area. The clast and matrix mineralogy (Tables 1 and 2) of this part of the Stemhaugen succession has close similarities with that at Ritlandsjønna, but there are differences in clast size, bed thickness and matrix content (Fig. 11). The beds are poorly developed with a low MPS/BTH ratio (average 0.17) and show crude reverse grading (Fig. 11). This succession probably also represents a subaerial, cohesive, debris-flow deposit. However, as it is highly eroded, subjected to local landslides and in many places covered by vegetation, a more precise interpretation is precluded.

Debris flows may undergo flow transformation during downslope movement, especially through mixing with water and dilution of the flow head, to become

a hyperconcentrated density flow or concentrated density flow, depending on the nature of the sediment concentration (Mulder & Alexander, 2001). A stratigraphical upward shift from a clast-supported to matrix-supported texture found within the LBU sediments at Svodene–Ritlandsfjellet and Stemhaugen (Figs. 5A and 11) may represent the flow transformation from a cohesive debris flow to a hyperconcentrated density flow/noncohesive debris flow (Mulder & Alexander, 2001; Gani, 2004). This flow transformation is probably due to the resurge of the seawater into the crater. The main mechanism for deposition from hyperconcentrated flows is frictional freezing that produces ungraded, or coarse-tail normally graded, gravel or gravelly sand and crudely or thickly stratified sand deposits. The matrix-supported beds of the LBU display a very crude normal grading (Figs. 5A and 11) with evidence of bottom traction carpets developing at the base of the beds (Fig. 5B). Abundant outsize and/or protruding clasts, in addition, suggest deposition from hyperconcentrated density flows transformed from the debris flows during downslope transport of coarse-grained, impact-derived sediments.

Sandstone Unit

The SU is well exposed in the Svodene–Ritlandsfjellet area in-between the LBU and the UBU, and displays some unique characteristics of density-controlled and turbiditic sedimentation, which are comparable to the sedimentation processes of a small, steep-slope, restricted, deep-basin setting, e.g., Crater Lake, Oregon, USA (Nelson et al., 1986). Relatively well developed conglomeratic sandstone beds were found at the Stemhaugen section and can be stratigraphically correlated with the lower part of the SU of the Svodene–Ritlandsfjellet area. The SU sediments probably resulted from gravity-controlled flow-transformation processes, i.e., from hyperconcentrated to concentrated and to turbidity currents (Mulder & Alexander, 2001). The different facies properties of the SU were compared to the typical characteristics of different density-/turbidity-controlled deposits (Mulder & Alexander, 2001; Haughton, et al., 2003; Gani, 2004) and possible depositional processes are discussed below.

Lower conglomeratic sandstone

This facies displays a gradational contact from the underlying matrix-supported conglomerate at both the Svodene–Ritlandsfjellet and the Stemhaugen sections. They are mostly homogeneous in nature and were probably deposited from either debris flows or hyperconcentrated density flows (Mulder & Alexander, 2001). A decrease in clast size and angularity, and increase in the quartz/feldspar ratio and matrix content compared to the underlying facies, can be related to a continuous reworking of the sediments during downslope transport (Figs. 12 and 13).

Parallel-bedded sandstones

The appearance of these sandstones clearly indicates a shift in depositional conditions from density flows to turbidity flows. Gani (2004) claimed that the main difference between turbidity currents and density flows is rheological, whereby a turbidity current is a completely Newtonian fluid and the dominant sediment-support mechanism is fluid turbulence. The turbidity-current deposits, i.e., 'turbidites', show fairly good grain sorting, with the upper part displaying normal grading without any floating clasts. Density flows are rheologically partly Newtonian fluids and partly non-Newtonian fluids, where dispersive grain pressure, fluid turbulence, escaping pore fluid and matrix strength are the dominant sediment support mechanisms (Gani, 2004). Density current deposits, i.e., 'densites', are ungraded, have floating clasts and are deposited through layer-by-layer accretion. The parallel-bedded sandstones of Ritland closely match the properties of turbidity deposits in terms of grain sorting, vertical bed stacking and absence of floating clasts. However, 1–3 mm-size mud clasts have been found in places. These low-density particles can be entrained by the upward component of turbulence, maintained in suspension and then settle gently (Mulder & Alexander, 2001). These sandstone beds are separated by thin, planar laminae (0.2–0.8 cm) consisting of fine-grained sand and silt that probably settled from suspension before another turbiditic event started to take place. Based on flow behaviour, Mulder & Alexander (2001) classified turbidity currents as surge, surge-like and quasi-steady turbidity currents. There is a continuum between the different types of turbidity current and one may transform into another as a result of sediment entrainment and dilution, producing changes in sediment concentration. Surge and surge-like turbidity flows are usually triggered by flow transformation through erosion and acceleration from flow types with a higher sediment concentration. These two turbidity-current classes generate sedimentary structures and bedforms comparable to those of the Bouma Tb–d (Bouma, 1962), but their duration is short and consequently related sedimentary structures are rare compared to the typical Bouma Tb–d (Mulder & Alexander, 2001).

The parallel-bedded sandstones of the Ritland successions do not reveal any complete development of Bouma sequences. The fining-upward trend from slightly conglomeratic bases (Fig. 7A) could be comparable to Bouma Ta. Upwards, the succession develops into finer-grained deposits with faint ripple marks (Fig. 7B) comparable to the Bouma Tb–c. The upper intervals of the Bouma sequence (Td–e) are absent within these Ritland sediments. Consequently, these sediments were probably deposited from surge or surge-like flows which evolved from precursory high-concentration flows during downslope transport of the sediments, and diluted gradually by continual addition of water and were eventually deposited in relatively distal parts of the crater basin as a turbidity fan.

The upper parts of the parallel-bedded sandstones are characterised by coarsening-upward developments (both individual beds and bed stacking) displaying some erosional scours and very faint ripple marks. The shift from the fining-upward to coarsening-upward stacking may suggest an increase in clastic input and energy conditions. Coarsening-upward stacking can be related to the renewed base-slope erosion and further reworking of the proximal sediments, deposited during fan-lobe progradation at the waxing phase (Kneller, 1995). A downslope reworking of these sediments is further indicated by the differences in the quartz/feldspar ratio between the sandstone facies (Figs. 12 and 13).

Middle homogeneous sandstone

The sandstone unit in the middle part is rather homogeneous with the local presence of boulder-size clasts of granitic/gneissic composition. These sediments were probably also deposited by turbidity currents. Transport of ~50-cm clasts under such energy conditions is very unlikely, and a rockfall is thus the most likely explanation. Since the clasts are angular and have a similar composition to the local basement, they probably fell down from the unstable crater wall. Similar rockfall features were also noted in the Gardnos crater-filling successions (Kalleson et al., 2008).

The cross-stratified, erosional-based sandstone beds were probably deposited by bypassing of the turbidity currents and represent a small-scale, channel mouth-bar deposit of a submarine-fan system. Mutti (1977) suggested that mouth bars are formed at the mouths of active channels through reworking of coarse-grained sediments deposited as excess load by bypassing of turbidity currents. The beds are characterised by large-scale cross laminae and consist of medium- to coarse-grained sands. Mutti (1977) interpreted these mouth-bar deposits as having formed in a regional-scale, deep-sea fan setting (Pyrenees basin); consequently, comparison with the small Ritland crater basin must take into account scale differences. Thus, the aerial extension of the sandstone unit in the Ritland impact structure was probably too modest to establish a channel-levee complex typical for a submarine fan setting.

Mineralogically, the cross-stratified sandstone beds are enriched in a calcite cement (Tables 1 and 2). The calcite cement has a poikilotopic texture, non-ferroan composition and probably formed during the early stages of diagenesis. (Fig. 14D). The cement within these beds may be of either organic or inorganic origin. During Early Cambrian time, Earth life was limited (mainly algae), poorly preserved and transported (low-relief sea-floor, temperate climate) (Brasier et al., 1992), so direct biogenic sources for the carbonate in these sandstone beds are unlikely except via, e.g., hydrothermal percolation from adjacent calcite-rich beds. Recent studies (Setså, 2011) have confirmed the presence of calcite-cemented beds outside the crater, underlying the ejecta bed.

Upper conglomeratic sandstone

The uppermost part of the sandstone unit represents a coexistence of the homogeneous and conglomeratic sandstone beds and can be compared to the 'linked debrites' described by Haughton et al. (2003) in a small, sand-rich fan system. The mechanism of deposition of these cogenetic beds (Haughton et al., 2003) in the Ritland succession can be the result of multiple breaching of the crater rim, where more water was added to the flow causing the flow to accelerate, resulting in increased slope erosion and reworking of the base-slope sediments. This could explain further clastic input to the flow. The flow started out as a viscous flow and the clast-rich conglomeratic beds were deposited. The flow then partitioned from a precursor debris flow into concentrated density flows during downslope movement, resulting in deposition of homogenous sandstone beds (Fig. 8C). Since flow transformations can be in both directions (cohesive-density; density-cohesive), these two bed types can coexist within a single flow event.

Upper Breccia Unit

The UBU sediments are well exposed at Svodene–Ritlandsfjellet and in the Bjødnabuhaugen area, representing a sedimentation pattern typical for marginal parts of a crater basin. They show well-developed wedge-shaped units developing from the crater rim towards the crater centre in a fan-like distribution (Fig. 9A). Individual fan lobes that developed from the southern crater rim (Svodene–Ritlandsfjellet) do not suggest bed-to-bed correlations with lobes along the northern (Bjødnabuhaugen) crater rim. The UBU sediments are probably missing at the Stemhaugen section as the sedimentary successions in this area were found only at lower elevations (425–455 m). Depositional mechanisms of the different facies types of these two depositional areas (Svodene–Ritlandsfjellet and Bjødnabuhaugen) are discussed in the following paragraphs.

Clast-supported breccia

The clast-supported breccia beds from the Svodene–Ritlandsfjellet and Stemhaugen sections could be interpreted as scree, rock-avalanche or debris-avalanche deposits. Bedforms produced by these three gravity-controlled processes are more or less similar but probably differ in matrix content due to differences in the degree of shattering, disintegration and pulverisation during downslope transport. Hewitt (1999) defined a 5% matrix content as 'matrix poor' and 25% as 'matrix rich' for rock-avalanche deposits from the Karakoram, Himalaya. The debris-avalanche deposits of the Milo Lahars sequence, studied by Calvari et al. (1998), revealed a 40% matrix content for the clast-supported beds. The matrix generated by these processes is compositionally identical to the clast composition in all these cases.

The matrix content of the clast-supported breccia beds from Svodene–Ritlandsfjellet and the

Bjødnabuhaugen area varies within the limits of 5% and 20%. Consequently, the matrix content of these clast-supported breccias is probably too low to reflect a debris-avalanche depositional mechanism according to Calvari et al. (1998). Interpretation of these beds based only on matrix content could be misleading as it relates to contributions from different sources. Rockfall, rockslide and rock avalanche represent a gradational spectrum of comparable gravity processes generated by failure of bedrock cliffs, and varying with respect to the size of the failed bedrock mass and the degree of shattering, disintegration and pulverisation (Blair & McPherson, 1994). These observations consequently suggest that the clast-supported breccia beds could have been deposited by any of the above-mentioned processes e.g., rockfall (scree), rock avalanche or debris avalanche, or a combination of all three, and deposited during the later stages of crater modification, probably post-dating SU deposition. The quartz/feldspar ratio of the clast-supported breccia beds from both the Svodene–Ritlandsfjellet and the Bjødnabuhaugen sections is significantly lower compared to other facies, suggesting a local source for these sediments. Minor differences in mineralogical composition, e.g., quartz/feldspar ratio, K-feldspar and mica content (Tables 1 and 2), of the clast-supported breccia beds between these sections are probably related to local compositional variations in the basement rocks.

Matrix-supported breccia/conglomerates

The characteristics of the matrix-supported breccia/conglomerate beds of the UBU match with those of typical debris-flow deposits which have probably been deposited in a subaqueous setting. Subaqueous debris-flow deposits have been discussed by Hampton (1972), Embley (1976), Nemec & Steel (1984) and Aksu & Hiscott (1992). These various deposits were discussed in the context of much wider basinal settings, but there are several similarities with the matrix-supported breccia/conglomerates of the Ritland crater. However, the clasts in the subaqueous debris-flow deposits commonly display better clast alignment and imbrications, poorly developed normal grading with the presence of wave-generated structures in sandy layers, and mud/silt interbeds (Nemec & Steel, 1984).

The matrix content in the matrix-supported breccia/conglomerate beds lies in the range 60–90% with an upward increase both at Svodene–Ritlandsfjellet and in the Bjødnabuhaugen area. Matrix-supported beds in the Svodene–Ritlandsfjellet section show a very crude normal grading with a significant upward increase in the matrix content. Some fluid-flow features and faint laminations have been found in the coarse-grained matrix of the Svodene section. All these characteristics suggest a subaqueous origin for these debris-flow deposits. The mineralogical composition of the matrix-supported beds from Svodene–Ritlandsfjellet is comparable to that in similar beds in the Bjødnabuhaugen area. Minor differences in the quartz/feldspar ratio and accessory minerals are probably related to compositional variations in the local basement rocks (Tables 1 and 2).

Parallel-bedded conglomeratic sandstone

The conglomeratic sandstones of the UBU from the Bjødnabuhaugen section can be interpreted as hyperconcentrated density-flow deposits (Mulder & Alexander, 2001), deposited during the retreating stage of an active fan setting. Development of hyperconcentrated flows during the retreating stage of small fans has been discussed by Mutti et al. (1996) and Falk & Dorsey (1998). Mulder & Alexander (2001) described similar identical characteristics in both the subaerial and the subaqueous settings. Sohn et al. (1999) discussed hyperconcentrated density-flow deposits in alluvial fan settings, showing thinly bedded (10–30 cm), well- to crudely-stratified sandstones sandwiched between 'debris-flow deposits' and 'stream-flow deposits', and interpreted the mechanism as a 'bipartite' division of flow.

The UBU sediments at the Bjødnabuhaugen section clearly indicate a well developed fan compared to the Svodene–Ritlandsfjellet fan. The MPS/BTH profile of the Bjødnabuhaugen section (Fig. 10) shows that the lower part of the profile consists of matrix-supported to conglomeratic sandstones, a middle part mostly consisting of clast-supported breccia/conglomerate and an upper part consisting of matrix-supported or conglomeratic sandstones showing an upward-fining trend. The bed thickness is also proportional to the clast-size distribution where a maximum bed thickness has been found in the middle part, with the beds thinning significantly in the lower and upper parts. Outsize clasts are still found within these thin sandstone beds, either floating or protruding. The coarsening- and thickening-upward trend from the lower to the middle part (Fig. 10) can be interpreted to represent progradation of a proximal-fan segment over distal-fan deposits. The fining- and thinning-upward trend from the middle to the upper parts (Fig. 10) probably represents the retreat of an active fan segment.

Depositional model—synthesis

The mineralogical composition of both the clasts and the matrix (Tables 1 and 2) of the crater-filling sediments of the 2.7 km-diameter Ritland impact structure suggests that they were derived from the impact-generated debris during different stages of crater modification and deposited as individual fan lobes prograding towards the crater centre (Fig. 15).

The palaeoenvironmental setting of the Ritland area is crucial for understanding the sedimentary processes that were active in and around the crater. According to Riis et al. (2011) the impact event took place after the

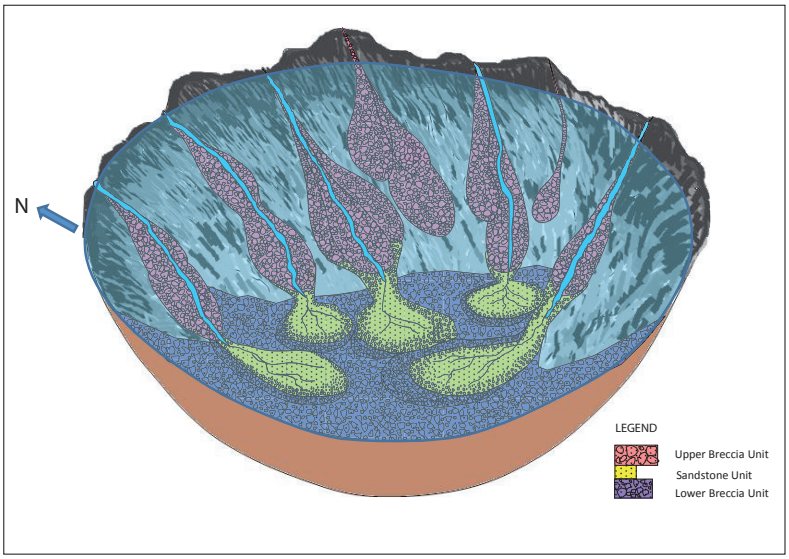

Figure 15. *Simplified conceptual model of the sedimentation processes of different sedimentary units in the Ritland crater. The fan at the right-hand side represents the Svodene–Ritlandsfjellet fan showing the possible field relationships between the three different sedimentary units. The Bjødnabuhaugen fan is to the left, especially showing the crater-filling sediments at higher stratigraphical levels; sediments lower in the stratigraphical column are not well exposed, or concealed. The Stemhaugen fan to the west has not been shown in the model as the model represents just one-half of the crater. The field relationships suggest that the Stemhaugen fan is relatively less well developed and was probably subjected to major sliding during the late syn-impact stage. The light blue shade represents the water-filled situation of the crater.*

Cambrian marine transgression, which suggests that an early epicontinental sea existed in the Ritland area. The Gardnos structure, which is assumed to have been roughly contemporaneous with the Ritland impact structure, was therefore probably formed in a similar geological setting of an epicontinental sea (Kalleson et al., 2008). The water depth during impact for other Fennoscandian impact craters in epicontinental sea settings are: Tvären (100–150 m; Ormö & Lindström, 2000), Kärdla (~50 m; Suuroja et al., 2002), Lockne (500–700 m; Ormö et al., 2007) and Granby (50–100 m; Brunn & Dahlman, 1982). The water depth of the contemporary epicontinental sea is one of the most important factors governing the sedimentation in the Ritland crater.

If the water depth during the impact event at the Ritland site was less than 100 m, the crater rim (110 m high) could have acted as a barrier preventing an instantaneous powerful resurge of the seawater into the crater, and the crater may thus have behaved initially as a subaerial target crater. The sedimentation pattern within the Ritland crater as presented here is fairly compatible with a subaerial target crater during the initial stages of impact, with a slow return of seawater afterwards. No specific evidence of powerful resurge processes have been found within the Ritland crater sediments. Generally, a resurge event within a crater would be represented by a sudden and enormous influx of seawater mixed with debris of varying grain size and shape washed out of the crater rim wall and mixed with ejecta and sediments from outside the impact area. The resurge will take place at the end of the crater modification stage, and 'resurge deposits' should be encountered with erosional bases towards the fall-back breccias (Sturkell, 1998). Resurge deposits can be distinguished from slump breccias by a marked fining-upward sequence due to gravitational separation of the suspended sediments. In the Swedish Tvären crater, a fining-upward sequence (60 m) has been interpreted as 'graded resurge deposits' with a sharp erosional contact to the underlying shock-metamorphosed breccia (Lindström et al., 1994; Ormö et al., 2007). The Lockne crater shows granulometric divisions in the resurge deposits related to differences in the flow dynamics of the resurge event, e.g., resurge proper, anti-resurge and oscillating resurge (Ormö et al., 2007). Sedimentary features, e.g., erosional scours, rip-up clasts, injection and deformation structures, are most likely to be encountered in the lower parts of the resurge deposits. However, in the case of coarse-grained sediments these features may not be present. Due to rapid settling of the suspended sediments, soft-sediment deformation and water-escape structures could also be found in the finer-grained sediments. The LBU sediments in the Ritland impact structure do not show any of these characteristics of 'resurge deposits', indicating a typical gravity-controlled sedimentation comparable to that in a subaerial target crater. The sedimentation started by slumping of the steep transient cavity walls and rim, and the sediments eventually slid down towards the crater centre as rock avalanches. With a gradual and slow resurge of seawater, the flow transformed into a mass-flow process with debris flows becoming hyperconcentrated density flows. The upward transition from clast-supported breccia to clast-supported conglomerate, and matrix-supported conglomerate to conglomeratic sandstone, clearly suggests that these sediments have been deposited by gradual and confined flow-transformation processes.

So far, differentiating the redeposited fall-back ejecta (French, 1998) from the slump-back breccias/slump debris within the crater has not been possible. In the case of a shallow water depth at the target site, most of the large ejecta blocks would have been thrown out into the sea, whereas very thin layers of fall-back ejecta materials consisting of smaller clasts and shocked particles would probably be encountered within the crater. In the lowermost part of the LBU, just above the strata of melt origin, there is a 20 cm-thick matrix-supported breccia bed (Figs. 3 and 4.). This unit may represent a possible ejecta layer mixed with slump-back materials.

The average quartz/feldspar ratio within the crater-filling sediments is significantly lower (0.20 XRD) than the quartz/feldspar ratios of the pre-impact sediments (0.93 XRD) (Setså, 2011), suggesting that the resurge of the reworked pre-impact sediments was fairly insignificant within the crater. The matrix mineral composition of the crater-filling sediments is similar to that of the basement breccia (Table 2), suggesting that these sediments were mostly derived from the fresh, unweathered, impact-related debris. Also, the mineralogical composition of the crater-filling sediments from the three different depositional areas does not vary much (Tables 1 and 2). The average quartz/feldspar ratio (XRD) of the LBU sediments from the Svodene–Ritlandsfjellet area (0.15) is comparable to that of the LBU sediments from the Stemhaugen area (0.20) (Table 2). Similar results have also been found for conglomeratic sandstones from the Svodene–Ritlandsfjellet (0.13) and Stemhaugen areas (0.20) (Table 1). The average quartz/feldspar ratio of UBU sediments from the Bjødnabuhaugen area (0.31) is slightly higher compared to the Svodene–Ritlandsfjellet area (0.16). K-feldspar dominates in the Svodene–Ritlandsfjellet sediments as compared to the sediments from other depositional areas. Among the other accessory minerals, sporadic enrichments of mica and amphibole are found in a few samples from all sites. These minor variations in mineral composition are probably related to compositional variations within the local basement rocks from where they have been derived. Minerals such as apatite, calcite, ankerite and mica have been found in a few samples, and are assumed to have been derived from the Cambrian sedimentary deposits (Bjørlykke & Englund, 1979), both from the pre-impact sediments outside the crater (Setså, 2011) and within the crater-filling sediments, suggesting that some inflow of extra-crater, pre-impact sediments occurred shortly after the impact event. Exceptionally rounded quartz grains probably represent the reworked pre-impact sediments that were transported within the crater-filling sediments. Enrichment of potassium (due to higher amounts of feldspar and mica) and titanium (due to the occurrence of diagenetically formed sphene and anatase) have been reported from the Neoproterozoic and Lower Cambrian sediments (Bjørlykke & Englund, 1979); these were also found within the LBU sediments from both the Svodene–Ritlandsfjellet and Stemhaugen areas.

The depositional conditions of the SU remain uncertain due to the very local occurrence of this unit in the field. Deposition of the SU in the Svodene section could be related to a local breaching of the crater rim. In the Ritland crater, the first breaching of the crater rim probably took place at the southwestern margin (Svodene–Ritlandsfjellet area) through which the seawater slowly resurged into the crater. The Kärdla crater (4 km in diameter) could be a close analogue to Ritland, formed in crystalline basement that was covered by just a few tens of metres of water (Puura & Suuroja, 1992). The Kärdla crater has a well developed rim wall. To the north and south the rim breached due to modification collapse followed by a rather low-energy inflow of sediment-laden water. The post-impact stratigraphy is relatively more complete within these 'resurge gullies' (Puura & Suuroja, 1992). The formation of resurge gullies has been explained as a consequence of an oblique impact and structural irregularities in the crystalline rim (Suuroja et al., 2002). The crater-filling history of the Ritland crater may thus have close similarities with the Kärdla, and probably involved a structural irregularity of the rim. Evidence of such structural irregularity at the western crater rim (Stemhaugen area) has been found (Fig. 2A) where the stratigraphy of the crater-filling sediments is less complete compared to the stratigraphy of the southwestern part. This may also be linked with an oblique angle of impact. A closer study on the distribution of ejecta (Kalleson et al., 2012) at Ritland may help to confirm this statement. The basinward-dipping beds of the SU with their fan-shaped geometry (Fig. 8) strongly suggest the establishment of some channel inlets or resurge gullies in the southwestern part of the crater through which the sediments were transported and eventually deposited in the distal part of the crater basin.

Considerable differences in the quartz/feldspar ratios and textural properties of the SU (Figs. 12 and 13) compared with the pre-impact sediments (Setså, 2011) suggest that highly reworked impact-derived debris is the main source of these sandstones. The low-relief, Early Cambrian landscape and epicontinental sea, with low-angle river-sea equilibrium, suggest a minimal clastic influx from outside the crater. In addition, the ground surge of the ejecta curtain during the cratering process may have swept out the thin, pre-impact, sedimentary cover almost entirely from the vicinity of the crater, as discussed in the case of Kärdla (Puura & Suuroja, 1992) and Gardnos (Kalleson et al., 2008). The major clastic influx in the SU was likely to have been derived from the impact-related debris which was intensely reworked during its downslope transport, and redeposited in the distal part of the basin as in Crater Lake, Oregon, USA, where fine-grained, well-sorted and graded sand layers were deposited in the distal part of the Crater Lake basin. These sediments were interpreted to have been transported by sheet-flow turbidity currents and deposited in a non-channellised submarine-fan system

(Nelson et al., 1986). The sediments of the SU were also probably deposited in a submarine-fan setting (Fig. 15). However, individual channel-levee complexes in the SU of the Ritland structure have so far not been detected, primarily due to the scarcity of field exposures. Sedimentary features related to the channellised flow, e.g., cross-bedding, ripple marks and scour marks, have been found in the SU, in contrast to the sheet-flow turbidity currents and non-channellised fan settings of Crater Lake.

The UBU sediments were probably deposited after the deposition of most of the suspended sediments (SU), thus post-dating the resurge event, although a synchronous origin of these two units cannot be ruled out. Field observations and crater morphology in the Svodene–Ritlandsfjellet area (Fig. 2A) suggest that the transport of these coarser clastics may be associated with the resurge gullies formed at the southwestern part of the crater during the late syn-impact stage. The erosional contact of the UBU to the underlying SU and the presence of abundant, large, angular granitic and gneissic clasts in the upper part of the SU could indicate a synchronous origin of these two units. Sandstones were deposited at the crater centre, probably from suspension currents, whereas scree, rock- or debris-avalanche processes were seemingly active in the steep crater walls. However, the fan-building processes probably continued through a significant span of time as indicated by the well-developed wedges and significant variations in clast size and a higher average quartz/feldspar ratio in the Bjødnabuhaugen area (Figs. 10 and 13). The sediments were derived from the continued local erosion of the unstable, steep, crater rim and wall, and deposited by different gravity-flow processes (Fig. 15), and the crater probably remained as a depression beneath the Cambrian epicontinental sea until it was filled with marine clays.

Conclusions

Based on field mapping and sedimentological study the late syn-impact and early post-impact sediments are classified into three units: i) Lower Breccia Unit, ii) Sandstone Unit and iii) Upper Breccia Unit. The textural zonation and the occurrence of dispersed particles of melt origin in the lower part of the LBU suggest a late syn-impact origin for these sediments. These particular sediments were deposited seconds after the impact, when the crater was behaving like a subaerial crater. Sedimentary signatures suggest that these sediments were deposited as rock-avalanche deposits (Fig. 15). Clast-supported conglomerates stratigraphically overlying these breccia beds show evidence of deposition from subaerial, cohesive, debris flows at an early post-impact stage (Fig. 15). Upwards, a clear shift from clast-supported to matrix-supported texture, representing a flow transformation from cohesive debris flows to hyperconcentrated density flows, might have arisen from a mixing with water and dilution of the flow head. This was probably caused by a resurge of the seawater with reduced energy, breaching and seeping through the unstable and weaker part of the crater rim, minutes after the impact. The localised breaching resulted in crater filling probably within hours/days, until finally suspension deposition dominated.

The SU probably represents the first suspension-dominated sedimentation in the Ritland crater. The parallel-bedded sandstones indicate a shift in depositional conditions from mass flows to more fluidal flows. These sediments were deposited as surge or surge-like turbidites. The coarsening-upward sandstones suggest an increase in clastic input possibly related to further slope erosion and reworking of the sediments deposited during the fan-lobe progradation (Fig. 15). Conglomeratic or breccia beds coexisting with the homogeneous sandstones can be related to the multiple breaching flows leading to increased slope erosion and further clastic input.

The UBU represents sedimentation in the marginal part of the crater basin. These sediments show well-developed wedges from the rim to the crater centre with a fan-like distribution. The clast-supported breccia beds appearing within this sedimentary unit probably accumulated as scree, rock-avalanche or debris-avalanche deposits (Fig. 15). The matrix-supported breccia/conglomerates were probably deposited as debris-flow deposits and were derived from the further reworking of the clast-supported sediments during downslope transport. The conglomeratic sandstone beds at the Bjødnabuhaugen section were probably deposited from hyperconcentrated density flows during the retreating stage of the fan setting. The crater was probably completely drowned soon after the resurge and remained as a depression beneath the Cambrian sea for a long time, eventually being filled with marine clays.

Acknowledgments. We express our sincere gratitude to the other Ritland project group members for their kind assistance and invaluable discussion. Adrian Read kindly corrected the language, while the thoughtful comments of referees Drs. Kevin Evans and Alex Deutsch are greatly appreciated. We are also grateful to the Sven Egil and Kari Sørensen family for lodging and transport during the field days at Ritland. The Research Council of Norway generously supported the three-year Ritland project; we greatly appreciate this. Finally, the lab technicians and the people of Ritland are acknowledged for their support and assistance.

References

Aksu, A.E. & Hiscott, R.N. 1992: Shingled Quaternary debris flow lenses on the north-east Newfoundland slope. *Sedimentology 39*, 193–206.

Andresen, A. 1982: *Stratigraphy and structural history of the Lower Palaeozoic metasediments on Hardangervidda, South Norway*. PhD thesis, University of California, 260 pp.

Bergström, J. & Gee, D.G. 1985: The Cambrian of Scandinavia. *In* Gee, D.G. & Sturt, B.A. (eds.): *The Caledonide Orogen—Scandinavia and related areas*, John Wiley & Sons, Chichester, pp. 247–271.

Bjørlykke, K. & Englund, J.O. 1979: Geochemical response to Upper Precambrian rift basin sedimentation and Lower Palaeozoic epicontinental sedimentation in South Norway. *Chemical Geology 27*, 271–295.

Blair, T.C. & McPherson, J.G. 1994: Alluvial fans and their natural distinction from rivers based on morphology, hydraulic processes, sedimentary processes, and facies assemblages. *Journal of Sedimentary Research A64*, 450–489.

Bouma, A.H. 1962: *Sedimentology of some flysch deposits: a graphic approach to facies interpretation*. Elsevier, Amsterdam, 168 pp.

Brasier, M.D., Anderson, M.M. & Corfield, R.M. 1992: Oxygen and carbon isotope stratigraphy of Early Cambrian carbonates in southeastern Newfoundland and England. *Geological Magazine 129*, 265–279.

Bruton, D.L. & Harper, D.A.T. 2000: A mid-Cambrian shelly fauna from Ritland, western Norway and its palaeogeographical implications. *Bulletin of the Geological Society of Denmark 47*, 29–51.

Bruton, D.L., Gabrielsen, R.H. & Larsen, B.T. 2010: The Caledonides of the Oslo Region, Norway—stratigraphy and structural elements. *Norwegian Journal of Geology 90*, 93–121.

Bruun, Å. & Dahlman, B. 1982: Den palaeozoiska berggrunden. *In* Wikman, H., Bruun Å, Dahlman, B. & Vidal, G (eds.): *Beskrivning till berggrundskartan Hjo NO*, Sveriges Geologiska Undersökning Afl20, pp. 76–109.

Calvari, S., Tanner, L.H. & Groppelli, G. 1998: Debris-avalanche deposits of the Milo Lahar sequence and the opening of the Valle del Bove on Etna volcano (Italy). *Journal of Volcanology and Geothermal Research 87*, 193–209.

Costa, J.E. & Williams, G.P. 1984: Debris flow dynamics. *U.S. Geological Survey, Open-file Report 84–606 (videotape)*.

Davies, T.R.H. 1982: Spreading of rock avalanches debris by mechanical fluidization. *Rock Mechanics 15*, 9–24.

Dons, J.A. & Naterstad, J. 1992: The Gardnos impact structure, Norway (abstract). *Meteoritics 27*, 215.

Dypvik, H. & Kalleson, E. 2010: Mechanisms of late synimpact to early postimpact crater sedimentation in marine-target impact structures. *Geological Society of America Special Papers 465*, 301–318.

Dypvik, H., Gudlaugsson, T.S., Tsikalas, F., Attrep, M., Ferrell, R.E. Jr., Krinsley, D.H., Mørk, A., Faleide, J.I. & Nagy, J. 1996: The Mjølnir structure—An impact crater in the Barents Sea. *Geology 24*, 779–782.

Dypvik, H., Plado J., Heinberg, C., Håkansson, E., Pesonen, L.J., Schmitz, B. & Raiskila, S. 2008: Impact structures and events—a Nordic perspective. *Episodes 31*, 107–114.

Earth Impact Effects Program, http://impact.ese.ic.ac.uk. (accessed 18.07.12).

Embley, R.W. 1976: New evidence for occurrence of debris flow deposits in the deep sea. *Geology 4*, 157–173.

Falk, P.D. & Dorsey, R.J. 1998: Rapid development of gravelly high-density turbidity currents in marine Gilbert type fan deltas, Lorento Basin, Baja California Sur, Mexico. *Sedimentology 45*, 331–349.

Folk, R.L. 1974: *Petrology of Sedimentary Rocks*. Hemphill Publishing, Texas, USA, 182 pp.

French, B.M. 1998: Traces of catastrophe: A handbook of shock-metamorphic effects in Terrestrial meteorite impact structures. *LPI Contribution No. 954*, Lunar and Planetary Institute, Houston, 120 pp.

French, B.M., Koeberl, C., Gilmour, I., Shirley, S.B., Dons, J.A. & Naterstad, J. 1997: The Gardnos impact structure, Norway: Petrology and geochemistry of target rocks and impactites. *Geochimica et Cosmochimica Acta 61*, 873–904.

Gani, M.R. 2004: From turbid to lucid: A straightforward approach to sediment gravity flows and their deposits. *The Sedimentary Record 2*, 4–8.

Goldschmidt, V.M., 1925: Ueber Fossilfürende untercambrische Basalablagerungen bei Ustaoset. *Fennia 45*, 1–11.

Gudlaugsson, S.T. 1993: Large impact crater in the Barents Sea. *Geology 21*, 291–294.

Hallam, A. 1981: *Facies interpretation and the stratigraphic record*. Freeman, Oxford, 291 pp.

Hampton, M.A. 1972: The role of subaqueous debris flows in generating turbidity currents. *Journal of Sedimentary Petrology 42*, 775–793.

Haughton, P.D.W., Barker, S.P. & Mccaferey, W.D. 2003: Linked debrites in sand-rich turbidite systems—origin and significance. *Sedimentology 50*, 459–482.

Henningsmoen, G. 1952: Early Middle Cambrian fauna from Rogaland, SW Norway. *Norsk Geologisk Tidsskrift 30*, 13–31.

Hewitt, K. 1999: Quaternary moraines vs catastrophic rock avalanches in the Karakoram Himalaya, northern Pakistan. *Quaternary Research 51*, 220–237.

Hubert, H.J. & Filipov, A.J. 1989: Debris-flow deposits in alluvial fans on the west flank of White Mountains, Owens Valley, CA, USA. *Sedimentary Geology 61*, 177–205.

Iverson, R.M. 1997: The physics of debris flows. *Reviews of Geophysics 35*, 245–296.

Kalleson, E., Dypvik, H. & Naterstad, J. 2008: Post-impact sediments in the Gardnos impact structure, Norway. *In* Evans, K., Horton, Jr. J.W., King, Jr. D.T. & Morrow J.R. (eds.): *The Sedimentary Record of Meteorite Impacts*, Geological Society of America Special Paper 437, pp. 19–41.

Kalleson, E., Corfu, F. & Dypvik, H. 2009: U–Pb systematics of zircon and titanite from the Gardnos impact structure, Norway: evidence for impact at 546 Ma? *Geochimica et Cosmochimica Acta 73*, 3077–3092.

Kalleson, E., Dypvik, H. & Nilsen, O. 2010: Melt-bearing impactites (suevite and impact melt rock) within the Gardnos structure, Norway. *Meteoritics and Planetary Science 45*, 798–827.

Kalleson, E., Riis, F., Setså, R. & Dypvik, H. 2012: Ejecta Distribution and Stratigraphy—Field Evidence from the Ritland Impact Structure. Abstract no. 1351, 43rd Lunar and Planetary Science Conference, Texas, USA.

Kalleson, E., Dypvik, H. & Riis, F. submitted: The melt-bearing impactites in the Ritland structure. *Meteoritics & Planetary Science.*

Kessler, L.G. & Bédard, J.H. 2000: Epiclastic volcanic debrites—Evidence of flow transformations between avalanche and debris flow processes, Middle Ordovician, Baie Verte Peninsula, Newfoundland, Canada. *Precambrian Research 101*, 135–161.

Knaust, D. 2004: Cambro-Ordovician trace fossils from the SW-Norwegian Caledonides. *Geological Journal 39*, 1–24.

Kneller, B.C. 1995: Beyond the turbidite paradigm: physical models for deposition of turbidites and their implications for reservoir prediction. *In* Hartley, A.J. & Prosser, D.J. (eds.): *Characterization of deep marine clastic systems*, Geological Society of London, Special Publication 94, pp. 31–49.

Larsen, V. & Steel, R.J. 1978: The sedimentary history of a debris flow-dominated alluvial fan: A study of textural inversion. *Sedimentology 25*, 37–59.

Lindström, M., Flodén, T., Grahn, Y. & Kathol, B. 1994: Post-impact deposits in Tvären, a marine Middle Ordovician crater south of Stockholm, Sweden. *Geological Magazine 131*, 91–103.

Martinsson, A. 1974: The Cambrian of Norden. *In* Holland, C.H. (ed.): *Lower Palaeozoic rocks of the world, Cambrian of the Brithish Isles, Norden and, Spitzbergen*, John Wiley & Sons, Chichester, pp. 185–283.

Melosh, H.J. 1987: The mechanics of large rock avalanches. *Geological Society of America, Reviews in Engineering Geology 7*, 41–49.

Melosh, H.J. 1989: *Impact cratering: a geological process*. Oxford University Press, New York, 245 pp.

Melosh, H.J. & Ivanov, B.A. 1999: Impact crater collapse. *Annual Review of Earth Planetary Sciences 27*, 385–415.

Morris, C., Sieve, B.J. & Bullen, H.A. 2008: E-Learning Module: Introduction to X-ray Diffraction. http://www.asdlib.org/onlineArticles/ecourseware/Bullen_XRD/XRDModule_index.htm (accessed. 01.05.11)

Mulder, T. & Alexander, J. 2001: The physical character of subaqueous sedimentary density flows and their deposits. *Sedimentology 48*, 269–299.

Mutti, E. 1977: Distinctive thin-bedded turbidite facies and related depositional environments in the Eocene Hecho Group (South-central Pyrenees, Spain). *Sedimentology 24*, 107–131.

Mutti, E., Davoli, G., Tinterri, R. & Zavala, C. 1996: The importance of fluvio-deltaic systems dominated by catastrophic flooding in tectonically active basins. *Science Geological Memoir 48*, 233–291.

Nelson, C.A., Meyer, A.W., Thor, D. & Larsen, M. 1986: Crater Lake, Oregon: A restricted basin with base-of-slope aprons of nonchannelized turbidites. *Geology 14*, 238–241.

Nemec, W. & Steel, R.J., 1984: Alluvial and coastal conglomerates: their significant features and some comments on gravelly mass-flow deposits. *In* Koster, L. H. & Steel, R. J. (eds.) *Sedimentology of Gravels and Conglomerates*, Canadian Society of Petroleum Geology Memoir 10, pp. 1–31.

Nielsen, A.T. & Schovsbo, N.H. 2007: Cambrian to basal Ordovician lithostratigraphy in southern Scandinavia. *Bulletin of the Geological Society of Denmark 53*, 47–92.

Nielsen, A.T. & Schovsbo, N.H. 2011: The Lower Cambrian of Scandinavia: Depositional Environment, Sequence Stratigraphy and Palaeogeography. *Earth Science Reviews 107*, 207–310.

Ormö, J. & Lindström, M. 2000: When a cosmic impact strikes the seabed. *Geological Magazine 137*, 67–80.

Ormö, J., Sturkell, E. & Lindström, M. 2007: Sedimentological analysis of resurge deposits at the Lockne and Tvären craters: clues to flow dynamics. *Meteoritics & Planetary Science 42*, 1929–1943.

Puura, V.A. & Suuroja, K. 1992: Ordovician impact crater at Kärdla, Hiiumaa Island, Estonia. *Tectonophysics 216*, 143–156.

Riis, F. 2001: En kraterstruktur i det subkambriske peneplanet ved Ritland, Ryfylke—sannsynligvis dannet ved meteorittnedslag (abstract). *Geonytt: Medlemsblad for Norsk Geologisk Forening*, 94.

Riis, F., Dypvik, H. & Krøgli, S.O. 2008: The Ritland Crater—An early Cambrian impact structure in West Norway (abstract # PIS–01805L). Abstract Volume, International Geological Congress, Oslo 6.–14. August 2008, Oslo, Norway (published online at http://www.cprm.gov.br/33IGC/1338980.html).

Riis, F., Kalleson, E., Dypvik, H., Krøgli, S.O. & Nilsen, O. 2011: The Ritland impact structure, southwestern Norway. *Meteoritics and Planetary Science 46*, 748–761.

Setså, R. 2011: *The Ritland impact structure: Characteristics and distribution of the ejecta layer and associated Lower Paleozoic sedimentary succession*. MSc thesis, University of Oslo, 111 pp.

Shuvalov, V., Dypvik, H., Riis, F., Kalleson, E. & Setså, R. 2012: Modelling the 2.7 km in diameter, shallow marine Ritland crater. *Earth, Planets and Moon 108*, 175–188.

Sigmond, E.M.O. 1978: Beskrivelse til det berggrunnsgeologiske kartbladet Sauda 1:250 000 (in Norwegian, English abstract). *Norges geologiske undersøkelse 341*, 1–94.

Sohn, Y.K., Rhee, C.W. & Kim, B.C. 1999: Debris flow and hyperconcentrated flood-flow deposits in an alluvial fan, Northwestern part of the Cretaceous Yongdong Basin, central Korea. *Journal of Geology 107*, 111–132.

Spjeldnæs, N. 1985: Biostratigraphy of the Scandinavian Caledonides. *In* Gee, D.G. & Sturt B.A (eds.): *The Caledonide Orogen—Scandinavia and Related Areas*, John Wiley & Sons, Chichester, pp. 317–329.

Sturkell, E.F.F. 1998: Resurge morphology of the marine Lockne impact crater, Jämtland, Central Sweden. *Geological Magazine 135*, 121–127.

Suuroja, K., Suuroja, S., All, T. & Flodén, T. 2002: Kardla (Hiiumaa Island, Estonia)—the buried and well-preserved Ordovician marine impact structure. *Deep-Sea Research II 49*, 1121–1144.

Tomczyk, M. 2010: *Post-impact sedimentation in the Ritland impact structure, South-western Norway*. MSc thesis, University of Oslo, 92 pp.

Wentworth, C.K. 1922: A scale of grade and class terms for clastic sediments. *Journal of Geology 30*, 377–392.

Paper 2

Late post-impact sedimentation in the Ritland impact structure, western Norway.

By

Azad, A. S., Dypvik, H., Riis, F. & Kalleson, E.

Norwegian Journal of Geology, 2013, *Vol. 93(1), p. 37-59 (in print).*

Late post-impact sedimentation in the Ritland impact structure, western Norway

Abdus Samad Azad, Henning Dypvik, Fridtjof Riis & Elin Kalleson

Azad, A.S., Dypvik, H., Riis, F. & Kalleson, E.: Late post-impact sedimentation in the Ritland impact structure, western Norway. *Norwegian Journal of Geology,* Vol 93, pp. 37–59. Trondheim 2013, ISSN 029-196X.

The crater-infilling successions of the 2.7 km-diameter, Ritland impact structure are classified as: (A) late syn-impact, (B) early post-impact and (C) late post-impact sediments. The late post-impact sediments represent later stages of crater sedimentation during stable crater conditions. The transition between the early post-impact and late post-impact crater sedimentation is marked by a ~6 m-thick succession exposed in the south-central part of the crater. The lowermost part of this succession consists of fine- to medium-grained sandstone, deposited from turbidity flows during the retreating or abandonment stage of earlier prograding submarine fans. Fine sandstones intercalated with silty shales in the middle part represent alternating episodes of turbiditic and suspension deposition. Upward transition of this facies into thick, dark-grey to black shales suggests establishment of anoxic to hypoxic bottom-water conditions where sediments were deposited during an extensive period of suspension deposition. Local coarse clastics exposed in the easternmost crater wall represent small-scale scree deposits, suggesting that submarine slides and reworking of the sediments were active processes for a long time after the impact.

Abdus Samad Azad, Henning Dypvik, Department of Geosciences, University of Oslo, PO Box 1047 Blindern, 0316 Oslo, Norway. Fridtjof Riis, Norwegian Petroleum Directorate, PO BOX 600, 4003 Stavanger, Norway. Elin Kalleson, Fyrstikkalleen skole, PO BOX 6660 Etterstad, 0609, Oslo, Norway.

E-mail corresponding author (Abdus Samad Azad): m.a.s.azad@geo.uio.no

Introduction

Crater-infilling sediments of the Cambrian Ritland impact structure of southwestern Norway have been grouped into three broad units: (A) late syn-impact, (B) early post-impact and (C) late post-impact (Azad et al., 2012). The late syn-impact and early post-impact sediments were discussed in Azad et al. (2012). The present paper deals with the later stages of crater sedimentation, representing a shift from the initial dramatic episodes of crater sedimentation (during the late syn- to early post-impact stages) to relatively stable sedimentation during the late post-impact stage. 'Late syn-impact' sedimentation (Dypvik & Kalleson, 2010) within impact craters starts by collapse of the transient cavity and slumping back into the crater by different gravity and mass-flow processes. In an idealised simple crater model, these could include rock avalanches, debris avalanches or debris flows, depending on the physical properties of the target rock, dry or wet target surface (e.g., subaerial, subaqueous/shallow marine, deep marine), crater size, degree of slope failure, and temporal fluidisation of the sediments (Melosh, 1989). The 'early post-impact' crater sedimentation is more erosion dominated and occurred under water-saturated conditions in the case of marine craters (Dypvik & Kalleson, 2010). Sediments are derived from the crater walls and rim and deposited by gravity-controlled processes, e.g., debris flows, turbidity flows (for more details see Dypvik & Kalleson, 2010 and Azad et al., 2012). The late post-impact sedimentation is suspension dominated, consists mostly of fine-grained sediments and commonly represents part of a widespread regional succession. The sedimentation of the late post-impact crater-filling deposits has major importance as it preserves the record of the transition between impact-related (late syn-impact and early post-impact) crater sedimentation and late post-impact geological history.

The Cambro–Ordovician successions in the Norwegian Caledonides were largely affected by thrust nappes directed to the southeast and east (Rey et al., 1997). Within the Caledonian Orogen, only a few thin successions are preserved autochthonously between the Precambrian peneplain and the Caledonian nappes (Bergström & Gee, 1985). The crater-filling sediments of the Ritland impact structure were deeply buried below the lowermost Caledonian nappe, and were scarcely affected by later thrusting. These well-preserved sedimentary successions were later exposed by tectonic activity and glacial erosion, providing opportunities to study the autochthonous Cambrian successions. The main objective of this study is to interpret the depositional mechanisms, sedimentary environments and possible sources of the late post-impact crater infills of the

Ritland impact structure. The study focuses in particular on the distribution, texture, mineralogical composition, structure and geometry of the late post-impact crater-filling sediments.

Geological setting

The Ritland structure is a 2.7 km diameter and 350 m deep, recently confirmed, simple impact structure, probably formed during the Early to Middle Cambrian period (Riis et al., 2011). At the present day, the structure shows remnants of an originally circular depression located in the mountainous terrain of Hjelmeland municipality, Rogaland, southwestern Norway (Fig. 1A). During the Cambrian, the granitic/gneissic sub-Cambrian peneplain was covered by a shallow but extensive epicontinental sea in which a thin unit of unconsolidated marine clays (10–20 m thick) accumulated, forming the target surface of the Ritland bolide impact. The water depth of the existing epicontinental sea was probably ≤100 m, assumed to be close to the size of the bolide (~115 m) (Azad et al., 2012; Shuvalov et al., 2012). Today, the sub-Cambrian peneplain is well exposed in the southeastern part of the crater, representing the remnants of a wide, flat, slightly undulating surface where the crater forms a topographic depression (Riis et al., 2011). The crater depression was initially filled by impact-derived coarser clastic material, e.g., breccias, conglomerates (Fig. 1B), mainly related to rock avalanches, while debris-flow and concentrated density-flow deposits dominated over rock avalanches during the early post-impact stage (Azad et al., 2012). Turbidity-current deposition dominated afterwards, when the crater was completely submerged by seawater. Different gravity-controlled sedimentary processes were also active, especially along the crater margins in the early post-impact stage (Azad et al., 2012). During the late post-impact stage, dark-grey to black marine clays were deposited (Fig. 1B). The Cambro–Ordovician sandstone covering the marine shales (Fig. 1B) represents a shallowing of the existing epicontinental sea (Knaust, 2004). At that time, the stable crater depression was apparently completely filled with sediments (Riis et al, 2011). The crater infills were subsequently deeply buried by the Caledonian thrust nappes (Fig. 1B) during the development of the Caledonian Orogen in Mid Silurian to Early Devonian time (Gee et al., 2008). Succeeding tectonic episodes during Late Palaeozoic to Cenozoic time, and finally several glacial episodes in the Quaternary period, helped to erode and expose the present-day impact structure.

Materials and methods

Detailed field investigations were carried out to map the late post-impact sediments exposed in the Svodene–Ritlandsfjellet and Dormålsknuten areas (Fig. 2). Sedimentary logs from both these sections were prepared to gain a better understanding of the lithofacies distribution. The lithofacies distribution map (Fig. 2) is based on a high-resolution, aerial-photo map with a contour interval of 5 m. Two geological profiles, from the crater centre to Svodene–Ritlandsfjellet (southwestern crater wall) (Fig. 3) and Dormålsknuten (northeastern crater wall) (Fig. 4), have been constructed to define the stratigraphical relationships of the late post-impact sediments to the late syn-impact and early post-impact sediments. Stratigraphical correlation has been made based on three logged sections to clarify our understanding of the Sandstone Unit–2 (Figs. 5, 6), which represents a transition in crater sedimentation (discussed in this paper) from early post-impact to the late post-impact stage. Another log has been prepared to plot the late post-impact clastics exposed in the Dormålsknuten area (Figs. 7, 8). Gamma measurements were made in the field using the portable RadiogramTM 4000 device. Natural gamma-ray activity was measured in counts per second (cps) for almost every individual bed within the succession to record significant variations in the radioactivity that would indicate any changes in the lithological continuity especially for the shale beds. The counter was placed in direct contact with the fresh bedding surfaces and kept there for at least 10 seconds to obtain optimal values for the natural gamma activity. Comparisons of the detailed sedimentological (Fig. 9) and mineralogical characteristics (Figs. 10, 11) between Sandstone Unit–1 (early post-impact) and Sandstone Unit–2 were made in order to establish the transition in depositional processes and sedimentary environment from the early post-impact to the late post-impact stage. The observations are presented in Table 1. A total of 37 thin sections have been examined under optical and scanning-electron microscopes. Modal compositions (400 grain counts) were determined for 29 of these (Table 2). Semiquantitative determination of mineralogical composition for 17 bulk samples is based on peak height (Morris et al., 2008) of data from XRD (X-ray diffraction) analysis, using a Philips X'Pert MPD, at the University of Oslo. The results are presented in Table 3. Quartz, K-feldspar, plagioclase, calcite, dolomite, mica, chlorite and pyrite were quantified with respective peak values of (d = 4.26 Å), (d = 3.24 Å, 3.25 Å), (d = 3.18 Å, 3.19 Å), (d = 3.03 Å), (d = 2.89 Å), (d = 10 Å), (d = 7 Å), (d = 2.71 Å). The Wentworth (1922) grain-size scale was used for grain-size classification. Folk's (1974) triangular diagram has been used for the classification of sedimentary rocks, e.g., conglomerate, conglomeratic sandstone, sandstone, etc. Based on field observations and mineralogical analyses, depositional models for the late-impact crater sedimentation are presented in Figs. 12 and 13.

Field observations

The late post-impact sediments of the Ritland impact structure have primarily been studied in two different depositional areas representing two different

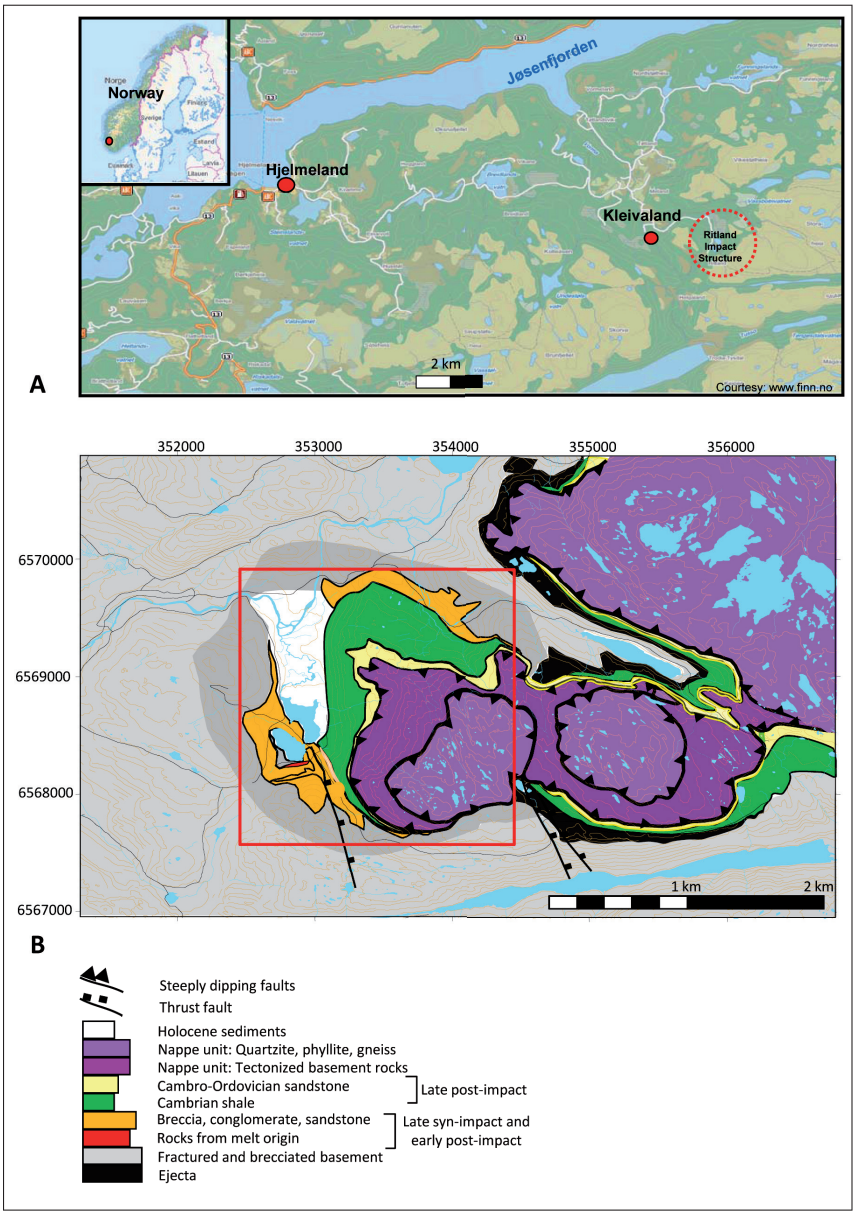

Figure 1. *(A) Location map of the Ritland impact structure. (B) Geological map of the Ritland impact structure based on topographic maps with rivers, lakes (blue), roads (black) and 20 m-interval contour lines (brown), showing the general outline of the crater-filling sedimentary succession and major lithological units inside and outside the crater (slightly modified from Riis et al., 2011); the bold red line indicates the area shown in Fig. 2.*

stratigraphical levels. The sediments exposed in the south-central part (Svodene–Ritlandsfjellet area) (Fig. 2) represent the transition in crater sedimentation from the early post-impact to the late post-impact stage, showing an overall fining-upward relation and indicating a gradual change from high-energy to low-energy sedimentation. The sediments exposed higher up along the northeastern crater wall (Dormålsknuten area) (Fig. 2) are interbedded with dark-grey to black shales. The Dormålsknuten section is located at higher elevations and stratigraphically younger compared to the Svodene–Ritlandsfjellet section, consisting of coarse clastics intercalated with dark-grey to black shales.

Svodene–Ritlandsfjellet area

The late syn-impact and early post-impact sedimentary succession in the Svodene–Ritlandsfjellet area was grouped

into three general stratigraphical units: (i) Lower Breccia Unit, (ii) Sandstone Unit and (iii) Upper Breccia Unit, described in detail by Azad et al. (2012). The sedimentary succession described in the present paper lies stratigraphically above the early post-impact Sandstone Unit, displaying a gradual upward transition into dark-grey to black shales in the central part of the crater (Figs. 2, 3). In this study, the early post-impact Sandstone Unit is renamed Sandstone Unit–1 and the overlying transitional sandstone succession is named Sandstone Unit–2 for clarity (Figs. 2, 3).

Sandstone Unit–2 has been logged at three different locations extending from south to north over a distance of about 100 m (Fig. 2). The beds dip with an angle of 4–7° towards the crater centre and represent a more basin-central location compared to Sandstone Unit–1 (Figs. 2, 3). Presently, the uppermost part of this succession is exposed 450 m above sea level, approximately 270 m below the reference level of the peneplain and stratigraphically located in the field on top of Sandstone Unit–1 and the Upper Breccia Unit (Fig. 3). However, the direct contact between Sandstone Unit–1 and Sandstone Unit–2 has not been found exposed in the field. The thickness of Sandstone Unit–2 is ~6 m, consisting dominantly of sandstones, silty shales and shales. The succession shows a gradational transition from fine- to medium-grained sandstone at the base to alternating layers of fine sand and silty shale in the middle, and dark-grey to black shales towards the top (Fig. 5). Within the succession it was possible to make just a few (four) palaeocurrent-direction measurements from the faint ripple marks. The ripple marks strike within the range 55–100°, indicating a northeastward flow direction (Fig. 2). Sandstone Unit–2 can be further subdivided into three facies types: (i) fine to medium sandstone, (ii) fine sandstone and iii) dark-grey to black shale (Fig. 5).

Fine to medium sandstone

These sandstones are light grey in colour, ~3 m thick, moderately sorted and planar bedded (Figs. 5, 6A). The thickness of the individual beds varies from 10 to 30 cm. The beds are commonly capped by thin silt laminae (10–20 mm thick) and show irregular or undulating erosive boundaries to the underlying beds (Fig. 6A). In a few places, ripple marks have been observed on the bedding-plane surfaces. The rippled beds are a few centimetres in thickness, consisting of silty sands with a typical ripple wavelength of 4 cm and height of 1 cm (Fig. 6B). In the lower part of the succession, a few beds display a concave-up relationship to the underlying beds, probably representing small scale (0.5 m) channels. The individual beds show internal fining-upward features and the overall development of this succession is homogeneous (Fig. 5). Gamma activity measurements in this succession show higher values (350–415 cps) compared to the overlying fine-sandstone and silty-shale facies (255–310 cps) (Fig. 5). A subrounded granitic clast, 40 cm diameter, has been observed embedded within the parallel-bedded sandstones, with associated conformable deformation of both overlying and underlying strata (Fig. 6C). Small-scale convolute laminations are seen in places within these sandstones. An increase in clay content in the sandstones has been recorded in the more distal part (northern part) of the succession. Sedimentary pyrites (diagenetic, 0.5 cm) and mud clasts (subrounded, 2 mm) have also been found. *Cruziana* ichnofacies, possibly *planolites* or *thalassinoides* (N.M. Hanken, pers. comm., 2012), have been observed within a few sandstone beds (Fig. 6D). A similar ichnofacies within these sediments has also been reported by Bruton et al. (1989). The traces are mostly horizontal, undulating, unbranched and convex in nature. Commonly, the length of the trace fossil varies from 10 to 25 cm and the width is 5–10 mm, and the track filled with material similar to that of the host rock. The trace fossils are found in silty sandstone, mostly on the bedding-plane surfaces (Fig. 6D).

Fine sandstone

The middle part of Sandstone Unit–2 is ~1.5 m thick and consists of alternating layers of dark-grey, parallel-bedded, fine sandstones and thinly laminated silty shales (Fig. 5). The thickness of individual fine-grained sandstone beds varies from 2 to 4 cm (Fig. 5). Some medium- to coarse-grained sandstone beds were also found, especially in the upper part of the succession (Fig. 5). The silty shale beds vary in thickness from 0.5 to 2 cm and show an upward increase in thickness (Fig. 5). The boundaries between individual beds are irregular, undulating and locally rippled. Individual beds show a fining upwards and the overall development is irregular/alternating (Fig. 5). Traces of Cruziana ichnofacies have also been found within the silty shale layers.

Dark-grey to black shale

The dark-grey to black shales overlie the fine-grained sandstone facies (Fig. 5). In the south-central part of the crater, the exposed thickness of this unit within the logged profile is only a metre (Fig. 5). In the central part of the crater, the dark-grey to black shale attains a maximum thickness of about 180 m (Riis et al., 2011) (Figs. 2, 3, 4). This shale has been referred to as bituminous shale by Knaust (2004) and contains early Middle Cambrian faunas of trilobites, brachiopods, hyoliths, sponge spicules and various problematica (Henningsmoen, 1952; Bruton et al., 1989). In the upper part of this shale unit, a bed of limestone concretions has been found containing an abundant inarticulate brachiopod fauna (Bruton & Harper, 2000). Based on the fossil content, Bruton & Harper (2000) suggested a correlation of this shale unit with the upper Middle Cambrian Limestone of southern Sweden. These shales are rich in organic matter, flaky, thinly laminated and commonly found with silty partings towards the overlying beds. They display a gradational transition from the silty shale at the base to dark-grey to black shale towards the top. The gamma readings in the lower part of the shale unit in the logged profile are low (215–270 cps) (Fig. 5).

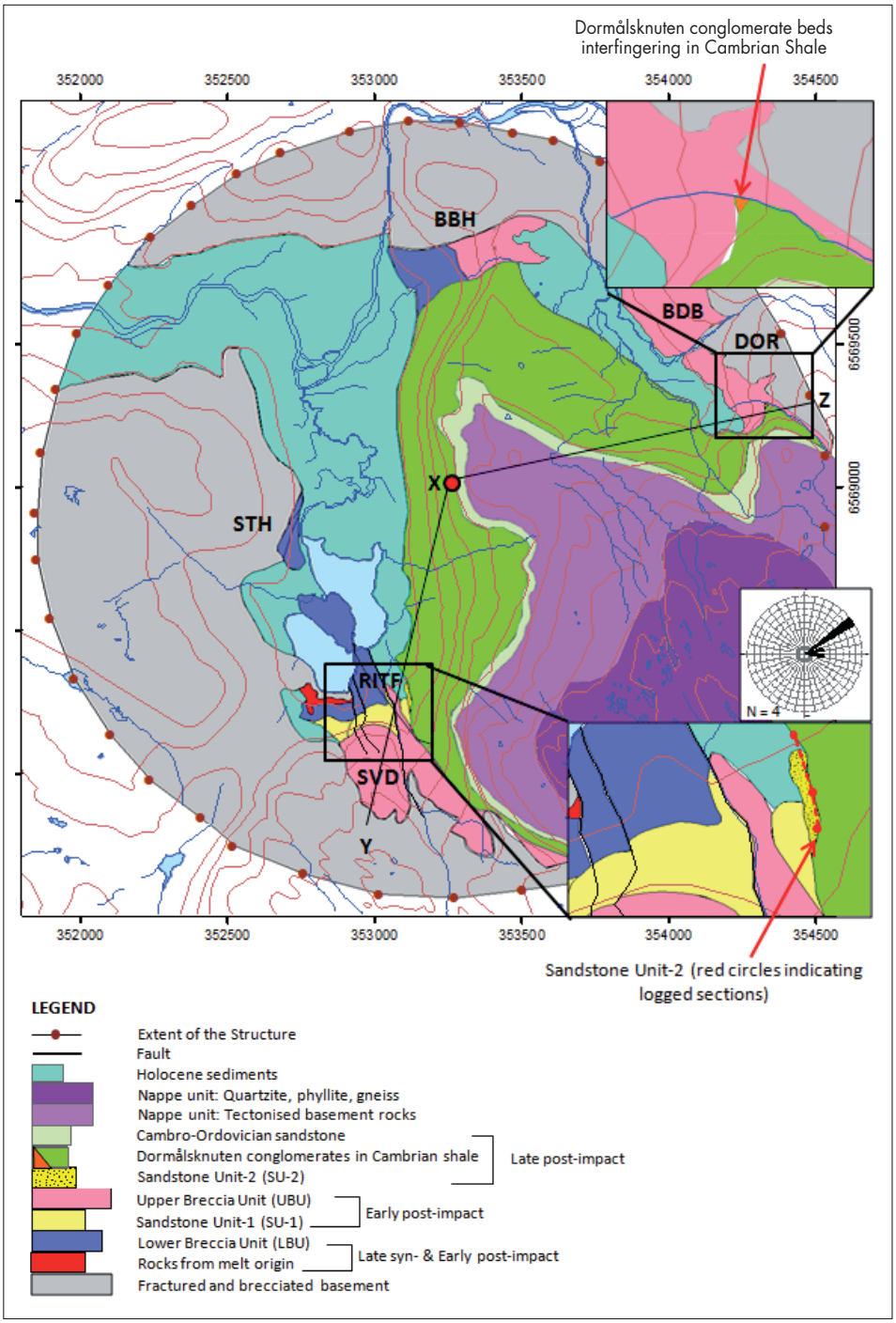

Figure 2. Lithofacies distribution map of the Ritland impact structure (modified from Azad et al., 2012). The Sandstone Unit–2 exposed in the RITF (Ritlandsfjellet) and SVD (Svodene) areas and the conglomerate beds in the DOR (Dormålsknuten) area are shown in two index figures. Other locations on the map are STH (Stemhaugen), BBH (Bjødnabuhaugen) and BDB (Bjødnabu). Rose diagram showing the palaeocurrent flow directions measured in Sandstone Unit–2. Two cross sections along X–Y and X–Z are shown in Figs. 3 and 4, respectively. A stratigraphical correlation (red dotted line, in index photo) of Sandstone Unit–2 is shown in Fig. 5.

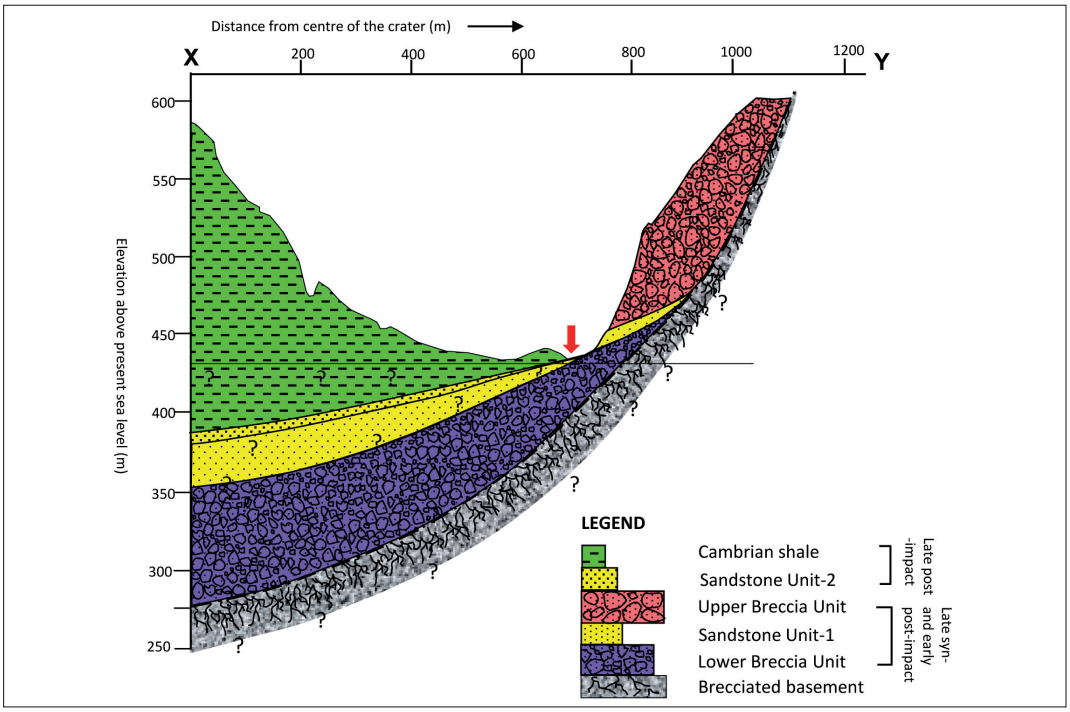

Figure 3. *Geological cross section (X–Y in Fig. 2) illustrating the stratigraphical relationship of Sandstone Unit–2 to other sedimentary units of the late syn-impact, early post-impact and late post-impact stages (Modified from Azad et al., 2012). The profile is drawn from the crater centre towards the Svodene–Ritlandsfjellet area. The base of the crater and the subsurface distribution of the different sedimentary units are drawn based on field observations and the numerical crater model of Shuvalov et al. (2012). The red arrow indicates the locations of the exposed sections of Sandstone Unit–2 within the profile.*

Dormålsknuten area

The Cambrian marine shales in the Dormålsknuten area show onlapping relations to the early post-impact breccias (Upper Breccia Unit) (Azad et al., 2012) in the northeastern crater wall (Fig. 7). The estimated thickness of this marine shale is ~180 m in the crater centre, thinning to almost zero along the crater margin (Fig. 4). At the present day, the top of the marine shale is located at higher elevations (720–760 m) in the northeastern crater wall compared to the crater centre (580 m), showing a concave-up geometric profile (Figs. 4, 7). The thickness of comparable marine shales found outside the crater (southeastern part) is about 35 m (Fig. 1B) (Kalleson et al., 2012). Knaust (2004) reported a thickness of this marine-shale unit outside the crater of about 20 m, possibly omitting the measurement of the 10–20 m-thick, pre-impact shales below the ejecta layer (Kalleson et al., 2012). Inside the crater, towards the top, this shale unit grades into silty shale and siltstone with numerous thin sandstone beds, containing abundant trace fossils (Knaust, 2004). This heterolithic rock grades further into a massive sandstone unit which can be mapped to a thickness of about 10 m inside the crater (Figs. 4, 7). This Cambro–Ordovician sandstone has been interpreted as a 'shoreface deposit' by Knaust (2004), probably deposited when the crater was totally filled with sediments. The autochthonous/parautochthonous unit of Cambrian sedimentary rocks is covered by a number of thrust sheets that involved the uppermost part of the crater-infill succession (Figs. 4, 7).

The contact of the Upper Breccia Unit (early post-impact) towards the brecciated basement is exposed extensively at higher elevations along the northeastern crater wall (Fig. 7). Deeper down, adjacent to this crater wall, the basement contact with the sedimentary breccias has not been found. The field observations and the modelled crater margin (Shuvalov et al., 2012) suggest that a thin veneer of early post-impact breccia (Upper Breccia Unit) stuck to the crater wall (Figs. 4, 7). The sedimentary succession in the Dormålsknuten area is characterised by clast-supported conglomerate beds interbedded with dark-grey to black shales (Figs. 7, 8A).

The thickness of the lowermost clast-supported conglomerate bed (bed–1) is about 1 m (Figs. 7, 8B).

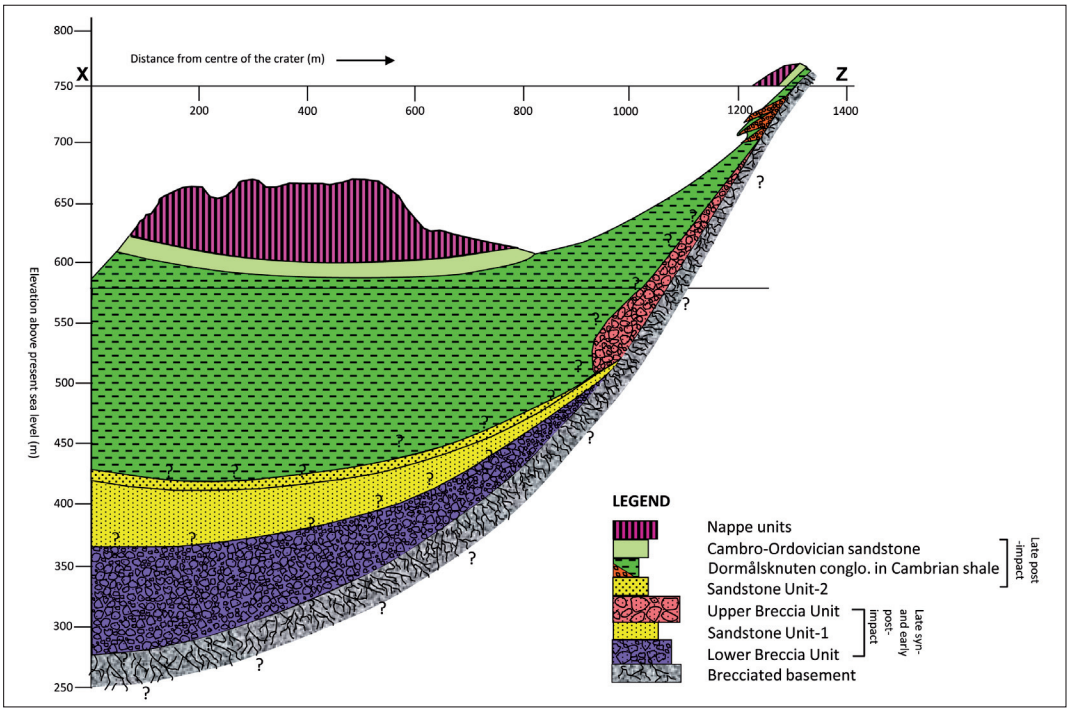

Figure 4. Geological cross section (X–Z in Fig. 2) illustrating the stratigraphical relationship of the Dormålsknuten clast-supported conglomerate beds (drawn in orange, the thickness and extent of the beds are not to scale) to other sedimentary units of the late syn-impact, early post-impact and late post-impact stages. The profile is drawn from the crater centre towards the Dormålsknuten area. The base of the crater and the subsurface distribution of the different sedimentary units are drawn based on field observations and the numerical crater model of Shuvalov et al. (2012).

It appears as a lens within black shale with a lateral extension of about 10 m (Fig. 8A). The bed thins towards the crater centre and dips at an angle of about 20°. The bed is poorly developed and shows an overall increase in the size of the clasts towards the top (Fig. 8B). The clasts are subangular to subrounded and similar in composition to the granitic/gneissic basement (Azad et al., 2012) (Fig. 8B), and range in size mostly from 5 to 15 cm; some larger clasts of 25–30 cm have also been found (Fig. 8B). The matrix content in the bed is fairly high (40–50%), consisting of a mixture of black clay and medium- to coarse-grained sand. The matrix is light grey to dark grey in colour, poorly sorted and has a similar composition to that of the clasts. In a few places, the matrix occurs as centimetre-thick irregular bands within this conglomerate bed (Fig. 8B). The overlying shale beds are deformed around the clasts of the conglomerate bed (Fig. 8B). Towards the top of the bed the larger clasts show possible imbrication or a tendency towards bedding-parallel alignments (Fig. 8B). The maximum clast size vs. bed thickness ratio for this bed is 0.2.

The clast-supported conglomerate bed in the middle (bed–2) is about 1.5 m thick, with a lateral extent of 15 m (Figs. 7, 8A), and also occurs as a lens in the dark-grey shale (Fig. 8A). The bed is poorly developed and the clasts display a slight increase in size in the upper part of the bed. Clast size typically ranges from 15 to 20 cm, with a few clasts up to 50 cm. The clasts and matrix have similar compositions to those in the underlying conglomerate bed (bed–1). This conglomerate bed (bed–2) also thickens towards the crater wall and thins to the crater centre. The maximum clast size vs. bed thickness ratio for this bed shows a higher value (0.4) than in the underlying bed (bed–1).

The uppermost, clast-supported, conglomerate bed (bed–3) is approximately 1 m thick and consists of clasts and matrix of a similar composition to those in bed–1 and bed–2, and occurs as a convex-up lens within shales. Detailed clast-size measurements of this bed were not made due to poor accessibility. Observation from a distance indicates that the average clast size is 15–20 cm; a few outsize clasts exceed 70 cm. The overall clast size increases upwards through the bed. Matrix content is fairly high (30–40%). The matrix shows centimetre-thick

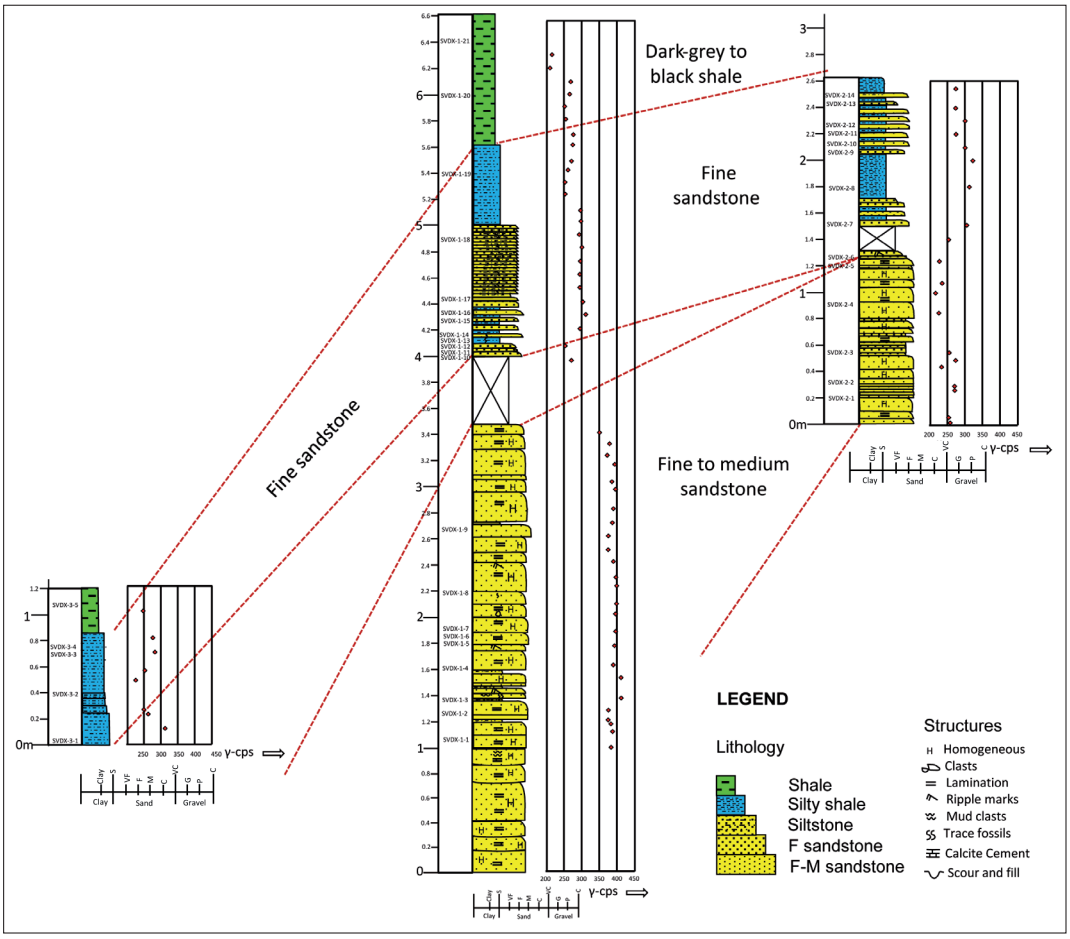

Figure 5. Stratigraphical correlation of Sandstone Unit–2 exposed in the Svodene–Ritlandsfjellet area (see Fig. 2 for geographical locations of the logged sections). The gamma-activity measurements (counts per second, cps) for individual beds are plotted next to the lithofacies column. The rock sample numbers are indicated to the left.

faint bands in a few places within the conglomerate. No obvious alignment or imbrication of the clasts was found. Two outsize clasts up to ~1.8 m in diameter have also been observed embedded within the dark-grey shale beds (at 5.5–6 m in the log) (Figs. 7, 8C). The clasts are granitic in composition, heavily fractured and sub-rounded to rounded in shape (Fig. 8C). The overlying shale layers show brittle deformation and a lamination bending around the clasts (Fig. 8C). Thin veneers of shale surrounding the clasts, marked in Fig. 8C, probably relate to the compaction of the unconsolidated clays during burial. A bed (2–4 cm thick) consisting of pebble-size granitic/gneissic clasts and very coarse-grained sand has been found within the thinly laminated, dark-grey to black shale beds (at 10.6 m in the log) (Figs. 7, 8D). The sandstone is light grey in colour, very poorly sorted and contains a black clayey matrix, and has a slightly erosional base to the underlying shale beds (Fig. 8D).

Comparison between Sandstone Unit–1 and Sandstone Unit–2

The sedimentological and mineralogical characteristics of Sandstone Unit–1 have been compared with those of Sandstone Unit–2 (Table 1) to decipher whether these sediments represent any clear transition in crater sedimentation. Sediments of Sandstone Unit–2 are texturally more mature compared to Sandstone Unit–1 (Table 1). The beds in Sandstone Unit–2 are parallel, well developed and commonly separated by

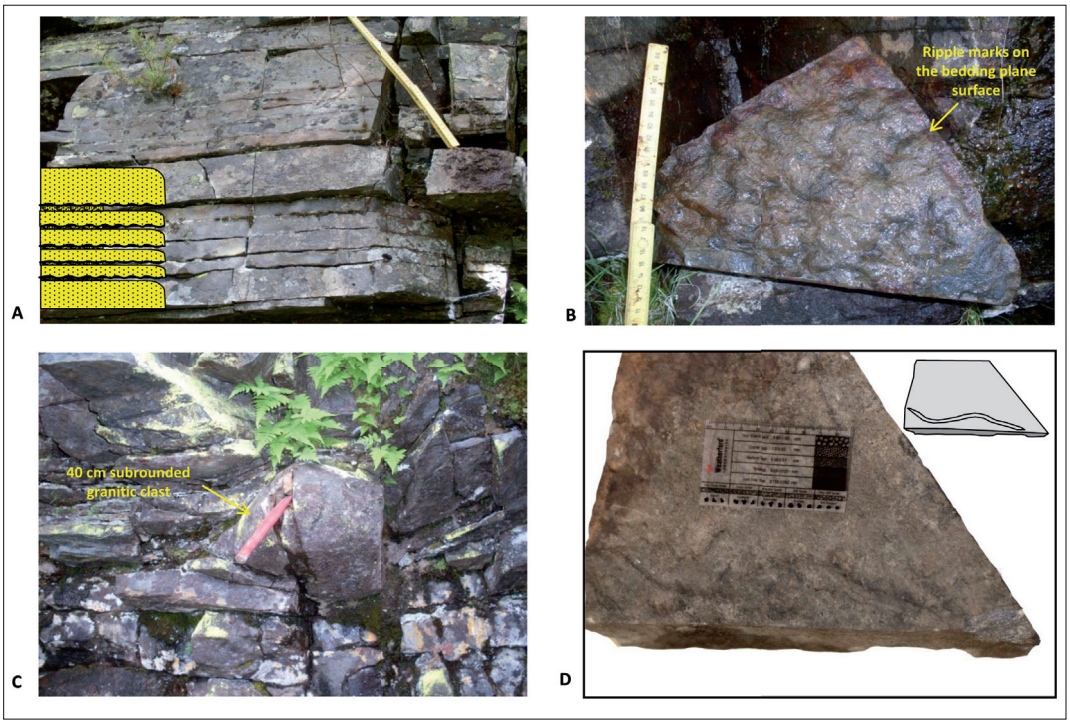

Figure 6. *Sedimentary features of the fine- to medium-grained sandstone facies of Sandstone Unit–2. (A) Parallel beds, commonly capped by thin silt laminae, showing irregular or undulating erosional boundaries to the underlying beds. (B) Faint ripple marks on the bedding planes are locally found (this piece was removed and placed vertically for better visualisation). (C) Granitic clast (40 cm in diameter) found embedded in the parallel-bedded sandstones; note the conformable deformation of the underlying and overlying beds. (D) Horizontal, undulating, unbranched and convex trace fossils (planolites) found within the lower sandstone beds.*

10–20 mm silt partings (Figs. 6A, 9B), in contrast to the more massive and relatively poorly developed beds in Sandstone Unit–1 (Fig. 9A). The contacts between the beds in Sandstone Unit–2 are mostly erosional and undulating (Fig. 6A), whereas gradational contacts are commonly found between the beds in Sandstone Unit–1. Both the individual beds and the overall succession of Sandstone Unit–2 show a gradual fining-upward trend accompanied by an upward decrease in bed thickness (Figs. 5, 9B). Sandstone Unit–1 is conglomeratic in its lower and upper parts and mostly homogeneous in the middle (Fig. 9A). Clasts in the conglomeratic beds in Sandstone Unit–1 are subangular to subrounded, granitic/gneissic in composition and vary in size from a centimetre up to a metre (Azad et al., 2012). Sandstone Unit–2 is mostly free of clasts, although one subrounded granitic clast (40 cm) has been recorded (Fig. 6C).

Sedimentary structures are comparatively poorly developed in both units. Very faint ripple marks occur in the parallel-bedded sandstones of Sandstone Unit–1 (see log, Fig. 9A), and some deformational structures are found in the homogeneous sandstone beds in the upper part of the unit (Azad et al., 2012). Sedimentary structures, especially ripple marks, are better developed in Sandstone Unit–2 (Fig. 6B). The ripple marks are mostly symmetrical and found in the finer-grained, silty sediments. Sandstone Unit–1 contains several 10–20 cm-thick (*c.* 2 m total thickness), calcite-cemented, low-angle cross-stratified beds (Fig. 9A) displaying erosional relationships to the underlying beds (Azad et al., 2012). The Sandstone Unit–2 beds are parallel and do not contain any calcite cement. Small-scale convolute laminations have been found within the silty shale layers of Sandstone Unit–2. Crenulated mud clasts (1–3 mm) occur in places within Sandstone Unit–1, and subrounded mud clasts (2 mm) are found in Sandstone Unit–2. Diagenetic pyrite has been found locally in Sandstone Unit–2, but only as an accessory phase in Sandstone Unit–1. Evidence of pressure solution has been found in Sandstone Unit–2, whereas no such compactional features have been observed in Sandstone Unit–1. Palaeocurrent flow measurements noted from, e.g., cross beds and ripple marks in both units show similar northeastward transport directions (Table 1). Trace fossils have not been observed in Sandstone

Unit–1, whereas Sandstone Unit–2 contains a few such tracks, especially on the bedding-plane surfaces. Sandstone Unit -2 sediments are generally quartz rich and feldspar poor, contrasting with the feldspar-rich and quartz-poor Sandstone Unit–1 (Table 1). Both the clast content (millimetre-sized clasts) and amount of matrix in Sandstone Unit–2 are lower as compared with the Sandstone Unit–1 (Table 1).

Mineralogical study

Sandstone Unit–2

The Sandstone Unit–2 sediments are mostly fine- to medium-grained, locally with coarse-grained sand and granitic/gneissic clasts (up to 4 mm). The grains are mostly subangular to subrounded (a few rounded), moderately to well sorted, tightly packed and show evidence of pressure solution. The grains display an upward-fining trend in a few thin sections. Mineralogical compositions of three different facies types of Sandstone Unit–2 are described below.

The average quartz content of the fine- to medium-grained sandstone facies is 42% (Table 2). Feldspar is the second most dominant mineral (28%) while mica (mostly biotite) and rock fragments (granitic and gneissic) make up the other primary constituents (Table 2). The XRD analyses show a higher content of plagioclase compared to K-feldspar (Table 3). Sericite forms the major authigenic phases (Table 2). Authigenic pyrite is commonly found, both as a grain-replacing (Fig. 10A) and a pore-filling phase. Titanite, phosphate (e.g., apatite, jarosite) and iron oxides (e.g., hematite) are other minor authigenic phases present as pore fillings and locally filling microfractures in grains. Discrete particles of apatite and titanite have also been found (Fig. 10B). Illite is another important authigenic mineral, forming thin coatings around quartz and feldspar grains (Fig. 10C). Organic matter (rounded, granular masses) and detrital heavy minerals, e.g., zircon, garnet, epidote and rutile, are other accessory phases.

The fine-sandstone facies has a slightly higher quartz content (44%) compared to the underlying facies (Table 2). However, the feldspar content of this facies is surprisingly low (3%) (Table 2). This low feldspar content reflects

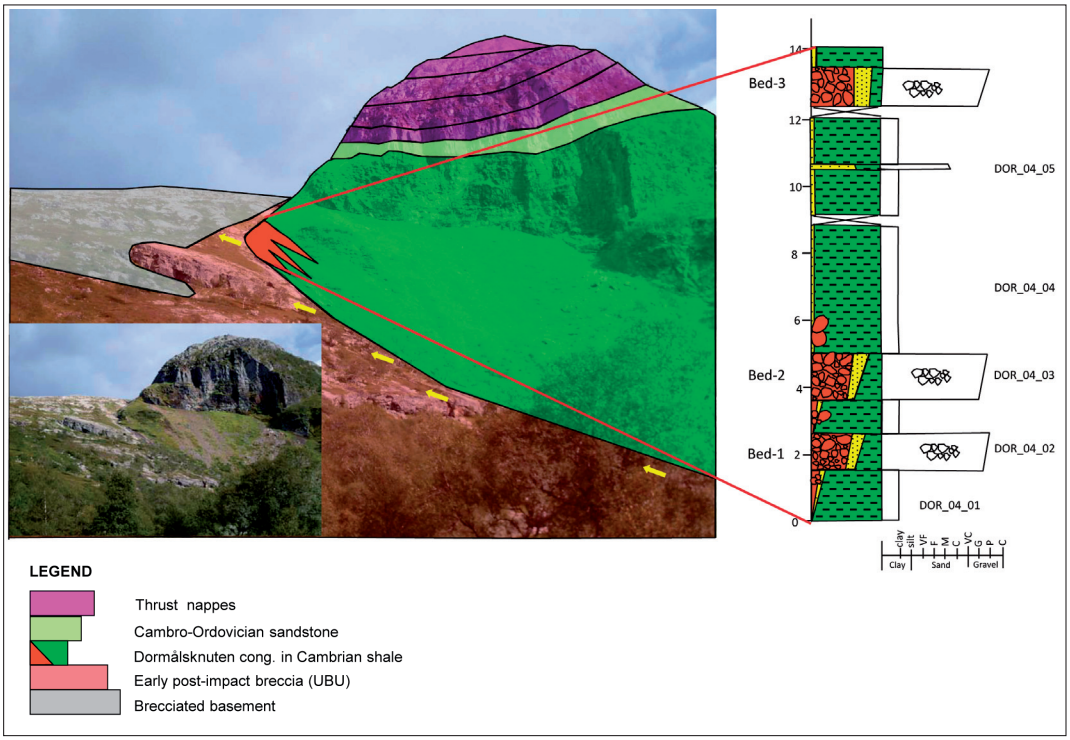

Figure 7. *The late post-impact Cambrian marine shale (green) showing an onlap relationship (indicated by yellow arrows) to the early post-impact breccias (Upper Breccia Unit) (shown in light brick red) in the Dormålsknuten area. The lower contact of the Upper Breccia Unit to the brecciated basement (light grey) has been found in the upper part of the crater wall. The Cambro–Ordovician sandstones overlying the Cambrian shale are shown in light green and the thrust sheets are in pink. The Dormålsknuten conglomerate beds (orange) interfinger with the Cambrian marine shale. To the right, a log profile of the Dormålsknuten conglomerate beds shows the intercalating conglomerate and marine shale. Rock sample numbers are shown next to the lithological column. The photo in the inset represents an uninterpreted section.*

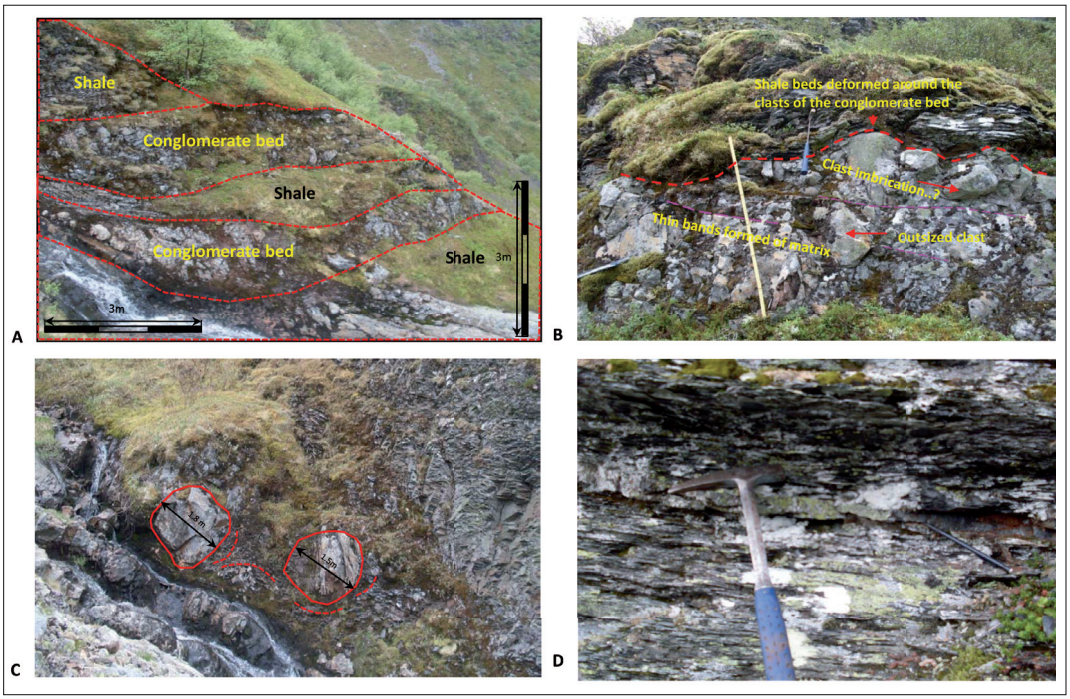

Figure 8. Dormålsknuten conglomerate beds in Cambrian shale. (A) The clast-supported conglomerate beds intercalated with dark-grey to black shale. (B) Clasts show an overall upward increase in size, with some outsize clasts, and a coarse-grained sandy matrix forming thin bands (shown by pink hatched line); photo from the lowermost conglomerate bed. (C) An outsize fractured clast (~1.8 m, granitic in composition) found embedded within the dark-grey to black shales. Note the deformation (dashed line) of the shale layers surrounding the clast. (D) A thin (2–4 cm) bed (indicated by the pencil head) consisting of small granitic clasts and very coarse-grained sand occurring within the thinly laminated, dark-grey to black shale unit.

intense sericitisation (28%) (Table 2). XRD analyses reveal a further decrease in K-feldspar and a corresponding increase in plagioclase (Table 3). Grains of both quartz and feldspar show an upward increase in roundness compared with the underlying facies. Fine-grained, recrystallised quartz and dark-grey to black illitic clay form the major part of the matrix (Fig. 10D). Authigenic pyrite (framboidal) and iron oxides (e.g., hematite) are the other significant authigenic minerals appearing within these sediments. Among other authigenic minerals, titanite and phosphates have been found in greater amounts compared with the fine- to medium-grained sandstones. Organic carbon and zircon are the other accessory phases.

Thin, mostly parallel and locally wavy laminations were observed in thin sections of the silty-shale facies rocks. The quartz and feldspar grains in the silty shales are angular to subangular, and show some a preferred orientation along the bedding planes. A few, angular, granitic clasts were also found within the silty shales. Fractures in the silty shale samples are filled with hematite. Fine-grained framboidal pyrite and granular organic carbon represent other important accessories.

The quartz/feldspar ratio (Fig. 11A) in Sandstone Unit–2 shows an upward increase. A significant increase in the quartz/feldspar ratio has been noted in Sandstone Unit–2 compared to Sandstone Unit–1 (Fig. 11A). XRD data reveal a decrease in K-feldspar content and a corresponding increase in plagioclase feldspar in Sandstone Unit–2 compared to Sandstone Unit–1 (Fig. 11B). The mica content (mostly biotite) shows an upward decrease. Among the authigenic minerals, Sandstone Unit–2 displays a significant increase in pyrite compared to Sandstone Unit–1 (Table 1). Sericite is the other authigenic phase commonly found in Sandstone Unit–2 sediments, showing an upward increase in the unit (Fig. 11C). Calcite and amphibole are absent in Sandstone Unit–2 sediments, but show a sporadic enrichment in Sandstone Unit–1. Increased amounts of apatite and titanite have also been noted in the sediments of Sandstone Unit–2.

Dormålsknuten conglomerate beds

The clast-supported, Dormålsknuten conglomerate beds have a lower average quartz content (26%) compared to Sandstone Unit–2 (43%) (Table 2). The low feldspar content in the conglomerate beds is attributed to the

higher amounts of sericite (Table 2). Dark-grey to black, illitic clay is the major matrix component, constituting 20–45% of the total sample (Table 2). Organic material and traces of pyrite have been found (Tables 2, 3). The coarse-grained sandstone bed in the shale unit (at 10.6 m in the log) (Figs. 7, 8D) has higher quartz and lower feldspar contents compared with the clast-supported conglomerate beds (Table 2).

Discussion

The late post-impact sediments in the Ritland impact structure have been studied sedimentologically and mineralogically. Sandstone Unit–2, exposed in the Svodene–Ritlandsfjellet area, consists of light-grey sandstones, dark-grey silty shales and black shales, representing a gradual upward transition from high-energy, oxygenated, crater-filling conditions to a low-energy, calm, stable, anoxic to hypoxic depositional regime. Field observations suggest that the clast-supported, Dormålsknuten conglomerate beds were deposited at later stages of crater sedimentation. The occurrence of the conglomerates as lenses within the dark-grey shale implies that mass-flow processes were intermittently active, interrupting long and quiet periods of clay deposition.

Svodene–Ritlandsfjellet area

The lowermost part of Sandstone Unit–2 (fine- to medium-grained sandstone facies) (Fig. 5) indicates a clear transition in crater sedimentation as evidenced by a greater textural maturity and increased quartz content as compared with the underlying Sandstone Unit–1 (Fig. 11A; Table 1) (Azad et al., 2012). Fine- to medium-grained sandstones (Fig. 6A) can be interpreted as turbidity deposits. The individual planar beds are marked by normal grading, erosional bases to the underlying beds, absence of floating clasts and a thin, silty sand capping; each bed represents a single turbidite flow event (Figs. 5, 6A). These turbiditic events may represent longer-duration, surge-like turbidity flows (Mulder & Alexander, 2001) as compared with the short-duration, surge-like turbidity flows of Sandstone Unit–1 (Azad et al., 2012). Relatively well-developed bedding and sedimentary structures (Fig. 9B) with upward-increasing bed thicknesses (Table 1) are suggestive of sustained

Table 1. *Comparison of sedimentological and mineralogical characteristics of Sandstone Unit–1 and Sandstone Unit–2.*

Sedimentary features	Sandstone Unit–1	Sandstone Unit–2
Texture and composition	Light-grey, fine- to medium-grained sand with common outsize clasts (cm size). Angular, subangular to subrounded grains. Moderate to poorly sorted.	Light-grey to dark-grey, fine- to medium-grained sand with few clasts (mm size). Fining-upward trend. Subangular to subrounded grains. Moderately sorted to well sorted.
Thickness of the succession	15–20 m	~6 m
Facies types	1. Upper conglomeratic sandstone. 2. Middle homogeneous sandstone. 3. Parallel-bedded sandstones. 4. Lower conglomeratic sandstone.	1. Dark grey to black shale. 2. Fine sandstone. 3. Fine to medium sandstone.
Bed thickness	Parallel-bedded sandstones are 10–20 cm thick. Homogeneous and conglomeratic sandstones vary from 1 to 1.5 m in thickness.	Fine to medium sandstones are 10–30 cm thick. Fine-sandstone beds vary from 2 to 4 cm in thickness. Silty shale beds vary within mm in thickness.
Bed type	Massive, less parallel, relatively poorly developed.	Parallel, well developed.
Bed contact	Graded mostly, the silty partings in the parallel-bedded sandstones are 20–80 mm.	Erosive, undulating, locally rippled, silt partings in fine to medium sandstone varies from 10 to 20 mm.
Conglomerate beds	Present in the upper and lower part. Commonly sandstone and conglomeratic beds locally coexist.	Total absence of conglomeratic beds, gradual fining-upward trend of the succession.
Clasts	Subangular granitic clasts (0.5–1m) commonly found.	Subrounded granitic clast (40 cm) found only in one place.
Sedimentary structures	Very faint ripples, low-angle cross beds, local crenulated mud clasts, convolute laminations in sand due to loading of the overlying conglomeratic beds.	Relatively well-developed ripples on the bedding-plane surface, local convolute lamination in silty shales and rounded mud clasts, absence of cross bedding.
Palaeocurrent directions	40° to 110°, northeastward.	55° to 100°, northeastward.
Trace fossils	Not found.	Horizontal, undulating, unbranched and convex.
Mineralogical composition (modal analysis, average)	Quartz: 24%, feldspar: 31%, mica: 9%, chlorite: 5%, calcite: 5%, rock fragments: 10%, matrix: 15%, heavy: 0.6%, sericite: 1%. Other accessory: amphibole, siderite.	Quartz: 43%, feldspar: 16%, mica: 4%, chlorite: 0.3%, calcite: 0%, rock fragments: 8%, matrix: 6%, heavy: 0%, sericite: 21%. Other accessory: pyrite (0.9%), titanite, apatite, hematite.

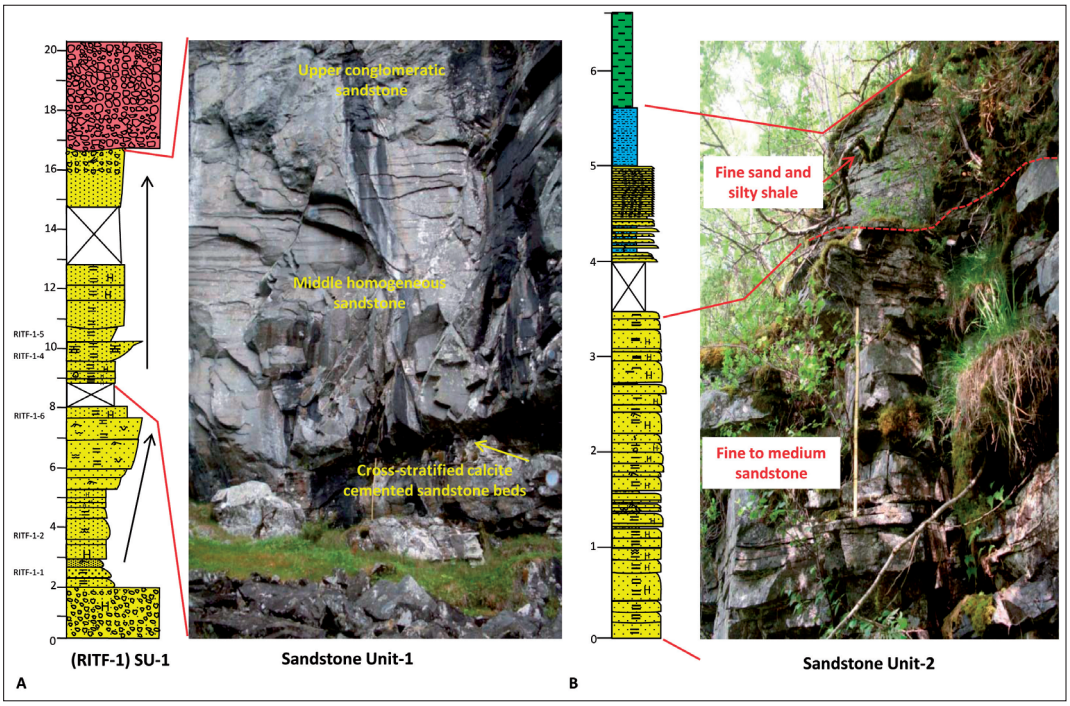

Figure 9. *Comparison of the sedimentary features between Sandstone Unit–1 and Unit–2. (A) Sedimentary log (modified from Azad et. al., 2012) of Sandstone Unit–1 (see legend in Fig. 5). The lower part of the succession shows a coarsening- and thickening-upward trend (indicated by the arrow), while the middle and upper parts are more homogeneous. The beds of this sandstone unit are massive, poorly developed, locally calcite cemented, cross stratified and ripple laminated, and contain subangular to angular clasts. (B) Sandstone Unit–2 is parallel-bedded, relatively well developed and individual beds show undulating and erosional contacts. The overall succession displays a fining- and thinning-upward trend. The overlying fine sand and silty shale beds are thin and occur as alternating layers of light to dark-grey fine sand and dark-grey silty shale.*

flows, contrasting with the impact-generated surges or short-duration, surge-like turbidity flows (Mulder & Alexander, 2001) of Sandstone Unit–1 (Azad et al., 2012). Such short-duration, surge-like turbidity flows are commonly triggered by flow transformation through erosion and acceleration from flow types with higher concentrations of sediment. Longer-duration, surge-like turbidity flows are generated by slope failure, consisting of a waxing flow head and waning body and tail (Mulder & Alexander, 2001). Each individual, fining-upward bed marked with an erosional base (Fig. 6A) can be related to individual events of slope failure, renewed base-slope erosion and further reworking of the slope sediments. Bouma T_{b-d} facies (Bouma, 1962) are relatively well developed in longer-duration, surge-like flows compared to the short-duration flows (Mulder & Alexander, 2001). However, the lowermost beds (fine- to medium-sandstone facies) of Sandstone Unit–2 do not reveal any complete developments of Bouma T_{b-d} sequences. The base of a typical sandstone bed of this facies is rather homogeneous and grades upward into silty sands with centimetre-thick, locally rippled beds (Fig. 6B) and can be compared to the Bouma T_{b-c} facies. The upper, fine-grained intervals of Bouma T_{d-e} are evidently absent within these sandstones.

The boulder-size granitic clast (40 cm) found within these sandstones (Fig. 6C) is unlikely to have been transported by turbidity currents and has probably derived from a rock fall from the granitic basement of the crater wall. The late post-impact crater wall was much more stable compared with the early post-impact stage, when angular granitic/gneissic clasts were released more frequently (Azad et al., 2012). The increased roundness of the clast (Fig. 6C) suggests that the crater infills were subjected to further reworking. The modest deformation of the sandstone beds around the clast (Fig. 6C) indicates that the clast rested in place while the sands were deposited at a slow, steady rate, eventually burying the clast. The occurrence of this isolated clast is unlike Sandstone Unit–1, where rapidly deposited, large, angular clasts are commonly found derived during the early post-impact stage of sedimentation (Azad et al., 2012). Comparable mineralogical compositions and palaeocurrent directions of Sandstone Unit–2 and Sandstone Unit–1 (Table 1) indicate that these sediments had a similar original source.

Table 2. *Mineralogical composition (vol.%, from thin-section study) of the different facies types of Sandstone Unit–2 from Svodene–Ritlandsfjellet and conglomerate beds from the Dormålsknuten area (400 grains were counted in each thin section to determine the percentages). The quartz/feldspar ratios of the individual samples are also presented in a separate column. Traces of some minerals studied from SEM/thin section have been added in the column at the far right.*

Sedimentary units	Depositional area	Facies	Sample no.	Quartz	Feldspar	Carbon-ates	Chlorite	Mica[1]	Matrix	Rock fragment	Pyrite	Hematite	Amphi-bole	Sericite	Organic matter	Qtz/ Felds.	Trace (SEM and XRD)
Late post-impact sediments	Svodene–Ritlandsfjellet	Fine sandstone	SVDX–02–14	30	1	0	0	1	39	14.5	2	1	0	11	0.5	30.00	
			SVDX–02–12	42	2	0	0	1	7	20	1	1	0	24	2	21.00	
			SVDX–02–10	35	1	0	0	2	17	17	0	1	0	24	3	35.00	
			SVDX–01–19	41	0.5	0	0	2	0.5	17.5	0	4	0	34.5	0	82.00	Illitic clay, zircon, apatite
			SVDX–01–18	46	2	0	0	2.5	6	10	0	3	0	30.5	0	23.00	
			SVDX–01–17	37	1	0	0	2	17.5	12.5	1	2.5	0	25	1.5	37.00	
			SVDX–01–16	39	2	0	0	0	13.5	15	1	0.5	0	28	1	19.50	Illitic clay
			SVDX–01–15	47	4	0	0	0	5	5	1	0	0	38	0	11.75	
			SVDX–01–14	54	7	0	0	2.5	0	0	1	2	0	32	1.5	7.71	
			SVDX–02–07	40	3	0	0	1	8	10	2	3	0	30	3	13.33	
			SVDX–02–06	49	6	0	0	4	0	4	1	12	0	22	2	8.17	Apatite, sphene
			SVDX–01–11	53	4	0	0	0	0	0	0	0	0	41	2	13.25	Apatite, jarosite
			SVDX–01–10	51	8	0	0	6	1	0	0	4	0	30	0.5	6.38	Titanite, apatite, zircon
		Fine to medium sandstone	SVDX–02–05	42	12	0	0	0	0	8	0	0	0	38	0	3.50	
			SVDX–02–04	38	33	0	0	8	2	5	0	0	0	13	1	1.15	
			SVDX–02–03	43	26	0	0	3	2	4	1	0	0	18	3	1.65	Titanite, zircon, apatite
			SVDX–02–01	40	21	0	2	3	0	9	0	1	0	24	0	1.90	
			SVDX–01–09	43	37	0	0.5	5	1	3	1	0	0	9	0.5	1.16	Zonation of pyrite, titanite
			SVDX–01–08	45	35	0	0	5	1	4	0	0	0	10	0	1.29	Pyrite, organic
			SVDX–01–07	43	30	0	1	8	3	7	2	0	0	6	0	1.43	
			SVDX–01–06	44	33	0.5	0	3	4	5	1	0	0	9	0	1.33	
			SVDX–01–05	39	28	0.5	0	7.5	5	3.5	0	0	0	16	0	1.39	Pyrite, organic
			SVDX–01–04	44	30	0	0	9	0	8	2	0	0	7	0	1.47	
			SVDX–01–03	46	23	0	3	7	1.5	3	0	0	0	16	0	2.00	Titanite, apatite, zircon, pyrite
			SVDX–01–02	42	25	0	2	3	4.5	6	4	0.5	0	13	0	1.68	Apatite, titanite, zircon, garnet
			SVDX–01–01	37	35	0	0	4	6	11	1	0	0	6	0	1.06	Apatite, titanite, zircon, illitic clay
	Dormåls-knuten	Coarse sand	DOR–04–05	37	8	0	0	2	22	7	0	0	0	24	0	4.63	
		Clast congl.	DOR–04–03	29	11	0	0	3	20	7	0	0	0	29	1	2.64	Pyrite
		Clast congl.	DOR–04–02	23	12	0	0	0	45	6	0	0	0	12	2	1.9	Hematite, pyrite

[1]'Mica' (mostly biotite) represents detrital/primary mica and 'sericite' represents secondary/authigenic mica, which mostly derived from alteration of K-feldspar.

An increased quartz/feldspar ratio (Fig. 11A) and decrease in feldspar, rock fragments, mica and matrix content in the fine- to medium-sandstone facies of Sandstone Unit–2 compared to that found in Sandstone Unit–1 (Table 1) suggest a gradual development of further reworking and weathering. The presence of authigenic pyrite, apatite and organic matter and the absence of calcite (Table 2) within the fine- to medium-grained sandstone facies (Sandstone Unit–2) indicate that sporadic, reducing, bottom-water conditions were established within the crater during the transitional stages.

Cruziana ichnofacies (here *planolites, thalassinoides*) are typical for the offshore transitional zones but have also been recorded in subtidal, poorly sorted, unconsolidated substrates (Pemberton et al., 1992). This ichnofacies is also found in the littoral to sublittoral parts of some estuaries, bays, lagoons and tidal flats. It generally represents low- to moderate-energy conditions at the fair-weather wave base, but in some cases may also be found in deeper, quieter waters (Pemberton et al., 1992). The ichnofauna appears at the upper surface (in silty layers) of the fine- to medium-grained sandstone beds (Sandstone Unit–2) as mostly simple, horizontal and cylindrical, sediment-filled burrows. They possibly represent fair-weather wave-base conditions with fairly low sedimentation rates or even periods of non-deposition. The crater was assumed to have been completely filled by seawater during the early post-impact stage (Azad et al., 2012); the presence of the *Cruziana* ichnofauna suggests that the water depth within the crater was in the order of 300 m. The 350 m of crater depth, a modelled rim height of about 115 m and an existing seawater depth of ≤100 m (Shuvalov et al., 2012) suggest that the crater rim was probably exposed to the atmosphere during the transitional stages of crater sedimentation. The occurrences of trace fossils in silty layers suggest a short-lived, quiet event of suspension deposition before the arrival of new turbidity currents. The low abundance and diversity of these trace fossils precludes the drawing of any major conclusion with regard to further changes in depositional conditions.

Alternating layers of dark-grey, parallel-bedded, fine sandstone and silty-shale in the middle part of Sandstone Unit–2 (Fig. 5) may represent repetitive cycles of turbiditic and suspension deposition. The individual sandstone beds of this facies type also show a fining-upward trend,

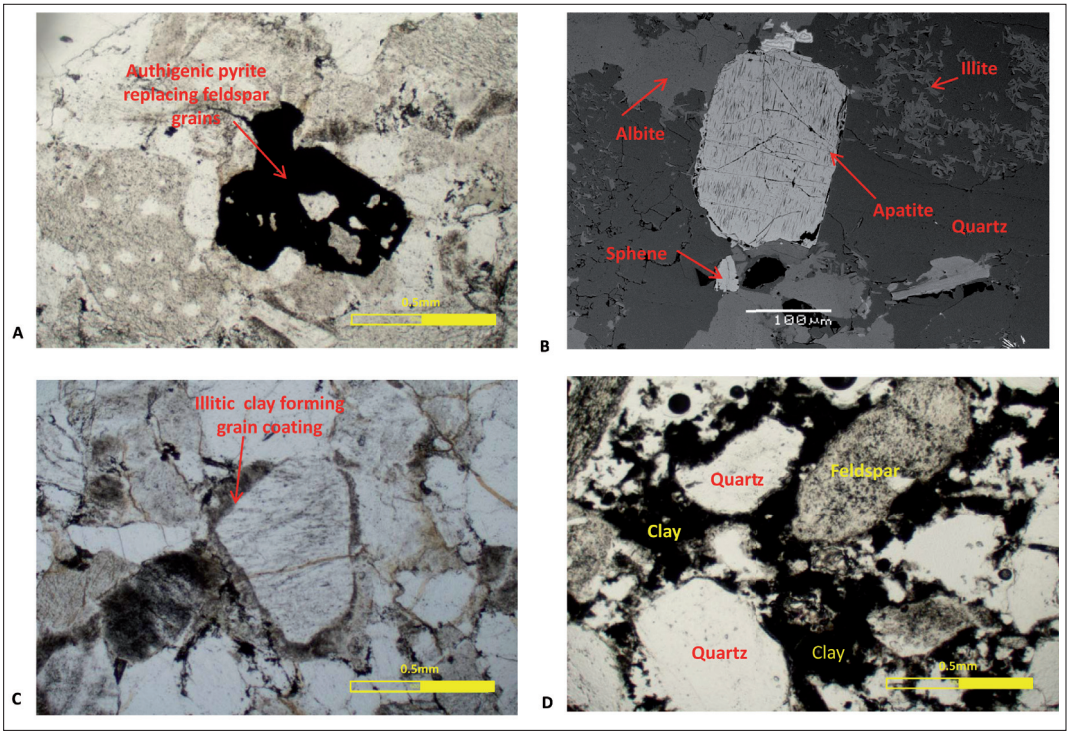

Figure 10. *Photomicrographs of Sandstone Unit–2. (A) Authigenic pyrite is commonly found both in the fine- to medium-grained sandstones and in the fine sandstones, replacing dissolved feldspar grains. (B) Discrete grains of apatite and titanite are more commonly found in the fine sand. (C) Illitic clay forming a thin coating around feldspar grains. (D) Dark-grey to black illitic clay and organic material found as a major pore-filling component in the fine sand and silty shale facies.*

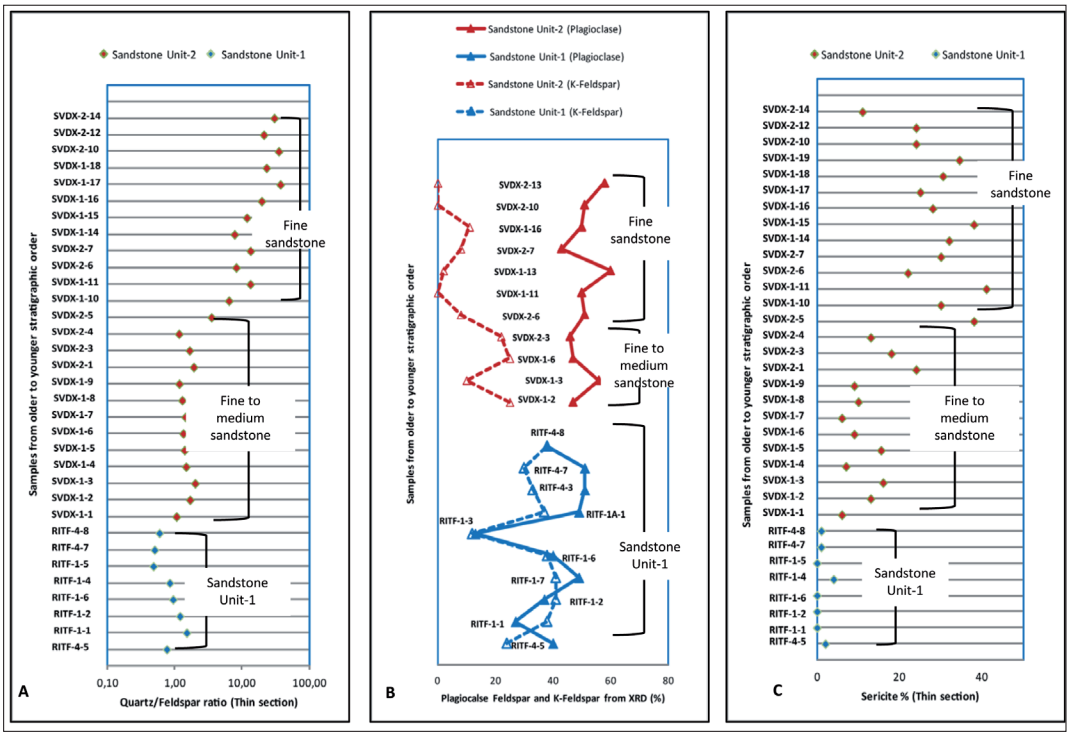

Figure 11. Comparison of mineralogical characteristics of Sandstone Unit–1 and Sandstone Unit–2. (A) Quartz/feldspar ratio (thin-section study) shows an upward-increasing trend from Sandstone Unit–1 to Sandstone Unit–2. (B) A decrease in K-feldspar (XRD %) and a corresponding increase in the plagioclase feldspar observed in Sandstone Unit–2 compared to Sandstone Unit–1. (C) Sericitisation (thin-section study) shows an upward increase that corresponds to the decreased feldspar contents from Sandstone Unit–1 to Sandstone Unit–2. See Fig. 9A (Sandstone Unit–1) and Fig. 5 (Sandstone Unit–2) for the rock sample positions in the lithological column.

erosional bases to underlying beds and centimetre-thick, undulating/rippled, silty-shale cappings, possibly reflecting individual turbiditic events. The intervals between the turbidity flows were possibly longer during this stage of crater sedimentation as the fine-grained sandstone beds are separated by 0.5–2 cm-thick, silty-shale layers deposited from suspension settling (Fig. 5). The overall fining-upward trend in this part of the succession, without any evidence of syn-depositional deformational structures or water-escape structures, suggests a further reduced rate of sedimentation. The upward decrease in thickness of sandstone beds (Fig. 5) also indicates a reduced clastic input. Local, medium- to coarse-grained sandstone beds can reflect a sudden increase in the energy conditions, e.g., related to base-slope failures and renewed erosion probably triggered by episodic storms. Increased thicknesses of the silty shales in the upper part of this facies (Fig. 5) indicate a progressive increase in seawater depth and establishment of suspension-dominated sedimentation. The increase in the quartz/feldspar ratio (Fig. 11A) and improved textural maturity of this facies compared to the underlying facies signify possible further reworking of the crater-filling sediments. The dark-grey to black, illitic clayey matrix (Fig. 10D) with increased organic content, and fine-grained authigenic pyrite and apatite (Tables 2, 3) reflects more stable and partly anoxic conditions prevailing within the crater.

The dark-grey to black shales overlying the fine-sandstone facies (Fig. 5) reflect a complete establishment of almost anoxic bottom-water conditions within the crater. This flaky, thinly laminated shale attains a thickness of about 180 m in the central part of the crater, indicating that the crater existed as a depression beneath the Cambrian sea for millions of years and eventually was filled by suspension settling deposits. Sporadic occurrences of angular to subangular quartz and feldspar grains and granitic clasts in the lowermost parts of the shale beds suggest that although hemipelagic sedimentation was dominant within the crater, clastic input from the crater walls had not completely died out. The presence of pyrite (Table 3) and organic matter in the upper part of the succession (Table 2) and lack of any trace fossils are suggestive of reduced ventilation under partly sediment-starved depositional conditions.

Table 3. *Mineralogical composition of the different facies types of Sandstone Unit–2 from Svodene–Ritlandsfjellet and conglomerate beds from Dormålsknuten area, obtained from XRD analysis (semiquantitative). Quartz/feldspar ratios of the individual samples are presented in a separate column. Peak values for quartz (d = 4.26 Å), K-feldspar (d = 3.24 Å, 3.25 Å), plagioclase (d = 3.18 Å, 3.19 Å), calcite (d = 3.03 Å), dolomite (d = 2.89 Å), mica (d = 10 Å), chlorite (d = 7 Å) and pyrite (d = 2.71 Å) were used for quantifying the minerals. Only the peak height has been considered for the semiquantitative analysis of these minerals (Morris et al., 2008).*

Sedimentary units	Depositional area	Facies	Sample no.	Quartz	Plagio-clase	K-feldspar	Calcite	Dolomite	Chlorite	Mica	Pyrite	Others	Quartz/ Felds.	Trace
Late post-impact sediments	Svodene–Ritlandsfjellet	Dark gray to black shale	SVDX–03–05	26	24	24	0	0	3	20	3	0	0.54	
			SVDX–01–20	25	0	3	0	0	1	71	0	0	8.33	
		Fine sandstone	SVDX–03–01	22	21	21	0	0	4	31	1	0	0.52	
			SVDX–02–13	32	58	0	0	0	0	10	0	0	0.55	
			SVDX–02–10	32	51	0	0	0	0	17	0	0	0.63	
			SVDX–01–16	27	50	11	0	0	0	12	0	0	0.44	
			SVDX–01–13	14	60	2	0	0	1	23	0	0	0.23	
			SVDX–02–07	32	43	8	0	0	0	13	1	3	0.63	Hematite
			SVDX–02–06	26	51	8	0	0	0	13	2	0	0.44	
			SVDX–01–11	31	50	0	0	0	0	16	0	3	0.62	Hematite
		Fine to medium sandstone	SVDX–02–03	26	46	22	0	0	1	5	0	0	0.38	
			SVDX–01–06	23	47	25	0	0	1	4	0	0	0.32	
			SVDX–01–03	25	56	10	0	0	3	6	0	0	0.38	
			SVDX–01–02	24	47	25	0	0	2	2	0	0	0.33	
	Dormålsknuten	Clast congl.	DOR–O4–03	25	48	21	0	0	0	6	0	0	0.36	Pyrite
		Clast congl.	DOR–O4–02	21	38	29	0	0	0	12	0	0	0.31	Pyrite
		Shale	DOR–O4–01	21	61	2	0	0	0	16	0	0	0.33	Pyrite

Dormålsknuten area

The clast-supported conglomerate beds in the Dormålsknuten area (Figs. 7, 8A) can be interpreted as submarine scree deposits that slid into unconsolidated, cohesive marine clays. The limited lateral and vertical extents of these possible scree beds (Fig. 7) compared to the extensive, early post-impact, breccia beds (Upper Breccia Unit) (Azad et al., 2012) suggest that the crater slopes were more stable and thus reduced the input of coarser clastics derived from the crater wall and rim during the later stages of crater infilling. An alternative interpretation of these beds is that they may represent debrites, possibly triggered by storm or precipitation-related, cohesive, debris-flow events.

'Screes' or 'talus' are downslope accumulations of rock fragments/rock falls produced by failure of cliffs encompassing the downward movement of individual, typically gravel-size clasts (Drew, 1873; Gardner, 1983). Scree deposits are considered to have formed by a granular flow mechanism, and bedforms produced by scree processes represent coarsening-upward arrangements of the clasts. In contrast, cohesive debris-flow deposits show *en masse* depositional characteristics, explaining the chaotic arrangement of the deposits. In debris flows, the cohesive strength of the matrix acts as the dominant clast-supporting mechanism; the matrix consists of fairly fine-grained sediments with a significant amount of clay-size particles (Costa & Williams, 1984; Mulder & Alexander, 2001; Gani, 2004). The diagnostic features of a cohesive debris-flow deposit include basal inverse grading (shear flow), an ungraded flow body (plug flow) and a sandy upper part (waterlain). The clast-supported conglomerate beds in the Dormålsknuten area do not show the well-developed basal reverse grading expected in cohesive debrites. The middle part of the conglomeratic beds is ungraded while the top part contains coarser clasts (Fig. 8B). Thin bands consisting of a sandy matrix have been found within the conglomeratic beds, but not at the upper surface of the bed. Consequently, the upward increase in clast size, poorly developed bedding, comparable clast and matrix composition (see below), and lens-like occurrence within the clay are more analogous to submarine scree deposits than to debris-flow deposits.

The clast composition of these conglomerate beds is comparable to the general basement composition of the area (granitic/gneissic) (Azad et al., 2012) indicating that these sediments have been derived from the erosion of the adjacent crater wall or rim. The matrix consists of significant amounts of clay with medium- to coarse-grained, angular to subangular quartz and feldspar, and small granitic/gneissic clasts (Table 2). The clay content of the matrix is probably sourced from pelagic sediments. The comparable clast and matrix mineralogical composition (granitic/gneissic) (Tables 2, 3) of the conglomerate beds suggests that the extra-crater sediment influx was not so significant in this later stage of crater sedimentation, and that the sediments were mostly derived from crater-slope erosion and reworking of the crater infills. The average quartz/feldspar ratio (2.2) in the matrix of these conglomerate beds (Table 2) is higher compared to the quartz/feldspar ratio (0.3) in the matrix of the early post-impact, clast-supported breccias (Upper Breccia Unit) (Azad et al, 2012). This suggests a further reworking of these sediments during later stages of crater sedimentation. Traces of pyrite (Table 3) and the organic content (Table 2) within the matrix suggest restricted, less ventilated conditions in the crater basin at the time that these conglomerate beds were deposited.

The outsize clasts within the dark-grey to black shales can be interpreted as deriving from rock falls into marine clays (Fig. 8C). Evidence of smearing of the clays around the clasts (Fig. 8C) also supports a rockfall mechanism. The brittle nature of the shale layers around the clasts and fracturing of the clasts (Fig. 8C) are probably related to compaction and Caledonian tectonics, which affected the upper parts of the crater infill. The thin (Fig. 8D) bed (at 10.6 m in the log) consisting of granitic clasts and coarse sand has probably resulted from crater-wall erosion and may represent a storm event, probably deposited from a hyperconcentrated density flow.

Depositional model synthesis

A thin (0–30 cm thick) layer of basal conglomerate has been found overlying the sub-Cambrian peneplain in the southwestern part, outside the crater, probably deposited from reworking of weathering products of the Precambrian basement rocks (Riis et al., 2011; Setså, 2011). This basal conglomerate, probably of Early Cambrian age, is overlain by a 10–20 m silty-shale layer (Setså, 2011) indicating the onset of the Early Cambrian marine transgression. This basal conglomerate and silty-shale unit represent the pre-impact sediments in the Ritland area, as evidenced by the overlying ejecta layer (Kalleson et al., 2012), suggesting a shallow-marine setting of the Ritland bolide.

The numerical modelling of the Ritland impact (Shuvalov et al., 2012), the distribution of the ejecta layers (Kalleson et al., 2012) and the sedimentary signatures within the crater infills (Azad et al., 2012) together indicate that the contemporary seawater depth during the Ritland impact event was ≤100 m. The depositional model in Fig. 12A represents crater sedimentation during the late syn-impact to early post-impact stage and has been discussed in detail in Azad et al. (2012). The depositional model presented in Fig. 12B represents crater sedimentation during the transitional stages (from early post-impact to late post-impact). A brief summary of the depositional processes during the late syn-impact to early post-impact interval is presented here to illustrate the link between the early post-impact and late post-impact stages of crater sedimentation.

The Ritland crater rim is considered to have formed subaerially in view of the crystalline target surface, shallow epeiric-sea setting and very thin, unconsolidated marine-clay cover. With the rim probably above sea level (Shuvalov et al., 2012), the initial Ritland crater sedimentation was thus also likely to have been subaerial (Azad et al., 2012). Sedimentation in the crater was initiated by the collapse of the transient cavity and rim; debris avalanched down towards the crater centre depositing the lower part of the Lower Breccia Unit (Azad et al., 2012) (Fig. 12A). Debris-flow deposition dominated (Fig. 12A) immediately after the rock avalanches as seawater resurged back into the crater. The numerical modelling (Shuvalov et al., 2012) and the sedimentary signatures of the lower part of the crater infills (Lower Breccia Unit) (Azad et al., 2012) suggest that the Ritland crater probably did not experience an instantaneous, powerful resurge of seawater. Water entered the crater through a breaching of the crater rim and eventually filled the crater. The crater rim remained exposed to the atmosphere (Fig. 12C) until it was inundated by later transgressions. Turbidity flows dominated in the central part of the water-filled crater cavity. The Sandstone Unit–1 (Table 1) represents turbidites from a minor submarine-fan setting prograding on to the crater floor (Fig. 12A). Along the steep crater walls, deposition of the coarser clastics (Upper Breccia Unit) continued, developing fans from the crater walls, prograding towards the crater centre (Fig. 12A). Through time, the crater cavity became more stable and the site for suspension deposition of fine-grained sediments (Sandstone Unit–2) (Fig.12B).

Sandstone Unit–2 was probably deposited during the retreating or abandonment phase (Fig.12B) of the earlier active, high-energy, minor submarine fans of the early post-impact stage (Sandstone Unit–1) (Azad et al., 2012) (Fig. 12A). The coarsening- and thickening-upward trend in the lower part and a rather homogeneous middle and upper part of the Sandstone Unit–1 (Fig. 9A) represent an upward transition from prograding-fan developments to a more stagnant situation during the later stages of early post-impact sedimentation. The fining- and thinning-upward trend (Figs. 5, 9B) of the succeeding transitional sandstones suggests that the active fans retreated during later stages of crater sedimentation (Fig.12B). The stratigraphical upward increase in the quartz/feldspar ratio (Fig. 11A) and sericite content (Fig. 11C) from early post-impact to the transitional sandstones, and a comparable mineral composition (Tables 2, 3) to that of the granitic and gneissic basement suggest that the reworking of the early post-impact crater-wall sediments was the major source of sediment supply within this closed, sediment-starved, crater basin during the later stages of crater sedimentation.

The extrabasinal sediment supply during Sandstone Unit–2 crater sedimentation was probably insignificant. Outside the crater, the extensively peneplained, epicontinental sea platform was dominated by a series of marine transgressions from the Early Cambrian onwards with little or no evidence of significant regressive phases before the end of the Cambrian (Nielsen & Schovsbo, 2011). Baltoscandia became extensively flooded and the clastic input was significantly reduced during this time. Similar conclusions were also suggested by Setså (2011) from studying the post-impact sediments outside the crater, e.g., the post-impact shale overlying the ejecta layer was characterised by a low quartz/feldspar ratio and greater amounts of pyrite, apatite and organic content, representing sediment-starved, anoxic ocean bottom conditions (Setså, 2011). The transitional sediments (Unit–2 time) inside the crater do not reveal any coarsening-upward trend, thus no regressive or prograding events were noted within the crater. A minimal supply of terrigenous clastics from outside the crater due to Early/Mid Cambrian, low-angle river profiles (Nielsen & Schovsbo, 2011) and reduced crater-slope erosion processes due to low-energy, depletive flow resulted in sediment-starved conditions within the crater. Fan building was probably abandoned in the early part of the late post-impact stage (Unit–2 time) and the crater was open mostly for suspension deposition over long time intervals. Increasing amounts of authigenic pyrite and organic matter, significant amounts of apatite, and an absence of trace fossils in the upper part of the succession support the interpretation of a gradual shift from high-energy, oxygenated (turbidity flows) to sediment-starved, low-energy, stagnant, less-ventilated, bottom-water conditions (suspension deposition).

The thickness of the Alum Shale unit in the crater centre is estimated to be 180 m (Riis et al., 2011). The sedimentation rate of the Alum Shale was extremely low, calculated at 3–8 mm per 1000 years (Berger, 1974) with only minor variations across the Baltoscandian platform (Thickpenny, 1984). The lithological variations are small within these shales with no apparent breaks observed; thus, zone thickness could be proportional to depositional duration (Thickpenny, 1984). An estimated time period for deposition of a 80–100 m-thick column of Alum Shale in the Skåne area, Sweden, is approximately 23–25 million years (Thickpenny, 1984). The sedimentation rate of the Alum Shale unit in the Ritland crater basin may have been slightly higher since the basin functioned as a closed depression beneath the epicontinental sea and would have received some clay influx from outside the crater. Assuming an upper limit of the sedimentation rate of 10 mm per 1000 years within the crater, the 180 m-thick shale unit in Ritland would have accumulated in 37.5 million years, probably covering the whole of the Middle to Upper Cambrian epoch. Although uncertainties related to compaction of the overburden and the effects of Caledonian tectonics have to be considered, it can be assumed that the crater was completely filled with marine clays by Late Cambrian time. The thickness variations of the Alum Shale unit inside (180 m) and outside (15–20 m) the crater suggest that the crater was completely filled by marine clays during this time.

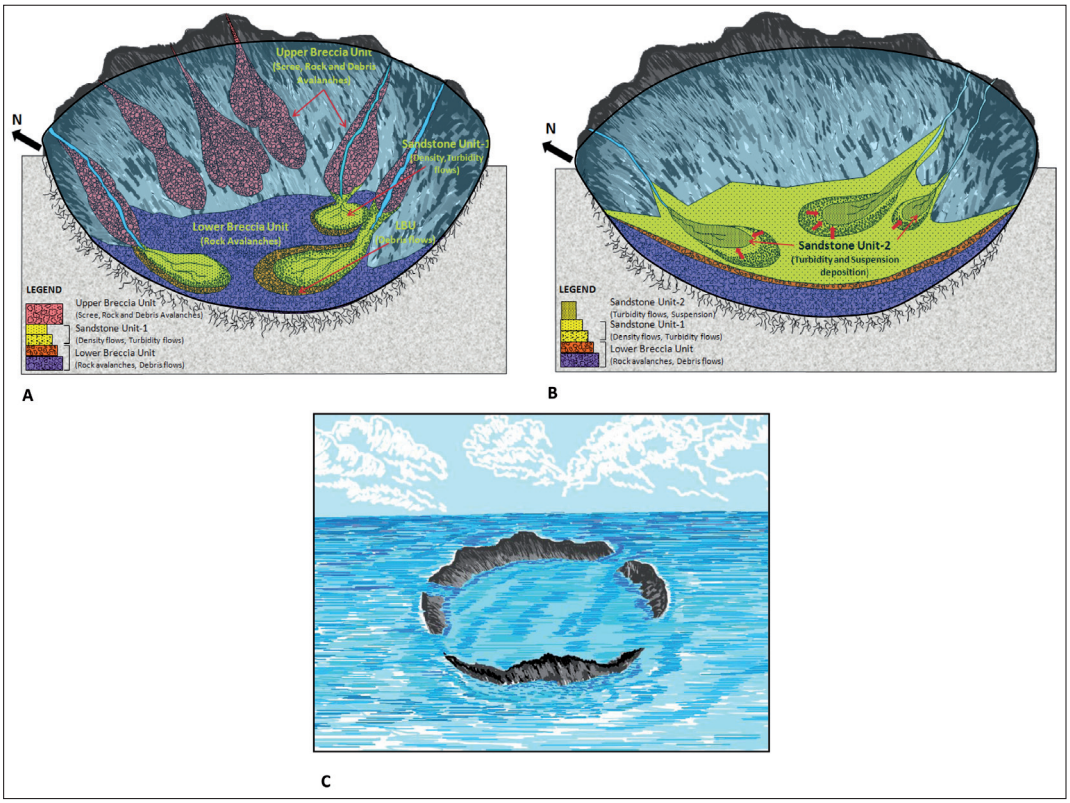

Figure 12. (A) Simplified depositional model (one half of the crater) representing the deposition of different sedimentary units in the Ritland crater during the late syn-impact and early post-impact stages (modified from Azad et al., 2012). (B) Model representing crater sedimentation during the transitional stage (early post-impact to late post-impact stage). The submarine fans were probably retreating (indicated by red arrow) due to a reduced clastic input from both inside and outside the crater. The channel abandonment processes were active, and the sediments were derived mostly from erosion and reworking of the crater-wall sediments. (C) Partially submerged crater within the Cambrian sea, with rims exposed to the atmosphere during the transitional stage.

The similar thickness (10 m) of the overlying Cambro–Ordovician sandstones (Knaust, 2004) inside and outside the crater confirms this observation.

The onlapping relations of the dark-grey shale on the early post-impact breccias exposed higher up in the northeastern crater wall in the Dormålsknuten area (Fig. 7) suggest a continued and prolonged interval of suspension deposition (Fig. 13). The clast-supported conglomerate beds in the northeastern part of the crater basin intercalated with the marine clays at an elevation of 700–720 m (Fig. 4) correspond to a depth of 50 m below the peneplain (the impact target surface), and 300 m above the base of the shale layer in the crater centre (Fig. 4). This implies that mass-flow processes, i.e., with development of screes, were active even in the very late stages of crater sedimentation (Fig. 13). The crater walls remained as escarpments beneath the epicontinental sea for millions of years.

The natural gamma-radiation measurements in the lower part of the dark-grey to black shale unit in the Svodene–Ritlandsfjellet area varies from 200 to 270 cps (Fig. 5), while in the upper middle part (Dormålsknuten area) the values range from 210 to 280 cps. These Alum Shale values are much lower than those in the fine- to medium-sandstone facies (350–415 cps) (Fig. 5) of Sandstone Unit–2 (Svodene–Ritlandsfjellet area). The higher gamma-radiation value within the fine- to medium-sandstone facies could be related to the higher average content of K-feldspar found in thin sections and XRD analyses (21%, Table 3). The surprisingly low gamma values of the dark-grey to black shales do not correspond with the typical highly radioactive characteristics of Alum Shale. Particularly the upper part of the Upper Cambrian Alum Shale in the Mjøsa region (Norway) and Øland (Sweden) is remarkable for its high (400–800 cps and 500–1000 cps, respectively) natural gamma activity due to high uranium concentrations (Dypvik, 1993). The lower gamma measurements in the shales of the Ritland

crater could probably be related to the lithological heterogeneity and variations in geochemical reactions due to the differences in oxygen and organic contents at the ocean bottom (Dypvik, 1993).

Late post-impact crater sedimentation dominated by suspension settling with a transitional (early post-impact to late post-impact) episode of turbidity flows has been observed in several terrestrial shallow-marine, impact craters. The Gardnos crater, assumed to have been roughly contemporaneous with the Ritland structure (Riis et al., 2011), is marked by a succession (25 m thick in the Branden core) of interbedded sandstones, siltstones and shales in the uppermost part of the crater-infilling succession, representing alternating episodes of turbidity flows and suspension deposition (Kalleson et al., 2008). In the Estonian Kärdla crater, a thick (>200 m) succession of carbonate sediments marks the late post-impact stage, deposited from suspension settling under sediment-starved, stable crater conditions (Ainsaar et al., 2002). A comparable geological setting in the Swedish Lockne crater also resulted in a thick sequence (>90 m) of carbonate sediments (Frisk & Ormö, 2007) during the late post-impact stage of crater sedimentation. In Virginia, USA, the Chikahominy Formation (94 m in the Eyreville core) consisting of finely laminated clays and silts with abundant sand-size foraminifera, shell fragments, glauconite and traces of pyrite and mica, represents the late post-impact sedimentation in the Chesapeake Bay impact structure. The Chikahominy Formation has been interpreted to have been deposited from suspension settling in a restricted offshore environment (Browning et al., 2009). The late post-impact sedimentation in the Flynn Creek crater, Tennessee, is marked by the deposition of black shales (up to 55 m thick), deposited over several hundred thousand years by alternating episodes of fine-grained turbidites and pelagic suspension settling (Schieber & Over, 2005).

The thickness of the late post-impact successions within these various craters is commonly many times higher compared to the coeval late post-impact succession outside the craters. The thickness of the Alum Shales in the central part of the Ritland structure is almost ten times higher compared to the thickness (20 m) outside the crater (Knaust, 2004). In the Kärdla crater, the late post-impact, Upper Ordovician limestone encountered in the crater centre is at least four times thicker than the equivalent limestone outside the crater (Ainsaar et al., 2002). The thickness of the Dalby Limestone in the Lockne crater also exceeds by several times that of the coeval Dalby Limestone outside the crater (Frisk & Ormö, 2007). The Flynn Creek crater has a thickness of black shale which is at least five times greater than the coeval Upper Devonian Chattanooga Shale (Schieber & Over, 2005). The Chickahominy Formation in the Eyreville core, drilled approximately in the crater centre, is also thicker compared to any other core drilled through this formation outside the crater (Edwards et al., 2009).

Summary

The Sandstone Unit–2 in the Svodene–Ritlandsfjellet area clearly represents a transitional phase between the early post-impact and late post-impact stages of crater sedimentation. The Ritland crater sedimentation during the late syn-impact and early post-impact stages was mainly controlled by gravity and mass flows, e.g., rock avalanches, screes, debris and turbidity flows (Azad et al., 2012), whereas during the late-post impact stage sedimentation was mostly suspension-dominated, interrupted by minor episodes of turbidity flows during the basal transitional phase.

The fine- to medium-sandstone facies of the transitional sandstones (Unit–2) is texturally more mature compared with the early post-impact sandstones (Unit–1) and interpreted to be derived from base-slope erosion and further reworking of the earlier crater infills. These sediments were probably deposited by turbidity currents during the retreating or abandonment stage of submarine fans that developed during the early post-impact stage. Through time, reduced rates of both crater-slope erosion and sediment supply from outside the crater resulted in a gradual, progressive establishment of suspension-dominated sedimentation. The dark-grey to black clayey matrix, with increased amounts of authigenic pyrite, apatite and organic matter within a fine-sandstone facies, represents more stable, calm and less-ventilated, bottom-water conditions in the crater basin. An upward transition of this facies into thick, dark-grey to black shales

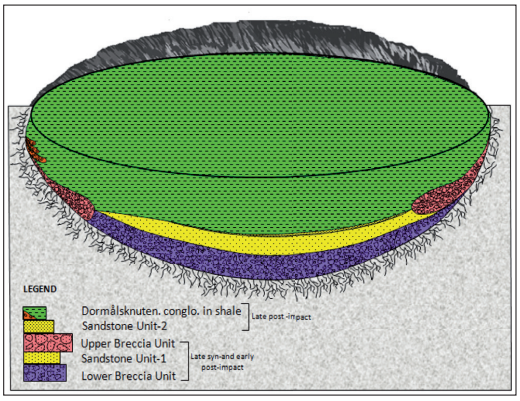

Figure 13. *Simplified depositional model (one half of the crater) representing depositional processes during the late post-impact stage. The clast-supported conglomerate beds in the Dormålsknuten area represent small-scale scree deposits (orange) sliding into the marine clay (green) as a result of occasional slope failures in the later stages of crater sedimentation.*

suggests a complete establishment of anoxic to hypoxic conditions where sediments were deposited during a protracted (millions of years) and quiet period of suspension deposition.

The scree deposits found in the Dormålsknuten area probably resulted from sporadic slope failures during the later stages of crater sedimentation. The small-scale scree beds, the metre-size clasts within the marine clay, and a few thin sandstone beds suggest that submarine slides, rock falls and reworking of the crater-wall sediments were active processes for a long time after the impact, occasionally depositing coarser materials between the long, quiet periods of suspension deposition.

Acknowledgments. We express our sincere gratitude to the other Ritland project-group members for their kind assistance and worthy discussion. Constructive and thoughtful comments of Drs. Kevin Evans and David Jolley helped to improve the manuscript. Adrian Read worked on improving the language, we appreciate his contribution. We are also grateful to the Sven Egil and Kari Sørensen family for their hospitality during the field days at Ritland. The Research Council of Norway generously supported the three-year Ritland project; we highly appreciate this. Finally, the laboratory technicians at the Department of Geosciences, University of Oslo, and the people of Ritland, are acknowledged for their support and assistance.

References

Ainsaar, L., Suuroja, K. & Semidor, M. 2002: Long-term effect of the Kärdla crater (Hiiumaa, Estonia) on Late Ordovician carbonate sedimentation. *Deep Research II: Topical studies in Oceanography 49*, 1145–1155.

Azad, A.S., Dypvik, H., Tomczyk, M., Kalleson, E. & Riis, F. 2012: Late syn-impact and early post-impact sedimentation in the Ritland impact structure, western Norway, *Norwegian Journal of Geology 92*, 405–431.

Berger, W.H. 1974: Deep sea sedimentation. *In* Burk, C.A. & Drake, C.L. (eds.): *The geology of continental margins*, Springer-Verlag, New York, pp. 231–241.

Bergström, J. & Gee, D.G. 1985: The Cambrian of Scandinavia. *In* Gee, D.G. & Sturt, B.A. (eds.): *The Caledonide Orogen – Scandinavia and related areas*, John Wiley & Sons, Chichester, pp. 247–271.

Bouma, A.H. 1962: *Sedimentology of some flysch deposits: a graphic approach to facies interpretation*. Elsevier, Amsterdam, 168 pp.

Bruton, D.L. & Harper, D.A.T. 2000: A mid-Cambrian shelly fauna from Ritland, western Norway and its palaeogeographical implications. *Bulletin of the Geological Society of Denmark 47*, 29–51.

Bruton, D.L., Harper, D.A.T. & Repetski, J.E. 1989: The stratigraphy and faunas of the Parautochthon and Lower Allochthon of southern Norway. *In* Gayer, R.A. (ed.): *The Caledonide geology of Scandinavia*, Graham & Trotman, London, pp. 231–241.

Browning, J.V., Miller, K.G., McLaughlin Jr., P.P., Edwards, L.E., Kulpecz, A.A., Powars, D.S., Wade, B.S., Feigenson, M.D. & Wright, J.D. 2009: Integrated sequence stratigraphy of the postimpact sediments from the Eyreville core holes, Chesapeake Bay impact structure inner basin. *In* Gohn, G.S., Koeberl, K., Miller, K.G. & Reimold, W.U. (eds.): *The ICDP–USGS deep drilling project in the Chesapeake Bay impact structure: Results from the Eyreville core holes*, Geological Society of America Special Paper 458, pp. 775–810.

Costa, J.E. & Williams, G.P. 1984: Debris flow dynamics. *U.S. Geological Survey, Open-file Report 84–606* (videotape).

Drew, F. 1873: Alluvial and lacustrine deposits and glacial records of the upper Indus Basin. *Geological Society of London Quaternary Journal 29*, 441–471.

Dypvik, H. 1993: Natural gamma activity – a possible aid in sedimentological framework. *Norsk Geologisk Tidsskrift 73*, 58–73.

Dypvik, H. & Kalleson, E. 2010: Mechanisms of late synimpact to early postimpact crater sedimentation in marine-target impact structures. *Geological Society of America Special Papers 465*, 301–318.

Edwards, L.E., Powars, D.S., Gohn, G.S., & Dypvik, H. 2009: Geologic columns for the ICDP–USGS Eyreville A and B cores, Chesapeake Bay impact structure: Sediment-clast breccias, 1096 to 444 m depth, *In* Gohn, G.S., Koeberl, K., Miller, K.G. & Reimold, W.U. (eds.): *The ICDP–USGS deep drilling project in the Chesapeake Bay impact structure: Results from the Eyreville core holes*, Geological Society of America Special Paper 458, pp. 51–90.

Frisk Å.M. & Ormö J. 2007: Facies distribution of post-impact sediments in the Ordovician Lockne and Tvären impact craters: Indications for unique impact-generated environments. *Meteoritics and Planetary Science 42*, 1971–1984.

Folk, R.L. 1974: *Petrology of Sedimentary Rocks*. Hemphill Publishing, Texas, 182 pp.

Gani, M.R. 2004: From turbid to lucid: A straightforward approach to sediment gravity flows and their deposits. *The Sedimentary Record 2*, 4–8.

Gardner, J.S. 1983: Accretion rates on some debris slopes in the Mt. Rae area, Canadian Rocky Mountains. *Earth Surface Processes and Landforms 8*, 347–355.

Gee, D.G., Fossen, H., Henriksen, N. & Higgins, A.K. 2008: From the early Paleozoic platforms of Baltica and Laurentia to the Caledonide orogen of Scandinavia and Greenland. *Episodes 31*, 44–51.

Henningsmoen, G. 1952: Early Middle Cambrian fauna from Rogaland, SW Norway. *Norsk Geologisk Tidsskrift 30*, 13–31.

Kalleson, E., Dypvik, H. & Naterstad, J. 2008: Post-impact sediments in the Gardnos impact structure, Norway. *In* Evans, K., Horton Jr., J.W., King Jr., D.T & Morrow J.R. (eds.): *The Sedimentary Record of Meteorite Impacts*, Geological Society of America Special Paper 437, pp. 19–41.

Kalleson, E., Riis, F., Setså, R. & Dypvik, H. 2012: Ejecta Distribution and Stratigraphy – Field Evidence from the Ritland Impact Structure. *43rd Lunar and Planetary Science Conference, Texas, U.S.A. Abstract # 1351*.

Knaust, D. 2004: Cambro–Ordovician trace fossils from the SW-Norwegian Caledonides. *Geological Journal 39*, 1–24.

Melosh, H.J. 1989: *Impact cratering: a geological process*. Oxford University Press, New York, 245 pp.

Morris, C., Sieve, B.J. & Bullen, H.A. 2008: E-Learning Module: Introduction to X-ray Diffraction. http://www.asdlib.org/onlineArticles/ecourseware/Bullen_XRD/XRDModule_index.htm (accessed 01.05.12).

Mulder, T. & Alexander, J. 2001: The physical character of subaqueous sedimentary density flows and their deposits. *Sedimentology 48*, 269–299.

Nielsen, A.T. & Schovsbo, N.H. 2011: The Lower Cambrian of Scandinavia: Depositional Environment, Sequence Stratigraphy and Palaeogeography. *Earth Science Reviews 107*, 207–310.

Pemberton, S.G., MacEachern, J.A. & Frey, R.W. 1992: Trace fossil facies models: Environmental and allostratigraphic significance. *In* Walker, R.G. & James, N.P. (eds.): *Facies Models: Response to Sea Level Change*, Geological Society of Canada, pp. 47–72.

Rey, P., Burg, J-P. & Casey, M. 1997: The Scandinavian Caledonides and their relationship to the Variscan belt. *In* Burg, J-P. & Ford, M. (eds.): *Orogeny through time*, Geological Society of London Special Publication 121, pp. 179–200.

Riis, F., Kalleson, E., Dypvik, H., Krøgli, S.O. & Nilsen, O. 2011: The Ritland impact structure, southwestern Norway. *Meteoritics and Planetary Science 46*, 748–761.

Schieber, J. & Over, D.J. 2005: Sedimentary fill of the Late Devonian Flynn Creek crater: a hard target marine impact. *In* Over, D.J.,

Morrow, J.R. & Wignall P.B. (eds.): *Understanding Late Devonian and Permian–Triassic Biotic and Climatic Events: Towards an Integrated Approach*, Developments in Palaeontology and Stratigraphy 20, pp. 51–69.

Setså, R. 2011: *The Ritland impact structure: characteristics and distribution of the ejecta layer and associated Lower Paleozoic sedimentary succession*. MSc thesis, University of Oslo, 111 pp.

Shuvalov, V., Dypvik, H., Kalleson, E. & Setså, R. 2012: Modelling the 2.7 km, shallow marine Ritland impact structure. *Earth Moon Planets 108*, 175–188.

Thickpenny, A. 1984: The sedimentology of the Swedish Alum Shales. *In* Stow, D.A.V. & Piper, D.J.W. (eds.): *Fine-grained Sediments: Deepwater Processes and Facies*, Geological Society of London Special Publication 15, pp. 511–525.

Wentworth, C.K. 1922: A scale of grade and class terms for clastic sediments. *Journal of Geology 30*, 377–392.

Paper 3

Sedimentation in marine impact craters - Insight from the Ritland impact structure.

By

Azad, A. S. and Dypvik, H.

Meteoritics and Planetary Science Journal, 2013, In Review.

Appendix

Conference Abstracts and Poster

Abstract # 1

Abstracts and Proceedings of the Geological Society of Norway,
Winter conference, 11-13 January, 2011, Stavanger, Norway

Syn-impact and early-post impact sedimentation in the Ritland impact structure, Western Norway

Azad, A. S.[1], Tomczyk, M.[2], Dypvik, H.[1], Kalleson, E.[1] & Riis, F.[3]

[1] Department of Geosciences, University of Oslo, 0316 Oslo, Norway
[2] Department of Geosciences, University of Bremen, 28359, Bremen, Germany
[3] Norwegian Petroleum Directorate, 4003 Stavanger, Norway

The crater infill sediments of the Ritland impact structure can be broadly classified in two sections: 1) syn-impact and early-post impact sediments and 2) post impact sediments. The syn- and early-post impact sediments (1) are composed of a minor melt succession and mostly coarse clastics; breccias, conglomeratic and arkosic sandstones. The post impact sediments (2) are fine grain sand- and siltstones and shales which formed at a rather stable crater situation. The syn- and early-post impact sediments, which are the topic of this presentation, broadly form three facies associations: i) lower breccia unit, ii) the sandstone unit and iii) upper breccia unit.

The lower breccia unit consists of melt-bearing rocks and authigenic breccias which overlying brecciated and fractured basement. The lower breccias form low angle wedges interfingering with thin melt-bearing rock succession. In general the sediments are clast supported along the base and more matrix rich towards the top, grading into conglomeratic sandstone beds. The clasts consist of basement gneisses and dispersed pegmatitic clasts, still carrying the original gneissic structure. The matrix-rich sediments at the top are marked by occasional well developed bedding and some possible fluidal features e.g., cross bedding, imbrications, and erosional scours. Preliminary observations suggests that the sediments of the lower breccia unit were deposited as freshly crushed, chemically unweathered fragments, derived from breakdown of the target rocks at the syn or early-syn stage of crater modification. The beds were deposited by gravity controlled processes e.g., landslide, slumping, and rock-avalanches. The matrix-rich sediments could represent debris-flow deposits, e.g., caused by breaching of the crater rim by subsurface or surface water bodies or even by precipitation.

The sandstone unit displays a lower gradational contact towards the lower breccias. These sandstones are laminated, parallel bedded in the lower part, cross stratified in the middle and massive in the uppermost layers. Macroscopically the sandstones are fine to medium grained, subangular to subrounded and appear well sorted. Low angle cross stratification, trough-cross bedding, ripple marks, mudflakes, scour and fill marks are present. Petrographic analyses demonstrate that these sandstones are enriched in feldspar, with occasional enrichments of calcite and quartz. The vertical stacking of these sediments reflects a shift in depositional conditions; from debris flows to density flows/turbidity flows. These successions were deposited during crater-lake configuration, possibly as alluvial fans/ fandeltas.

The upper breccia unit is exposed in topographically higher elevations along the steep crater walls. The sediments are mostly clast supported, but a few meters of matrix-supported breccia and conglomeratic beds have been found in both the lower and upper parts of this unit. The matrix is relatively coarse grained, showing weak lamination or fluid flow features especially in the upper part. In the southern area (Svodene), the upper breccia unit displays an erosional contact to the underlying sandstone unit, while an erosional contact to the fractured basement characterizes the south-western rim. The overall observations of the upper breecia unit suggest gravity controlled sedimentation e.g., scree or debris flows due to erosion of the unstable crater wall and crater rim in the later crater modification stage.

Abstract # 2

30th Nordic Geological Winter Meeting,
09-12 January, 2012, Reykjavik, Iceland

ORAL
IS 1

Post impact sedimentation in the Ritland impact structure, Western Norway

Abdus Samad Azad[1], Henning Dypvik[1], Elin Kalleson[1], Fridtjof Riis[2]
[1]*University of Oslo, OSLO, Norway*
[2]*Norwegian Petroleum Directorate, STAVANGER, Norway*

The crater infill sediments of the Ritland impact structure can be classified as: A) syn-impact B) early-post impact, and C) post impact sediments. The syn- and early-post impact sediments are composed of a minor, basal melt unit succeeded by a relatively thick succession of coarse grained clastics; breccias, conglomeratic and arkosic sandstones. The post impact sediments consist of finer grained clastics representing a rather stable crater situation and succeeded by regionally developed extensive clastic sequences.

The post impact sediments are exposed in the central and at the eastern part of the crater, showing onlapping relations to the upper part of the early-post impact sediments. The post impact sediments consist of a lower unit (~6 m thick) of fine to medium grained sandstones, succeeded by very fine sand and silty-shales in the upper part, overlain by a thick (estimated 180 m) unit of dark grey to black shales. Evidences of bioturbation, possibly *planolites, thalassinoides* has been found within the sandy sediments indicating the establishment of Early Cambrian life within the crater. The transition to black shales indicates that more stable and anoxic conditions started to prevail within the crater.

Higher up along the easternmost crater wall, the early-post impact to post impact transition is marked by three clast-supported breccia beds interbedded with dark grey to black shales. The breccia beds are composed of decimetre sized, sub-angular to sub-rounded clasts of granitic and gneissic origin, with bed thickness ranging from 1-2 m. The matrix consists of a mix of fine to medium grained sand and dark grey to blackish clay. The breccia beds have limited lateral extent (10 to 20 m) and, thin towards the crater centre. Towards bed tops some thin beds (2 cm) consisting of medium to coarse grained sand have been found intercalating with thinly laminated dark grey shales and silty shales. Submarine slides and reworking of sediments were active processes along the crater wall for a long time after impac occasionally depositing coarser material between the long and quiet periods of clay deposition.

This study will focus on the sedimentological and mineralogical aspects of the transitional sediments (early-post impact to post impact) inferring to their depositional mechanism the paleoenvironmental conditions and their possible source areas.

SEDIMENTATION IN THE RITLAND IMPACT STRUCTURE, WESTERN NORWAY.

A. S. Azad[1], H. Dypvik[1], E. Kalleson[1] and F. Riis[2]

[1] Department of Geosciences, University of Oslo, P.O. Box 1047, Blindern, NO-0316 Oslo, Norway (m.a.s.azad@geo.uio.no, henning.dypvik@geo.uio.no and elinkal@geo.uio.no)

[2] Norwegian Petroleum Directorate, P.O. Box 600, NO-4003 Stavanger, Norway (Fridtjof.Riis@npd.no).

Introduction: Syn- and post-impact sedimentation within impact craters often start by collapse of the transient cavity and sediment transportation towards the crater centre by different gravity and mass flow processes. These could include rock avalanches, debris avalanches, scree and debris flows depending on the physical properties of the target rock, degree of slope failure, and temporal fluidization of the sediments [1]. The sedimentary processes also vary depending on the overall paleo-geographical setting of the target area (subaerial, subaqueous/shallow marine, deep marine) [2]. In the Ritland case the target area was a shallow epeiric sea, with basement rocks covered by a thin blanket of sediments. In such shallow water setting a crater rim is formed in much the same way as for land-target craters in contrast to deep marine impacts lacking well developed crater rims [3]. The crater rim height and its relation to the sea water depth during impact may significantly control the sedimentation in such craters. An instantaneous powerful resurge of sea water might not be expected if the crater rim is high enough compared to the sea water depth. Sea water may eventually fill the crater with reduced resurge energy through breaching of the crater rim and mass flow events such as debris flows and suspension flows would dominate in the water filled crater soon after the rock-avalanches/debris-avalanches processes. Suspension-dominated sedimentation e.g., turbidity currents are to be expected dominating in a later stage with a comparatively stable crater cavity [4].

Ritland Impact Structure: Ritland is the third and most recently confirmed Norwegian impact structure, located in the Hjelmeland municipality, Rogaland, western Norway (Fig. 1) [5]. The structure shows a nearly circular depression (2.7 km in diameter and 350 m deep) excavated in the gneissic Precambrian terrain. The crater was probably formed during Cambrian time, filled by sediments and eventually deeply buried [5]. Several succeeding events of uplift, erosion, and finally the Pleistocene glaciations helped to disclose the structure. At present, highly deformed and fractured basement rocks and the exposed crater filling sediments display the remnants of this simple impact structure. The sub-Cambrian peneplain, covered by a thin (5-15 m) marine Cambrian sedimentary cover and about 100 m of water, probably was the target surface of the Ritland impact [5]. Detailed study of the sedimentary features of the Ritland impact structure has not yielded evidence of powerful resurge within the crater. The crater rim was probably elevated above sea level, damming more powerful instantaneous resurge. Delayed and reduced resurge effects may be suggested in Ritland crater as evidenced by the characteristics of the crater filling sediments, partly described below.

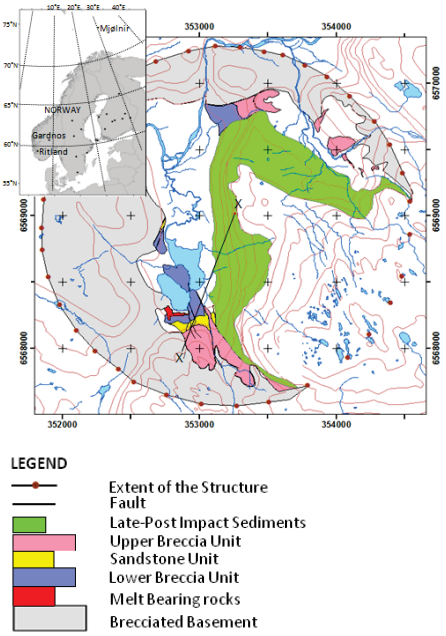

Fig. 1: Lithofacies distribution map of the Ritland impact structure. Red dot (point X) indicates the reconstructed crater centre, the cross section along XX′ is shown in Fig. 2

Sedimentary Units: The crater infill sediments of the Ritland impact structure (Fig. 1) can be broadly classified as: A) syn-and early post impact sediments and B) late-post impact sediments. The syn- and early-post impact sediments are composed of a minor, basal melt-rock unit succeeded by a relatively thick succession of coarse grained clastics; breccias, conglomeratic and arkosic sandstones. These were deposited at the early stages of crater modification and can further be subdi-

vided into; i) Lower Breccia Unit (LBU) ii) Sandstone Unit (SU) and iii) Upper Breccia Unit (UBU) (Fig. 1). The succeeding late-post impact sediments consist of finer grained clastics; forming a thin lower unit of very fine sand and silty-shales in the lower part, overlain by a thick unit of dark grey to black shales.

Sedimentary Processes: The lower-most LBU sediments (Figs. 1, 2) were sourced from intense *in situ* brecciated transient cavity walls and rims, particles eventually sliding down towards the crater centre and deposited as rock-avalanches. Clast supported breccia with similar clast and matrix composition compared to the basement breccia (target surface) as well as occurrences of dispersed, reworked melt particles in the lower-most part of the Lower Breccia Unit and a basal melt bearing rock unit underneath (Fig. 2) suggest that these sediments were deposited during an early stage of crater modification. Debris flow deposits dominates on top of these avalanche formations, probably reflecting prevailing water saturated conditions due to delayed resurge of the sea water through the breached crater rim. The rock debris was transported down from the unstable crater walls and rim as multiple depositional lobes.

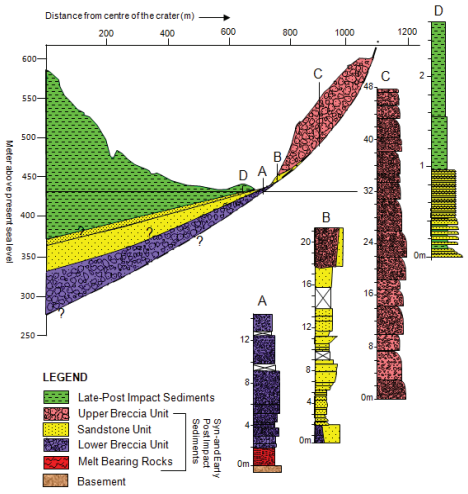

Fig. 2 Geological cross section (XX/ in Fig.1) illustrating stratigraphic relation of the different sedimentary units. The sections A, B, C, and D show the generalized stratigraphy of the crater filling successions based on field lithologs.

A marked shift from clast-supported to matrix-supported texture appears in the upper part of the Lower Breccia Unit sediments. This transition represents a shift towards hyperconcentrated density flows, generated by mixing of water and dilution at the flow head with gradual entrance of sea water into the crater. The crater eventually filled with water and suspension-dominated sedimentation dominated. The Sandstone Unit (Fig. 2) were probably deposited by turbidity currents under submarine fan settings towards the centre of the crater basin and the sediments may have been derived from base-slope erosion and further reworking of the crater wall sediments. The Upper Breccia Unit sediments represent the marginal part of the crater basin where the sediments were derived from renewed, local erosion of the steep, unstable crater wall and rim. These sediments wedge out from the rim to the crater centre showing fan like distribution. Different gravity and mass flow processes dominates within this unit. The late-post impact sediments (Fig. 2) were deposited during a long (millions of years) and quiet period of sedimentation through suspension-deposition during mainly anoxic bottom water conditions.

References:

[1] Melosh H.J. (1989) New York: Oxford University Press. 245. [2] Dypvik H. and Jansa L.F. (2003) *Sedimentary Geology.* 161, 309-337. [3] Ormö J. and Lindström M. (2000) *Geological Magazine.* 137, 67-80. [4] Dypvik H. and Kalleson E. (2010) *Geological Society of America.* 465, 301-318. [5] Riis F., Kalleson E., Dypvik H., Krøgli S. O. and Nilsen O. (2011) *Meteoritics and Planetary Science.* 46, 748-761

SEDIMENTATION IN THE RITLAND IMPACT STRUCTURE, WESTERN NORWAY

A. S. Azad[1], H. Dypvik[1], E. Kalleson[1] and F. Riis[2]
1 Department of Geosciences, University of Oslo, P.O. Box 1047, Blindern, NO-0316 Oslo, Norway
2 Norwegian Petroleum Directorate, P.O. Box 600, NO-4003 Stavanger, Norway

Introduction

Ritland is a 2.7 km diameter, 350 m deep simple impact structure, located in western Norway (Fig. 1). The crater was probably formed during Cambrian time, filled by sediments and eventually deeply buried. Several succeeding events of uplift, erosion, and finally the Pleistocene glaciations disclosed the structure [1].

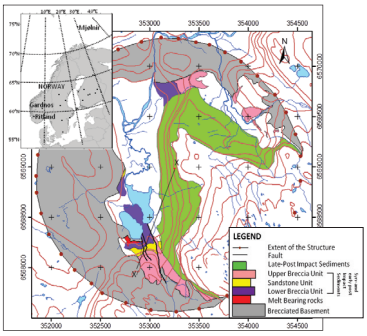

Fig. 1. Lithofacies distribution map of the Ritland impact structure. The cross section along XX′ is shown in Fig. 2

The study is aimed to understand the mechanism of different sedimentary processes to deduce crater filling history. Detailed field mapping of the sedimentary successions and mineralogical study were done.

Sedimentary Units

The crater infill sediments of the Ritland impact structure can be broadly classified as: A) syn-and early post impact sediments and B) late-post impact sediments. The syn- and early-post impact sediments can be subdivided: i) Lower Breccia Unit (LBU) ii) Sandstone Unit (SU) and iii) Upper Breccia Unit (UBU) (Figs. 1 & 2). The succeeding late-post impact sediments consist of finer grained clastics; forming a thin lower unit of very fine sand and silty-shales, and overlained by thick unit of dark grey to black shales (Fig. 2).

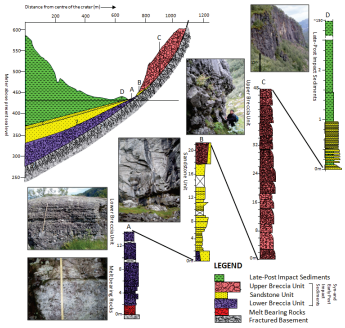

Fig. 2 Geological cross section (XX′ in Fig.1) The sections A, B, C, and D show the generalized stratigraphy. Photos along side shows the dramatic differences in facies types.

Depositional Model

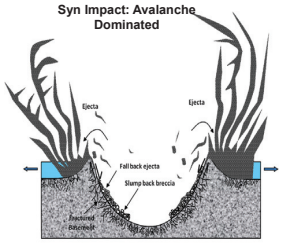

Fig. 3.A Sedimentation started with intense *in situ* brecciation and slumping of the transient cavity walls and rims.

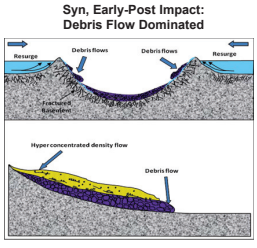

Fig. 3.B Debris flow dominated as water saturated conditions prevailed. Debris flows transformed into hyperconcentrated density flows [2] afterwords.

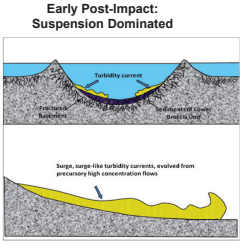

Fig. 3.C The crater eventually filled with sea water and the suspension currents under submarine fan settings dominated.

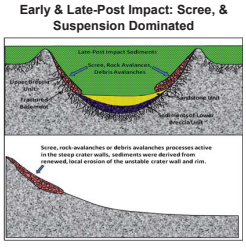

Fig. 3.D Scree, rock or debris avalanches were active along steep crater walls. Suspension-deposition continued in the crater centre.

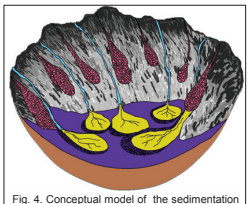

Fig. 4. Conceptual model of the sedimentation processes of different sedimentary units of Ritland impact structure

Conclusions

The lower-most LBU sediments were sourced from intense *in situ* brecciation and slumping of the steep transient cavity walls and rims and eventually slided down towards the crater centre and deposited as rock-avalanches (Fig. 3.A).

Debris flows dominated immediately after the rock avalanches as water saturated conditions start to prevail due to delayed resurge of the sea water through the breached crater rim (Fig. 3.B & 4). Debris flows transformed into hyperconcentrated density flows [2] by mixing of water and dilution at the flow head with gradual entrance of sea water into the crater as indicated by the upper part of the LBU sediments (Fig. 3.B).

The crater eventually filled with sea water and the SU sediments were deposited by turbidity currents under submarine fan settings (Fig. 3.C & 4).

The Upper Breccia Unit sediments represent the marginal part of the crater basin (Fig. 3.D & 4) and were derived from renewed, local erosion of the steep, unstable crater wall and rim and deposited as scree, rock-avalanches or debris avalanches. The late-post impact sediments were deposited during a long (millions of years) and quiet period of sedimentation during mainly anoxic bottom water conditions (Fig. 3.D).

Reference:
[1] Mulder T., & Alexander J., 2001: The physical character of subaqueous sedimentary density flows and their deposits. *Sedimentology.* 48, 269-299.
[2] Riis F., Kalleson E., Dypvik H., Krøgli S. O. and Nilsen O. 2011: The Ritland impact structure, southwestern Norway. *Meteoritics and Planetary Science.* 46, 748-761